

# LOADDEF USER MANUAL

LoadDef v. 1.1.4

HILARY R. MARTENS<sup>1</sup>, LUIS RIVERA<sup>2</sup>, AND MARK SIMONS<sup>3</sup>

<sup>1</sup>*Department of Geosciences, University of Montana, Missoula, MT, USA*

<sup>2</sup>*Institut de Physique du Globe de Strasbourg (UMR7516), Université de Strasbourg/CNRS, Strasbourg, France*

<sup>3</sup>*Division of Geological and Planetary Sciences, California Institute of Technology, Pasadena, CA, USA*



Caltech

February 17, 2021

© 2020

**Hilary R. Martens, Luis Rivera, Mark Simons**

All Rights Reserved

## Abstract

`LoadDef` is a `Python`-based toolkit for modeling the spheroidal deformation-response of a spherically symmetric, non-rotating, elastic, and isotropic (SNREI) Earth to a variety of applied forces, including surface mass loading and gravitational fields. We designed the toolkit with ease-of-use in mind, such that it may be a resource for both experienced Earth-deformation modelers as well as newcomers to the field. Love numbers are generated by integrating the equations of motion for spheroidal deformation through a spherically-symmetric planetary model using Runge-Kutta techniques, with appropriate boundary conditions applied at the surface. The planetary model may be radially heterogeneous and optionally include a fluid layer. To quantify the effects of small perturbations to the density and elastic structure on the deformation-response, the toolkit also includes a module to compute partial derivatives of Love numbers with respect to perturbations in the density, bulk modulus, and shear modulus. Load Green's functions (displacement, gravity, strain, and tilt) are derived from combinations of load Love numbers in three separate reference frames (CE, CM, CF). The displacement load Green's functions may then be convolved with local- to global-scale models of surface mass loading to derive predicted surface displacements at user-defined geographic locations.

## Preface

### 0.1 About This Document

This document is a user manual accompanying the `LoadDef` software. Section 1 discusses how to access and install the software. Section 2 describes how to access certain datasets that may be used with the software, some of which require registration and license agreements. We then explain the structure of the main `LoadDef` modules, including optional arguments and file formats, in Section 3. In Section 4, we provide several examples showing how to perform some of the primary functions of the software. A description of the theory and methods fundamental to the modeling objectives for which the code is designed is provided in Section 5. References are provided at the end of the document.

### 0.2 Attribution

The `LoadDef` software is a product of Hilary Martens’s PhD studies at Caltech in collaboration with Mark Simons (Caltech) and Luis Rivera (Université de Strasbourg). We distribute the software free of charge with the hope that you may find it useful in your own research and educational pursuits. In the normal scientific practice, we request that you recognize the efforts of the authors by citing the appropriate peer-reviewed paper(s) in presentations and publications.

We aim to continue supporting and developing `LoadDef` based on community input, and we also welcome opportunities to collaborate as co-author(s) on project applications that make use of `LoadDef`. If you have any questions about the software or would like to discuss a particular project idea further, please get in touch! Thanks! ([hilary.martens@umontana.edu](mailto:hilary.martens@umontana.edu))

#### **To acknowledge use of this software, please cite:**

1. Martens, H.R., L. Rivera, and M. Simons (2019), “LoadDef: A Python-based toolkit to model elastic deformation caused by surface mass loading on spherically symmetric bodies,” *Earth & Space Science*, **6**: 1–13, doi:10.1029/2018EA000462.

#### **Additional publications** associated with the software include:

2. Martens, H.R., and M. Simons (2020), “A comparison of predicted and observed ocean tidal loading in

Alaska,” *Geophys. J. Int.*, **223**(1): 454–470, doi:10.1093/gji/ggaa323.

3. Martens, H.R., L. Rivera, M. Simons, and T. Ito (2016), “The sensitivity of surface mass loading displacement response to perturbations in the elastic structure of the crust and mantle,” *J. Geophys. Res. Solid Earth*, **121**: 3911–3938, doi:10.1002/2015JB012456.

4. Martens, H.R., M. Simons, S. Owen, and L. Rivera (2016), “Observations of ocean tidal load response in South America from sub-daily GPS positions,” *Geophys. J. Int.*, **205**(3): 1637–1664, doi:10.1093/gji/ggw087.

**For additional information**, you may also be interested to consult:

Martens, Hilary R. (2016), “Using Earth deformation caused by surface mass loading to constrain the elastic structure of the crust and mantle,” Dissertation (Ph.D.), California Institute of Technology. doi:10.7907/Z9N29TX7.  
<http://resolver.caltech.edu/CaltechTHESIS:04102016-211741759>

### 0.3 Support

LoadDef is based upon work supported by the National Science Foundation Geophysics Program funding under Grant No. EAR-1417245 as well as by the National Science Foundation Graduate Research Fellowship to HRM under Grant No. DGE-1144469. This software is based upon work supported by the NASA Earth and Space Science Fellowship to HRM under Grant No. NNX14AO04H as well as by NASA EPSCoR funding under Grant No. NNX15AK40A.

### 0.4 Request for Comments

We welcome comments, suggestions, and corrections aimed at improving the software and documentation. Please report errors, inaccuracies, typos, comments, and suggestions to Dr. Hilary Martens at the University of Montana ([hilary.martens@umontana.edu](mailto:hilary.martens@umontana.edu)).

### 0.5 LoadDef Software License and Copyright Notice

**Copyright (c) 2014–2020 Hilary R. Martens, Luis Rivera, Mark Simons**

LoadDef is distributed under the GNU General Public License version 3:

*LoadDef* is free software: you can redistribute it and/or modify it under the terms of the GNU General Public License as published by the Free Software Foundation, either version 3 of the License, or any later version.

*LoadDef* is distributed in the hope that it will be useful, but WITHOUT ANY WARRANTY; without even the implied warranty of MERCHANTABILITY or FITNESS FOR A PARTICULAR PURPOSE. See the GNU General Public License for more details.

You should have received a copy of the GNU General Public License along with *LoadDef*. If not, see <https://www.gnu.org/licenses/>.

# Contents

<b>Abstract</b>	<b>ii</b>
0.1 About This Document . . . . .	iii
0.2 Attribution . . . . .	iii
0.3 Support . . . . .	iv
0.4 Request for Comments . . . . .	iv
0.5 LoadDef Software License and Copyright Notice . . . . .	iv
<b>Preface</b>	<b>v</b>
<b>1 Download and Installation</b>	<b>1</b>
1.1 Installation with Anaconda (RECOMMENDED) . . . . .	1
1.2 Installation with Other Package Managers . . . . .	2
1.3 Additional Notes on Optional Python Modules . . . . .	4
<b>2 Data Access</b>	<b>6</b>
2.1 Land-Sea Mask . . . . .	6
2.2 Surface Mass Loading . . . . .	6
2.2.1 Global Ocean Tide Models . . . . .	6
2.2.2 Local Ocean Tide Models . . . . .	7
2.2.3 Non-Tidal Ocean Models . . . . .	7
2.2.4 Atmospheric Models . . . . .	8
<b>3 Main Programs</b>	<b>9</b>
3.1 Love Numbers . . . . .	9
3.2 Love Number Partial Derivatives . . . . .	13
3.3 Load Green's Functions . . . . .	17
3.4 Displacement Response to Surface Mass Loading . . . . .	21
3.5 Formatting Surface Mass Load Models for Input to LoadDef . . . . .	25
<b>4 Examples</b>	<b>26</b>
4.1 Computing Love Numbers . . . . .	27
4.2 Computing Love-Number Partial Derivatives . . . . .	27
4.3 Computing Load Green's Functions . . . . .	29
4.4 Generating a Land-Sea Mask . . . . .	30
4.5 Preparing a Load Model . . . . .	30

4.5.1	Harmonic Loads . . . . .	31
4.5.2	Time-Series Loads . . . . .	32
4.6	Predicting Load-Induced Surface Displacements . . . . .	32
4.7	Utility Functions . . . . .	33
4.7.1	Station Grid . . . . .	33
4.7.2	Plotting Results . . . . .	34
4.7.3	Custom Earth Models . . . . .	35
4.7.4	Conversion of Harmonic Displacements to Horizontal Particle Motion Ellipses . . . . .	35
<b>5</b>	<b>Deformation Modeling</b>	<b>37</b>
5.1	Introduction . . . . .	37
5.2	Love Number Computation . . . . .	37
5.2.1	Introduction . . . . .	37
5.2.2	Equilibrium Equations for Material Deformation . . . . .	39
5.2.3	Linear Elastic Constitutive Relation . . . . .	40
5.2.4	Solutions to the Equations of Motion . . . . .	43
5.2.5	Reduction of the Equations of Motion to First Order . . . . .	46
5.2.6	Non-dimensionalization . . . . .	48
5.2.7	Starting Solutions: Power Series Expansion . . . . .	49
5.2.8	Starting Solutions: Homogeneous Sphere . . . . .	50
5.2.9	Runge-Kutta Integration . . . . .	52
5.2.10	Fluid Layers . . . . .	53
5.2.11	Boundary Conditions at Solid-Fluid Interfaces . . . . .	54
5.2.12	Surface Boundary Conditions . . . . .	54
5.2.13	Load Love Numbers . . . . .	58
5.2.14	Potential Love Numbers . . . . .	59
5.2.15	Shear Love Numbers . . . . .	60
5.2.16	Stress Love Numbers and Degree-1 Modes . . . . .	60
5.2.17	Numerical Considerations . . . . .	62
5.2.18	Starting Radius within the Mantle . . . . .	62
5.2.19	Asymptotic Solutions . . . . .	62
5.3	Load Green's Functions . . . . .	63
5.3.1	Introduction . . . . .	63
5.3.2	Kummer's Transformation and Series Convergence . . . . .	67
5.3.3	Legendre Sums . . . . .	71
5.3.4	Legendre Sums: Limit as $\theta \rightarrow 180^\circ$ . . . . .	72



5.3.5	Legendre Polynomial Recursion Relations . . . . .	72
5.3.6	Legendre Polynomial Recursion Relations: Limit as $\theta \rightarrow 180^\circ$ . . . . .	75
5.3.7	Disk Factor . . . . .	75
5.3.8	Reference Frames . . . . .	76
5.4	Convolution Methods . . . . .	78
5.4.1	Integration Mesh . . . . .	80
5.4.2	Interpolation and Integration of Load Green's Function . . . . .	81
5.4.3	Convolution Procedure . . . . .	83
5.4.4	Additional Considerations . . . . .	85
<b>References</b>		<b>86</b>

# 1 Download and Installation

LoadDef may be downloaded from GitHub under <https://github.com/hrmartens/LoadDef/>.

Questions about the download and installation of LoadDef should be directed to Dr. Hilary Martens at:

[hilary.martens@umontana.edu](mailto:hilary.martens@umontana.edu).

LoadDef is compatible with Python2 and Python3, but Python3 will be prioritized for future versions. LoadDef has been tested on Ubuntu and Debian Linux systems.

## 1.1 Installation with Anaconda (RECOMMENDED)

To install all packages using Anaconda (recommended), we suggest first creating a new environment.

First, you will need to install Anaconda on your system, if you haven't done so already:

<https://www.anaconda.com>

Next, at the command line, run the following three lines:

```
conda config --prepend channels conda-forge
conda config --set channel_priority strict
conda create -n LDEF python=3.7 basemap mpi4py scipy netCDF4 pyshp shapely
```

The commands above only need to be executed once on your system. From now on, each time you wish to run LoadDef, you only need to activate the LDEF environment (see next command).

To activate the new LDEF environment, run:

```
conda activate LDEF
```

If the command above did not work for you (e.g. for older versions of Anaconda), then you can try:

```
source activate LDEF
```

You're all set! LoadDef should now be ready to use.

To deactivate the new environment when you are finished, you can run:

```
conda deactivate
```

## 1.2 Installation with Other Package Managers

Several Python modules are required to use LoadDef. Most are quite standard. We recommend that modules be installed using a package-management system, such as Anaconda, apt-get, python-pip, or macports. We recommend Anaconda, since administrator privileges are not required.

Required modules include:

1. **numpy**
2. **scipy**
3. **matplotlib**
4. **math**
5. **sys**
6. **os**
7. **netCDF4**
8. **datetime**
9. **mpi4py**

Optional, but recommended, Python modules include:

1. **mpl.toolkits.basemap**
2. **shapefile**
3. **shapely**
4. **pyproj**

If you are using Ubuntu (Linux), you may install packages using apt-get and python-pip. Both require administrator privileges. To install python-pip using apt-get:

```
sudo apt-get install python-pip
```

To search for additional packages using apt-get:

```
apt-cache search []
```

To search for Python packages:

```
pip search []
```

To install most standard Python packages:

```
sudo pip install []
```

For example:

```
sudo pip install numpy
sudo pip install scipy
sudo pip install matplotlib
sudo pip install math
sudo pip install sys
sudo pip install os
sudo pip install datetime
```

The **mpi4py** package requires a pre-installed and working MPI distribution:

<https://mpi4py.scipy.org/docs/usrman/install.html>.

On a system running **Ubuntu 14.04.5 Linux**, we have found that all required packages for the **mpi4py** module may be installed using `apt-get`:

```
sudo apt-get install python-mpi4py
```

On a desktop PC running **Windows 10 with an Ubuntu Linux subsystem**, we installed the **mpi4py** module using the following sequence of commands:

1. **Optional:** If `python-mpi4py` was already installed using `apt-get`, first run:

```
sudo apt-get remove python-mpi4py
```

2. **Optional:** Ensure that `apt-get` is up-to-date:

```
sudo apt-get update
```

```
sudo apt-get -y upgrade
```

3. **Optional:** Search for available OpenMPI packages by running:

```
apt-cache search openmpi
```

4. Install OpenMPI:

```
sudo apt-get install libopenmpi-dev
```

5. Install mpi4py using python-pip:

```
sudo pip install mpi4py
```

**Note:** It is possible that problems may arise at run-time related to the SciPy sub-package `special`. In the `/LOADGF/LN/fundamental_solutions_homsph.py` function, the line near the top reading “from `scipy.special` import **sph\_jn**” may need to be modified to read “from `scipy.special` import **spherical\_jn** as **sph\_jn**”.

### 1.3 Additional Notes on Optional Python Modules

The following modules are not required to use the primary functionalities of `LoadDef` (e.g., computing Love numbers and Green’s functions), but are required to import and interpret certain load and coastline databases. The `basemap` addition to the `mpl_toolkits` module helps to improve the efficiency of grid interpolation for the convolution of Green’s functions with a load model.

If not using Anaconda, the optional modules may be installed using `apt-get` and `python-pip`.

For example, on Ubuntu Linux:

```
sudo apt-get install python-mpltoolkits.basemap
```

```
sudo pip install pyshp
```

```
sudo pip install shapely
```

```
sudo pip install pyproj
```

```
sudo pip install netCDF4
```

The `pyshp` module includes the `shapefile` module.

If you do not have access to `mpl_toolkits.basemap`:

`/LoadDef/CONVGF/CN/interpolate_load.py`

must be modified by commenting *out* the import of `mpl_toolkits.basemap` (top of script), commenting *out* the reference to the `basemap.interp` function, and commenting *in* the reference to the `scipy.interpolate.RectBivariateSpline` function.

If you do not have access to **shapefile**, **shapely**, and/or **pyproj**:

`/LoadDef/GRDGEN/utility/process_add_shapefile.py`, which generates a land-sea mask for Antarctica, will not be available.

If you do not have access to **netCDF4**, you will not be able to read certain load models in netCDF format.

You may also comment out the import of **netCDF4** in `CONVGF/utility/read_AmpPha.py`, and instead use load models in plain-text format.

## 2 Data Access

### 2.1 Land-Sea Mask

Global bathymetric and topographic datasets, such as ETOPO1 (Amante & Eakins, 2009), may be used to generate a land-sea mask. The land-sea mask may then be refined using local models where available. For Antarctica, for example, coastline information is available from the Scientific Committee on Antarctic Research (SCAR) Antarctic Digital Database (ADD).

ETOPO1: <https://www.ngdc.noaa.gov/mgg/global/global.html>

ADD: <http://www.add.scar.org/home/add7>

### 2.2 Surface Mass Loading

#### 2.2.1 Global Ocean Tide Models

**FES2014** is the most recent installment in a series of tidal atlases produced by the “French Tidal Group” under the generic name of “Finite Element Solution (FES)” (Le Provost et al., 1994; Lyard et al., 2006; Carrère et al., 2012). The FES2014 atlas, generated by assimilating satellite altimetry observations into a global hydrodynamic model, provides the complex-valued amplitudes of 32 tidal harmonics on a  $0.0625^\circ \times 0.0625^\circ$  grid. The model may be accessed from AVISO after site registration and license agreement:

[www.aviso.altimetry.fr/en/data/products/auxiliary-products/global-tide-fes.html](http://www.aviso.altimetry.fr/en/data/products/auxiliary-products/global-tide-fes.html).

**TPXO8-Atlas**, developed at Oregon State University, integrates a global tidal solution (TPXO8) with a multitude of high-resolution local solutions produced for shelf and coastal regions at several locations around the world (Egbert et al., 1994; Egbert & Erofeeva, 2002; Egbert et al., 2010). Tidal amplitudes and phases are provided on a global grid of  $\frac{1}{30}^\circ$  resolution for the harmonics  $M_2$ ,  $S_2$ ,  $N_2$ ,  $K_2$ ,  $K_1$ ,  $O_1$ ,  $P_1$ ,  $Q_1$ , and  $M_4$ . Additional long-period and compound tidal harmonics ( $M_f$ ,  $M_m$ ,  $MS_4$ , and  $MN_4$ ) are provided on a  $\frac{1}{6}^\circ$ -resolution grid. Satellite altimetry data from the TOPEX/Poseidon and Jason missions are assimilated into global solutions of the Laplace Tidal Equations (LTEs) to generate TPXO8. Tide gauges are primarily used for validation, particularly in the shelf and coastal regions. The model may be accessed from Oregon State University: [volkov.oce.orst.edu/tides/](http://volkov.oce.orst.edu/tides/).

**EOT11A**, a purely empirical ocean tide model generated from a harmonic analysis of multi-mission satellite altimetry data, provides amplitudes and phases for thirteen tidal harmonics (Savcenko & Bosch, 2012). The harmonic analysis was performed on the combined altimetry residuals, using FES2004 (Lyard et al., 2006) as a reference model. The model may be accessed from: <ftp://dgfi.tum.de/pub/EOT11a/>.

**HAMTIDE11A** (Hamburg direct data Assimilation Methods for TIDEs) provides amplitude and phase information for nine tidal harmonics on a regular grid of  $0.125^\circ$  resolution. A direct minimization of model and observational residuals using least-squares inversion generates the HAMTIDE11A atlas. The model may be accessed from: <ftp://ftp-icdc.cen.uni-hamburg.de/hamtide/>.

**GOT4.10c**, available by request from Dr. Richard Ray at the Goddard Space Flight Center (GSFC), is the latest release in a series of global ocean tide models developed by Dr. Ray at GSFC (Ray, 1999; Ray & Egbert, 2004; Ray, 2013). The model is generated by performing a harmonic analysis of satellite altimetry residuals with respect to an *a priori* hydrodynamic model. The satellite altimetry observations of sea-surface height were corrected for tidal geocenter variations induced by the loading (Desai & Ray, 2014).

**DTU10**, developed and distributed by The Technical University of Denmark, is a global ocean tide model with  $0.125^\circ \times 0.125^\circ$  resolution. The model may be accessed from: [http://www.space.dtu.dk/english/Research/Scientific/\\_data\\_and\\_models/Global/\\_Ocean/\\_Tide/\\_Model](http://www.space.dtu.dk/english/Research/Scientific/_data_and_models/Global/_Ocean/_Tide/_Model).

### 2.2.2 Local Ocean Tide Models

Tidal predictions near coastlines and in shallow seas are less reliable than in the open ocean due to nonlinearities in the tidal equations and limited empirical constraints (e.g., Ray et al., 2011). The high-resolution, local ocean tide models may be obtained from Oregon State University (Egbert & Erofeeva, 2002; Egbert et al., 1994, 2010): [volkov.oce.orst.edu/tides/region.html](http://volkov.oce.orst.edu/tides/region.html).

Additional providers of local tidal models are listed in Agnew (2013), and the references therein. Local models for Canadian waters have also been developed by Lambert et al. (1998).

### 2.2.3 Non-Tidal Ocean Models

**ECCO2**: NASA's *Estimating the Circulation and Climate of the Oceans* (ECCO) consortium provides time series of non-tidal ocean loading (NTOL) on global grids (e.g., Stammer et al., 2002). A recent install-



ment of the consortium, the ECCO2 model, includes daily estimates of ocean bottom-pressure potential anomalies on a global grid of resolution  $0.25^\circ \times 0.25^\circ$  from 1992 onward. The ECCO2 estimates of bottom-pressure anomalies are diagnostic quantities derived from anomalous water-column height (e.g., van Dam et al., 1997). It is recommended that global-spatial and temporal averages be removed from the ECCO2 bottom-pressure anomalies to account for drifts in the global balance of evaporation and precipitation (D. Menemenlis and H. Zhang, personal communication). Moreover, the ECCO2 simulations of ocean-bottom pressure anomalies do not include the effects of atmospheric or tidal forcing (D. Menemenlis, personal communication). To first-order, however, the ocean-bottom pressure does not change with variations in atmospheric pressure due to the inverted barometer effect, but could have issues on timescales less than a few days. <https://ecco.jpl.nasa.gov>

#### 2.2.4 Atmospheric Models

Estimates of the atmospheric surface pressure on global grids are routinely computed by reanalysis centers such as the European Centre for Medium-Range Weather Forecasts (ECMWF) and the National Centers for Environmental Prediction/National Center for Atmospheric Research (NCEP/NCAR).

**ECMWF:** ECMWF models are distributed with six-hour temporal resolution on global grids of  $0.75^\circ \times 0.75^\circ$  spatial resolution. ECMWF uses data assimilation techniques to incorporate a range of space- and land-based empirical weather measurements into general circulation models. Variations in atmospheric pressure tend to be largest at high latitude due to geostrophic force balance (e.g., Wunsch & Stammer, 1997). <https://www.ecmwf.int/en/research/climate-reanalysis>

**NCEP/NCAR:** NCEP/NCAR models are distributed with six-hour temporal resolution on global grids. <https://www.esrl.noaa.gov/psd/data/gridded/data.ncep.reanalysis.html>

### 3 Main Programs

LoadDef includes four main programs, located in the **working** directory:

- **run\_ln.py** | Computes potential, load, shear, and stress Love numbers
- **run\_pl.py** | Computes partial derivatives of Love numbers
- **run\_gf.py** | Computes displacement, gravity, tilt, and strain load Green's functions
- **run\_cn.py** | Computes surface displacements caused by surface mass loading

#### 3.1 Love Numbers

The program **run\_ln.py**, located in the **working** directory, computes potential, load, shear, and stress Love numbers. The input planetary model is assumed to be spherically symmetric, non-rotating, elastic, and isotropic (SNREI), and should be in the following format: radius (km), Vp (km/s), Vs (km/s), density (g/cc).

##### REQUIRED INPUTS:

1. **Planet Model** : radius (km), Vp (km/s), Vs (km/s), density (g/cc)
  - :: Assumed to be spherically symmetric, non-rotating, elastic, and isotropic (SNREI)
  - :: May include one internal fluid layer (e.g. Earth's outer core), or be entirely solid

##### OPTIONAL INPUTS AND DEFAULTS:

1. **startn** : Starting value for spherical harmonic degrees (for Love numbers)
  - Default is 0
2. **stopn** : Ending value for spherical harmonic degrees (for Love numbers)
  - Default is 10000
3. **period.hours** : Forcing period (in hours)
  - Default is 12.42 (M<sub>2</sub> period)

4. **r\_min** : Minimum radius for variable planetary structural properties (m)  
Default is 1000
5. **interp\_emod** : Optionally interpolate the planetary model to a different resolution  
Default is False (see LOADGF/LN/prepare\_planet\_model.py)
6. **kx** : Order of the spline fit for the planetary model (1=linear; 3=cubic)  
Default is 1 (recommended)
7. **delim** : Delimiter for the planetary model file  
Default is None (Whitespace)
8. **inf\_tol** : Integration starting radius,  $r$ , for which  $(\frac{r}{a})^n$  drops below tolerance 'inf\_tol'  
Default is 1E-5
9. **rel\_tol** : Integration tolerance level (relative tolerance)  
Default is 1E-13
10. **abs\_tol** : Integration tolerance level (absolute tolerance)  
Default is 1E-13
11. **backend** : Specify ODE solver  
:: Recommended to only use `dop853` or `dopri5` solvers, since they integrate only to a specified stopping point (no overshoot, like `lsoda` and `vode`)  
Default is `dop853`
12. **nsteps** : Specify maximum number of (internally defined) steps allowed during each call to the ODE solver  
:: For more information, see `Scipy.Integrate.Ode` manual pages  
Default is 3000
13. **num\_soln** : Set number of solutions for each integration (integer)  
:: Note that integration step size is adaptive based on the specified tolerance, but solutions are

only computed at regular intervals determined by this user-specified value

Default is 100

14. **G** : Universal gravitational constant

Default is  $6.672\text{E-}11 \text{ (m}^3 \text{ kg}^{-1} \text{ s}^{-2}\text{)}$

15. **nmaxfull** : Maximum spherical harmonic degree for which integration will be performed through the full planet. Beyond nmaxfull, the integration will begin in the mantle.

Default is None (the parameter will be estimated from inf\_tol within integrate\_odes.py)

16. **file.out** : Extension for the output files

Default is “.txt”

#### OUTPUT FILES:

1. **Load Love Number Output File**

“output/Love\_Numbers/LLN/lln\_” + **file.out**

2. **Potential Love Number Output File**

“output/Love\_Numbers/PLN/pln\_” + **file.out**

3. **Stress Love Number Output File**

“output/Love\_Numbers/STR/str\_” + **file.out**

4. **Shear Love Number Output File**

“output/Love\_Numbers/SHR/shr\_” + **file.out**

#### OUTPUT VARIABLES:

1. Spherical harmonic degrees,  $n$  (array)
2. Vertical-displacement load Love numbers,  $h'$  (array)
3. Horizontal-displacement load Love numbers,  $nl'$  (array)
4. Gravitational-potential load Love numbers,  $nk'$  (array)

5. First-order asymptotic solution for  $h'$  (float)
6. First-order asymptotic solution for  $nl'$  (float)
7. First-order asymptotic solution for  $nk'$  (float)
8. Second-order asymptotic solution for  $h'$  (float)
9. Second-order asymptotic solution for  $nl'$  (float)
10. Second-order asymptotic solution for  $nk'$  (float)
11. Vertical-displacement potential/tide Love numbers,  $h$  (array)
12. Horizontal-displacement potential/tide Love numbers,  $nl$  (array)
13. Gravitational-potential potential/tide Love numbers,  $nk$  (array)
14. Vertical-displacement stress Love numbers,  $h_{\text{str}}$  (array)
15. Horizontal-displacement stress Love numbers,  $nl_{\text{str}}$  (array)
16. Gravitational-potential stress Love numbers,  $nk_{\text{str}}$  (array)
17. Vertical-displacement shear Love numbers,  $h_{\text{shr}}$  (array)
18. Horizontal-displacement shear Love numbers,  $nl_{\text{shr}}$  (array)
19. Gravitational-potential shear Love numbers,  $nk_{\text{shr}}$  (array)
20. Planet radius (float, m)
21. Planet mass (float, kg)
22. Integration points (array of radial distances)
23. Solutions for spheroidal deformation due to loading as a function of radius (array)
24. Solutions for spheroidal deformation due to a potential field as a function of radius (array)
25. Solutions for spheroidal deformation due to stress conditions as a function of radius (array)

- 26. Solutions for spheroidal deformation due to shear forcing as a function of radius (array)
- 27. Lamé parameter  $\lambda$  at the surface (float, Pa)
- 28. Lamé parameter  $\mu$  at the surface (float, Pa)

### 3.2 Love Number Partial Derivatives

The program **run\_pl.py**, located in the **working** directory, computes the partial derivatives of Love numbers with respect to the bulk modulus, the shear modulus, and density (Okubo & Saito, 1983; Martens et al., 2016a). The program initially calls the same subroutines as **run\_ln.py** to compute the solution vectors (solutions to the equations of motion as a function of radius), and then uses the solution vectors to compute partial derivatives as a function of radius. As a result, many of the inputs and outputs are the same as for **run\_ln.py**. Note that if a specific file extension is specified and is identical to an extension used to compute Love numbers during a previous run of **run\_ln.py**, the old Love number files will be overwritten.

#### REQUIRED INPUTS:

1. **Planet Model** : radius (km), Vp (km/s), Vs (km/s), density (g/cc)
  - :: Assumed to be spherically symmetric, non-rotating, elastic, and isotropic (SNREI)
  - :: May include one internal fluid layer (e.g. Earth's outer core), or be entirely solid

#### OPTIONAL INPUTS AND DEFAULTS:

1. **startn** : Starting value for spherical harmonic degrees (for Love numbers)
  - Default is 0
2. **stopn** : Ending value for spherical harmonic degrees (for Love numbers)
  - Default is 10000
3. **period.hours** : Forcing period (in hours)
  - Default is 12.42 (M<sub>2</sub> period)
4. **r\_min** : Minimum radius for variable planetary structural properties (m)
  - Default is 1000

5. **interp\_emod** : Optionally interpolate the planetary model to a different resolution  
Default is False (see LOADGF/LN/prepare\_planet\_model.py)
6. **kx** : Order of the spline fit for the planetary model (1=linear; 3=cubic)  
Default is 1 (recommended)
7. **delim** : Delimiter for the planetary model file  
Default is None (Whitespace)
8. **inf\_tol** : Integration starting radius,  $r$ , for which  $\left(\frac{r}{a}\right)^n$  drops below tolerance 'inf\_tol'  
Default is 1E-5
9. **rel\_tol** : Integration tolerance level (relative tolerance)  
Default is 1E-13
10. **abs\_tol** : Integration tolerance level (absolute tolerance)  
Default is 1E-13
11. **backend** : Specify ODE solver  
:: Recommended to only use `dop853` or `dopri5` solvers, since they integrate only to a specified stopping point (no overshoot, like `lsoda` and `vode`)  
Default is `dop853`
12. **nsteps** : Specify maximum number of (internally defined) steps allowed during each call to the ODE solver  
:: For more information, see `Scipy.Integrate.Ode` manual pages  
Default is 3000
13. **num\_soln** : Set number of solutions for each integration (integer)  
:: Note that integration step size is adaptive based on the specified tolerance, but solutions are only computed at regular intervals determined by this user-specified value  
Default is 100

14. **G** : Universal gravitational constant

Default is  $6.672\text{E-}11 \text{ (m}^3 \text{ kg}^{-1} \text{ s}^{-2}\text{)}$

15. **nmaxfull** : Maximum spherical harmonic degree for which integration will be performed through the full planet. Beyond nmaxfull, the integration will begin in the mantle.

Default is None (the parameter will be estimated from inf\_tol within integrate\_odes.py)

16. **plot\_figure** : Reproduce Figure 1 from Okubo & Endo (1986) as a sanity check.

Default is False

17. **par\_out** : Extension for the output filenames

Default is “partials.txt”

#### OUTPUT FILES:

##### 1. Load Love Number Output File

“output/Love\_Numbers/LLN/lln\_” + **par\_out**

##### 2. Potential Love Number Output File

“output/Love\_Numbers/PLN/pln\_” + **par\_out**

##### 3. Stress Love Number Output File

“output/Love\_Numbers/STR/str\_” + **par\_out**

##### 4. Shear Love Number Output File

“output/Love\_Numbers/SHR/shr\_” + **par\_out**

##### 5. Partial Derivative Output File (one file per spherical-harmonic degree)

“output/Love\_Numbers/Partials/lln\_n” +  $n$  + “\_” + **par\_out**

#### OUTPUT VARIABLES:

1.  $\frac{\partial}{\partial \mu} h_{\text{potential}}(r)$

2.  $\frac{\partial}{\partial \mu} l_{\text{potential}}(r)$



3.  $\frac{\partial}{\partial \mu} k_{\text{potential}}(r)$
4.  $\frac{\partial}{\partial \kappa} h_{\text{potential}}(r)$
5.  $\frac{\partial}{\partial \kappa} l_{\text{potential}}(r)$
6.  $\frac{\partial}{\partial \kappa} k_{\text{potential}}(r)$
7.  $\frac{\partial}{\partial \rho} h_{\text{potential}}(r)$
8.  $\frac{\partial}{\partial \rho} l_{\text{potential}}(r)$
9.  $\frac{\partial}{\partial \rho} k_{\text{potential}}(r)$
10.  $\frac{\partial}{\partial \mu} h_{\text{load}}(r)$
11.  $\frac{\partial}{\partial \mu} l_{\text{load}}(r)$
12.  $\frac{\partial}{\partial \mu} k_{\text{load}}(r)$
13.  $\frac{\partial}{\partial \kappa} h_{\text{load}}(r)$
14.  $\frac{\partial}{\partial \kappa} l_{\text{load}}(r)$
15.  $\frac{\partial}{\partial \kappa} k_{\text{load}}(r)$
16.  $\frac{\partial}{\partial \rho} h_{\text{load}}(r)$
17.  $\frac{\partial}{\partial \rho} l_{\text{load}}(r)$
18.  $\frac{\partial}{\partial \rho} k_{\text{load}}(r)$
19.  $\frac{\partial}{\partial \mu} h_{\text{shear}}(r) (h_{\text{stress}}(r) \text{ for } n = 1)$
20.  $\frac{\partial}{\partial \mu} l_{\text{shear}}(r) (l_{\text{stress}}(r) \text{ for } n = 1)$
21.  $\frac{\partial}{\partial \mu} k_{\text{shear}}(r) (k_{\text{stress}}(r) \text{ for } n = 1)$
22.  $\frac{\partial}{\partial \kappa} h_{\text{shear}}(r) (h_{\text{stress}}(r) \text{ for } n = 1)$
23.  $\frac{\partial}{\partial \kappa} l_{\text{shear}}(r) (l_{\text{stress}}(r) \text{ for } n = 1)$

24.  $\frac{\partial}{\partial \kappa} k_{\text{shear}}(r)$  ( $k_{\text{stress}}(r)$  for  $n = 1$ )
25.  $\frac{\partial}{\partial \rho} h_{\text{shear}}(r)$  ( $h_{\text{stress}}(r)$  for  $n = 1$ )
26.  $\frac{\partial}{\partial \rho} l_{\text{shear}}(r)$  ( $l_{\text{stress}}(r)$  for  $n = 1$ )
27.  $\frac{\partial}{\partial \rho} k_{\text{shear}}(r)$  ( $k_{\text{stress}}(r)$  for  $n = 1$ )

### 3.3 Load Green's Functions

The program **run\_gf.py**, located in the **working** directory, computes displacement, gravity, tilt, and strain Green's functions for load-induced spheroidal deformation.

#### REQUIRED INPUTS:

1. **Love-Number File:** Output *load* Love number file from **run\_ln.py**

#### OPTIONAL INPUTS AND DEFAULTS:

1. **theta** : Angular distances at which to compute the load Green's functions (list format; degrees)

Default is:

```
theta = [0.0001, 0.001, 0.01, 0.02, 0.03, 0.04, 0.06, 0.08, 0.1, 0.16, 0.2, 0.25, 0.3,
0.4, 0.5, 0.6, 0.8, 1.0, 1.2, 1.6, 2.0, 2.5, 3.0, 4.0, 5.0, 6.0, 7.0, 8.0, 9.0,
10.0, 12.0, 16.0, 20.0, 25.0, 30.0, 40.0, 50.0, 60.0, 70.0, 80.0, 90.0, 100.0,
110.0, 120.0, 130.0, 140.0, 150.0, 160.0, 170.0, 180.0]
```

2. **a** : Planet mean radius (m)

Default is 6371000.

3. **me** : Planet mean mass (kg)

Default is 5.976E24

4. **lmda\_surface** : Value of lambda elastic (Lamé) parameter at planet's surface (Pa)

Default is 3.422E10

5. **mu\_surface** : Value of the shear modulus at planet's surface (Pa)  
Default is 2.662E10
6. **g\_surface** : Value of acceleration due to gravity at planet's surface ( $\text{m s}^{-2}$ )  
Default is 9.81
7. **disk\_factor** : Include a disk factor to improve convergence of the LGFs in the far field  
Default is True
8. **angdist** : Angular distance (in degrees) beyond which the disk factor will be included  
Default is 10 (if disk\_factor = True)
9. **disk\_size** : Radius of the disk in degrees  
Default is 0.1 (if disk\_factor = True)
10. **apply\_taper** : Option to apply a taper to the series summation in the computation of the LGFs.  
The taper mimics the recursive averaging described in Guo et al. 2004 (Eqs. 23 and 24).  
Default is True
11. **grn\_out** : Extension for the output Green's function files  
Default is 'grn.txt'

#### OUTPUT FILES:

1. **Green's Function Output File (CE Frame)**  
"output/Greens\_Functions/ce\_" + **grn\_out**
2. **Green's Function Output File (CM Frame)**  
"output/Greens\_Functions/cm\_" + **grn\_out**
3. **Green's Function Output File (CF Frame)**  
"output/Greens\_Functions/cf\_" + **grn\_out**

#### OUTPUT VARIABLES:

1. Vertical-displacement load Green's function, CE frame
2. Horizontal-displacement load Green's function, CE frame
3. Vertical-displacement load Green's function, CE frame (normalized by  $10^{12}a\theta$ , where  $a$  is planet's radius in meters and  $\theta$  is angular distance in radians)
4. Horizontal-displacement load Green's function, CE frame (normalized by  $10^{12}a\theta$ )
5. Vertical-displacement load Green's function, CM frame
6. Horizontal-displacement load Green's function, CM frame
7. Vertical-displacement load Green's function, CM frame (normalized by  $10^{12}a\theta$ )
8. Horizontal-displacement load Green's function, CM frame (normalized by  $10^{12}a\theta$ )
9. Vertical-displacement load Green's function, CF frame
10. Horizontal-displacement load Green's function, CF frame
11. Vertical-displacement load Green's function, CF frame (normalized by  $10^{12}a\theta$ )
12. Horizontal-displacement load Green's function, CF frame (normalized by  $10^{12}a\theta$ )
13. Gravity load Green's function, indirect (elastic) component, CE frame
14. Gravity load Green's function, indirect (elastic) component, CE frame (normalized by  $10^{18}a\theta$ )
15. Gravity load Green's function, indirect (elastic) component, CM frame
16. Gravity load Green's function, indirect (elastic) component, CM frame (normalized by  $10^{18}a\theta$ )
17. Gravity load Green's function, indirect (elastic) component, CF frame
18. Gravity load Green's function, indirect (elastic) component, CF frame (normalized by  $10^{18}a\theta$ )
19. Tilt load Green's function, indirect (elastic) component, CE frame
20. Tilt load Green's function, indirect (elastic) component, CE frame (normalized by  $10^{12}(a\theta)^2$ )

21. Tilt load Green's function, indirect (elastic) component, CM frame
22. Tilt load Green's function, indirect (elastic) component, CM frame (normalized by  $10^{12}(a\theta)^2$ )
23. Tilt load Green's function, indirect (elastic) component, CF frame
24. Tilt load Green's function, indirect (elastic) component, CF frame (normalized by  $10^{12}(a\theta)^2$ )
25. Strain load Green's function,  $\theta\theta$  component, CE frame
26. Strain load Green's function,  $\lambda\lambda$  component, CE frame
27. Strain load Green's function,  $rr$  component, CE frame
28. Strain load Green's function,  $\theta\theta$  component, CE frame (normalized by  $10^{12}(a\theta)^2$ )
29. Strain load Green's function,  $\lambda\lambda$  component, CE frame (normalized by  $10^{12}(a\theta)^2$ )
30. Strain load Green's function,  $rr$  component, CE frame (normalized by  $10^{18}a\theta$ )
31. Strain load Green's function,  $\theta\theta$  component, CM frame
32. Strain load Green's function,  $\lambda\lambda$  component, CM frame
33. Strain load Green's function,  $rr$  component, CM frame
34. Strain load Green's function,  $\theta\theta$  component, CM frame (normalized by  $10^{12}(a\theta)^2$ )
35. Strain load Green's function,  $\lambda\lambda$  component, CM frame (normalized by  $10^{12}(a\theta)^2$ )
36. Strain load Green's function,  $rr$  component, CM frame (normalized by  $10^{18}a\theta$ )
37. Strain load Green's function,  $\theta\theta$  component, CF frame
38. Strain load Green's function,  $\lambda\lambda$  component, CF frame
39. Strain load Green's function,  $rr$  component, CF frame
40. Strain load Green's function,  $\theta\theta$  component, CF frame (normalized by  $10^{12}(a\theta)^2$ )
41. Strain load Green's function,  $\lambda\lambda$  component, CF frame (normalized by  $10^{12}(a\theta)^2$ )

- 42. Strain load Green's function,  $rr$  component, CF frame (normalized by  $10^{18}a\theta$ )
- 43. Direct (Newtonian) effect of gravity (normalized by  $10^{18}a\theta$ )
- 44. Direct (Newtonian) effect of tilt (normalized by  $10^{12}(a\theta)^2$ )

### 3.4 Displacement Response to Surface Mass Loading

The program **run\_cn.py**, located in the **working** directory, computes predicted surface displacements caused by surface mass loading. The required inputs to **run\_cn.py** include displacement load Green's functions for a SNREI planetary model, which may be generated using **run\_gf.py**, and a load model.

#### REQUIRED INPUTS:

1. **rfm** : Reference frame (Blewitt, 2003)  
 :: Used for input and output filenames
2. **grn\_file** : Displacement load Green's function file output from **run\_gf.py**
3. **norm\_flag** :  
 :: True = Displacement load Green's functions normalized by the Farrell (1972) convention  
 Format:  $[\theta, u_{\text{norm}}, v_{\text{norm}}]$   
 $\theta$  is the angular distance (degrees)  
 $u_{\text{norm}}$  is the vertical-displacement load Green's function (normalized by  $10^{12}a\theta$ , with  $\theta$  in radians)  
 $v_{\text{norm}}$  is the horizontal-displacement load Green's function (normalized by  $10^{12}a\theta$ , with  $\theta$  in radians)  
 :: False = Load Green's function file output directly from **run\_gf.py**
4. **loadfile\_directory** : Full path to the directory containing the input load files
5. **loadfile\_prefix** : Prefix for the input load files  
 :: The load-file directory will be searched for all files starting with this prefix  
 :: Note: For load files organized by date, the end of the filename must be in the format

yyyymmddhhmns.txt

:: Note: For load files not organized by date, the files may be organized by a unique filename ending (e.g. tidal harmonic)

:: Note: Output filenames will be determined in part by the extension following the last underscore character in the load-file name

:: **General format for the load files:** [Latitude (degrees, +N), Longitude (degrees, +E), Amplitude (m), Phase (degrees)]

6. **loadfile\_format** : File format for the load models

:: Acceptable formats include: “nc” (netCDF) and “txt” (plain text)

:: See: /GRDGEN/load\_files/ directory for scripts to generate LoadDef-compatible files of both formats for common load models.

7. **time\_series** : Flag for whether or not the files are organized by date

:: False = All files matching the directory and prefix criteria will be analyzed

:: True = Files are organized by date and will be filtered by date

:: Note: If true, filenames must end in the format yyyymmddhhmns.txt

8. **first\_date** : First date of the time series [year, month, day, hour, minute, second]

:: Note: Only used if **time\_series** is set to true

9. **last\_date** : Last date of the time series [year, month, day, hour, minute, second]

:: Note: Only used if **time\_series** is set to true

10. **regular** : Flag for whether or not the load grid is regular (rectangular)

:: True = Grid is regular (speeds up interpolation)

:: False = Grid is not regular (if unsure, select false)

11. **ldens** : Density of the surface mass load ( $\text{kg m}^{-3}$ )

:: For oceanic loads, suggested density is 1030.0 (default)

:: For atmospheric loads, suggested density is 1.0

12. **lsmask\_type** : Type of land-sea mask

:: 0 = Do not mask either the ocean or the land (retain full model)

:: 1 = Mask out the land (retain the ocean load)

:: 2 = Mask out the oceans (retain the load over the land areas)

13. **lsmask\_file** : Full path and filename of the land-sea mask

:: Format = [Latitude (degrees, +N), Longitude (degrees, +E), Mask Value (0=ocean; 1=land)]

:: Note: The land-sea mask may be irregular and sparse

14. **sta\_file** : File containing the prediction locations for the convolution

:: Format: [Latitude (degrees, +N), Longitude (degrees, +E), Station/Point Name (string)]

15. **outstr** : Additional string to append to output filenames (e.g. “\_2019”)

:: Format: String

#### OPTIONAL INPUTS AND DEFAULTS:

1. **load\_density** : Density of the surface mass load ( $\text{kg m}^{-3}$ )

Default is 1030.0

2. **rad** : Mean radius of the planet (m)

Default is 6371000.

3. **Mesh Parameters** :

(a) **delinc1** : Angular-distance (degrees) increment for inner zone

Default is 0.0002

(b) **delinc2** : Angular-distance (degrees) increment for zone 2

Default is 0.001

(c) **delinc3** : Angular distance (degrees) increment for zone 3

Default is 0.01

(d) **delinc4** : Angular distance (degrees) increment for zone 4

Default is 0.1



(e) **delinc5** : Angular distance (degrees) increment for zone 5

Default is 0.5

(f) **delinc6** : Angular distance (degrees) increment for outer zone

Default is 1.0

(g) **izb** : Inner zone boundary (degrees;  $0 < \text{izb} < \text{z2b}$ )

Default is 0.02

(h) **z2b** : Zone 2 boundary (degrees;  $\text{izb} < \text{z2b} < \text{z3b}$ )

Default is 0.05

(i) **z3b** : Zone 3 boundary (degrees;  $\text{z2b} < \text{z3b} < \text{z4b}$ )

Default is 1.0

(j) **z4b** : Zone 4 boundary (degrees;  $\text{z3b} < \text{z4b} < \text{z5b}$ )

Default is 10.0

(k) **z5b** : Zone 5 boundary (degrees;  $\text{z4b} < \text{z5b} < 180$ )

Default is 90.0

(l) **azminc** : Azimuthal increment (degrees)

Default is 0.1

(m) **mass.cons** : Option to enforce mass conservation by removing the spatial mean from the load grid

Default is False

#### OUTPUT FILES:

1. Predicted displacements at the specified convolution grid-point/station locations for each load file

“output/Convolution/cn\_” + **unmasked region** + “\_” + **cnv\_out**

#### OUTPUT VARIABLES:

1. East-component amplitude (mm)
2. East-component phase (degrees)

3. North-component amplitude (mm)
4. North-component phase (degrees)
5. Vertical-component amplitude (mm)
6. Vertical-component phase (degrees)

### 3.5 Formatting Surface Mass Load Models for Input to LoadDef

The **general format for the load model** must be:

Latitude [degrees, +N], Longitude [degrees, +E], Amplitude [m], Phase [degrees]

If the load is not a harmonic (e.g. not of tidal origin), then the phase should be set to zero.

Load grids may be provided in netCDF or plain-text format (see **GRDGEN/load\_files** for automatic conversion of common datasets). Load models come in a wide variety of formats, and conversion to a LoadDef-standard format prior to input into the convolution allows for simplified program modules and greater ease of generating custom models. Note that small differences (e.g. fraction of a micron) can arise in the predicted load-induced surface displacements computed by `run_cn.py`, since the precision of the floating point values written to the netCDF and plain-text files can be different.

**Note:** In general, LoadDef is not currently set-up to handle very high-resolution load models, unless they are only local in extent. The memory usage can increase dramatically for very high-resolution grids, particularly during the grid interpolations. That said, LoadDef can currently handle most global-scale ocean-tide model grids as well as modern atmospheric and non-tidal oceanic pressure grids on modest computational systems. In addition to memory and storage, run-time also increases with finer grid resolution.

Scripts within the **GRDGEN/load\_files** folder are already set up to generate LoadDef-formatted grids from common datasets, such as the TPXO8-Atlas and FES2014 ocean-tide models, ECMWF atmospheric models, and ECCO2 non-tidal oceanic-pressure models.

## 4 Examples

Assuming that the required `Python` modules have been properly installed (see Sec. 1), the `LoadDef` working directory contains prepared example scripts that illustrate the main functions of the software.

The example scripts are `run_ln.py`, `run_pl.py`, `run_gf.py`, and `run_cn.py`, which compute Love numbers, partial derivatives of Love numbers, load Green’s functions, and predicted load-induced surface displacements, respectively. The `input` directory contains an Earth model (PREM), a pre-generated land-sea mask, and descriptions on how to access common load models. Once downloaded, many of the common load models may be converted into `LoadDef` format using utility scripts in the `GRDGEN/load_files/` folder. The example scripts are already set up to derive Love numbers and load Green’s functions based on the provided data files in the `input` directory, with the exception of `run_cn.py`, which requires that a load model be downloaded first and then converted to `LoadDef` format; more details on the conversion procedure are discussed below.

In general, the scripts *should* be run in a particular order. An output file from the Love-number program `run_ln.py`, for example, may be used as input to the Green’s-function program `run_gf.py`. The Green’s functions are then used as input to the convolution program `run_cn.py`. Both `run_ln.py` and `run_pl.py` may be run simply by specifying an Earth model as input (nothing more is required).

All scripts are `MPI` compatible to reduce overall computation time. To run the `run_ln.py` script, for example, using `X` number of parallel processors:

```
mpirun -np X run_ln.py
```

To run the script in serial-processing mode:

```
mpirun -np 1 run_ln.py
```

or, on some systems, you may simply type:

```
run_ln.py
```

The following sections provide more detailed information on each program.

## 4.1 Computing Love Numbers

To demonstrate how to compute Love numbers using `LoadDef`, we have prepared a script in the `working` directory called `run_ln.py` to generate Love numbers based on PREM structure.

The program is MPI compatible to improve computational efficiency. From within the `working` directory, the script may be run by typing:

```
mpirun -np X python run_ln.py
```

where `X` specifies the number of processors to use. For serial computations, specify `X = 1`. The specified number of processors should not exceed the number of jobs to be run.

Note that the top of the script includes a section for user inputs. An input Earth model is required, and we have selected PREM as an example. We also specify an optional parameter: an extension for the output filename. Without specifying a specific extension, the program would have defaulted to “.txt”. To override the default value, we had to specify the parameter within the call to the main Love-number function (`compute_love_numbers.main`), which may be found at the bottom of the `run_ln.py` script.

For a list of additional optional input parameters, see Sec. 3.1. Importantly, the default integration parameters, including relative and absolute convergence tolerances, may be easily changed by passing in alternative values for the appropriate variables.

The program generates four output files: potential (PLN), load (LLN), shear (SHR), and stress (STR) Love numbers. Each file contains a particular type of Love numbers (PLN, LLN, SHR, or STR) for each spherical harmonic degree selected for the computation. By default, the program computes Love numbers from  $n = 0$  to  $n = 10000$ , though the range may be modified using optional input parameters.

The output files are placed in an `output` directory, which will be created automatically if one does not already exist. The results from `run_ln.py` will specifically be placed under `output/Love_Numbers/`.

## 4.2 Computing Love-Number Partial Derivatives

To demonstrate how to compute Love-number partial derivatives using `LoadDef`, we have prepared a script in the `working` directory called `run_pl.py` to generate partial derivatives (with respect to the elastic moduli and density) based on PREM structure.

The program is MPI compatible to improve computational efficiency. From within the `working` directory, the script may be run by typing:

```
mpirun -np X python run_pl.py
```

where `X` specifies the number of processors to use. For serial computations, specify `X = 1`. The specified number of processors should not exceed the number of jobs to be run.

The program `run_pl.py` only requires an Earth model as input (specified in the “user inputs” section at the top of the script). To compute partial derivatives, the program first computes Love numbers (using the `compute_love_numbers.main` function) and then uses the output parameters as input to a partial-derivative function (`compute_lnpartials.main`). Thus, the program calls the same subroutines to compute the Love numbers as `run_ln.py`. That said, it can still be worthwhile to have both programs (`run_ln.py` and `run_pl.py`). In particular, use-cases not requiring partial derivatives have no need for the additional functionality of `run_pl.py`. Furthermore, although `run_pl.py` does generate Love-number output files, some use-cases might only require partial derivatives for a few spherical-harmonic degrees. In this case, the number of spherical-harmonic degrees contained within the Love-number output file would be insufficient for input to the Green’s-function program. As with `run_ln.py`, the range of spherical-harmonic degrees computed may be specified as optional inputs. In `run_pl.py`, we demonstrate how to restrict the range to  $n = 0 - 4$ . Partial derivatives will only be computed for degrees within the specified range.

Whenever partial derivatives for  $n = 1$  are computed, a figure called `Okubo_Endo_Fig1.eps` may optionally be generated and placed under `output/LoveNumbers/Partials/`. The figure reproduces Figure 1 from Okubo & Endo (1986) as a sanity check. The block of code used to generate the figure may be activated or inactivated within the script: `LOADGF/PL/lnpartials.py`.

Additional output files include partial derivatives for the load, potential, and shear Love numbers. All results are placed under the folder `output/LoveNumbers/Partials/`. The prefix of each filename indicates whether the partial derivatives correspond to load (`lln`), potential (`pln`), or shear (`sln`) Love numbers. For the case of  $n = 1$ , the partial derivatives with the prefix “`sln`” correspond instead to stress Love numbers. One file is output for each type of Love number (`lln`, `pln`, or `sln`) and each spherical harmonic degree.

In addition, Love-number files are created in the same way as `run_ln.py`, and will only include Love

numbers for the spherical-harmonic degrees used for computation of the partial derivatives.

### 4.3 Computing Load Green’s Functions

The script `run_gf.py`, also located in the `working` directory, is already set up to use the output from `run_ln.py` to generate load Green’s functions (LGFs) for displacement, gravity, strain, and tilt in three different reference frames (CE, CM, and CF). Note that `run_ln.py` must *finish* running (and have generated the necessary output files) prior to running `run_gf.py`. Since PREM structure was used to compute the Love numbers, we specify a special file extension within the “user inputs” section at the top of the `run_gf.py` script to indicate that the LGFs correspond to PREM structure. Additional optional parameters may be specified in the call to `compute_greens_functions.main` at the bottom of the script. See Sec 3.3 for more information on the optional inputs.

The program is MPI compatible to improve computational efficiency. From within the `working` directory, the script may be run by typing:

```
mpirun -np X python run_gf.py
```

where `X` specifies the number of processors to use. For serial computations, specify `X = 1`. The specified number of processors should not exceed the number of jobs to be run.

Three output files are generated, one per reference frame, and placed under `output/Greens.Functions`. The prefix of each filename corresponds to the reference frame (CE, CM, or CF). The columns of the output files are: angular distance from the load point (“theta”, degrees); radial displacement (m/kg); horizontal displacement (m/kg); normalized radial displacement ( $[m/kg] \times [10^{12} a\theta]$ , where  $a$  is Earth’s radius and  $\theta$  is the angular distance in degrees); normalized horizontal displacement ( $[m/kg] \times [10^{12} a\theta]$ ); elastic component of gravity ( $\times 10^{18} a\theta$ ); elastic component of tilt ( $\times 10^{12} [a\theta]^2$ ); strain component  $\varepsilon_{rr}$  ( $\times 10^{18} a\theta$ ); strain component  $\varepsilon_{\theta\theta}$  ( $\times 10^{12} [a\theta]^2$ ); strain component  $\varepsilon_{\lambda\lambda}$  ( $\times 10^{12} [a\theta]^2$ ); ratio of elastic to Newtonian components of gravity ( $\times 10^{18} a\theta$ ); and the ratio of elastic to Newtonian components of tilt ( $\times 10^{12} [a\theta]^2$ ).

Tilt and strain LGFs are the slowest to converge, and their accuracy is directly affected by the precision of the Love numbers. To further speed convergence, a disk factor may be applied in the far field. Parameters associated with the application of the disk factor may be easily changed by passing alternative values to the appropriate variables. See Sec 3.3 for more information on the optional inputs.

## 4.4 Generating a Land-Sea Mask

Most surface mass loads are not global in extent. The ocean tides, for example, are zero in amplitude over land areas. Although mass-load models continue to improve in resolution every year, it can still be useful to apply a land-sea mask, whereby every point covered by the mask is ensured to be zero-amplitude. As another example, the continents and the oceans respond differently to atmospheric pressure forcing, and it may therefore be desirable to only apply the atmospheric load over land areas. A land-sea mask specifies which grid points are over land and which grid points are over water.

The format for the land-sea mask used by `LoadDef` is very simple: **latitude** (degrees, +N), **longitude** (degrees, +E), and a **land-sea flag**. The flag should be zero (0) for water areas and one (1) for land areas. A utility script called `landsea_mask.py`, within the `GRDGEN/landsea_mask/` directory, may be used to convert ETOPO1, and optionally a refined Antarctic coastline, into a land-sea mask (Amante & Eakins, 2009). A second utility script called `antarctic_mask.py`, also within the `GRDGEN/landsea_mask/` directory, may be used to convert the Antarctic Digital Database (ADD) into a refined land-sea mask around the Antarctic <http://www.add.scar.org/>.

## 4.5 Preparing a Load Model

The format for load models used by `LoadDef` is designed to be accessible and general. `LoadDef` requires either a netCDF or plain-text file with geographic coordinates (latitude, longitude) and an amplitude and phase value for each coordinate location. In other words, the format is simply [latitude, longitude, amplitude, phase]. For non-harmonic loads, the phase may simply be set to zero. When the phase is set to zero, all values in the amplitude parameter are assumed to load the planet at the same moment in time.

The netCDF and/or plain-text files for common load models may be generated using the scripts in the `GRDGEN/load_files/` folder. The netCDF files are significantly more efficient, both in terms of storage and processing speed, but the plain-text files are more straight-forward to manipulate and interpret. Note that small differences (e.g. fraction of a micron) can arise in the predicted load-induced surface displacements computed by `run_cn.py`, since the precision of the floating point values written to the netCDF and plain-text files can be different.

For predicting load-induced surface displacements using the convolution algorithm (`run_cn.py`), the load

model will be linearly interpolated onto an integration mesh. The resolution of the integration mesh may be adjusted using optional input parameters to `run_cn.py`. The load value mapped to each cell of the integration mesh will be integrated over the area of the cell. The grid interpolations typically take the longest time to run (for very high-resolution grids, the interpolation might take up to a few minutes or more to complete). Thus, the resolution of the load grid, as well as the resolution of the integration mesh (an optional parameter for the convolution algorithm), affects the run-time as well as the precision. That said, the inputs (load model and integration mesh) are adjustable to meet the specific needs of individual projects. Moreover, if the load is on a regular grid, this may be specified in the call to the convolution algorithm (within the `run_cn.py` script) to speed up the computation. For loads on irregular grids, the convolution algorithm can handle the model but will take longer to run. If the model is local (as opposed to global) in extent, then the model should be surrounded by a grid of zero-amplitude values, such that the linear-interpolation algorithm will set areas beyond the local model to zero.

#### 4.5.1 Harmonic Loads

Examples of harmonic loads include the ocean tides. To prepare an ocean-tide model for input into `LoadDef`, you can use the `gen_otl.py` utility in the `GRDGEN/load_files/` folder. We have included instructions for downloading various ocean-tide models within the `input/LoadModels/` folder. Some of the models may be downloaded straight away, and others require the acceptance of license agreements. For scientific and/or educational purposes, the models are generally available.

The `GRDGEN/load_files/gen_otl.py` script is already set up to read in several common ocean-tide models. The script will prepare an ocean-tide model for input into `LoadDef`, as well as, optionally, for plotting using the Generic Mapping Tools (GMT) (Wessel et al., 2013). Note that the three user-inputs at the top of the script are set to the  $M_2$  harmonic of the TPXO8-Atlas model, which is a recently released high-resolution ocean-tide model, but the parameters may easily be changed to read in a different model or harmonic instead (see the “user inputs” section at the top of the script). Since the TPXO8-Atlas model is defined on a high-resolution global grid, the script may take a few minutes or so to write out the necessary grid files. Lower resolution grids can be prepared in far less time.

For the examples presented here, we will assume that the  $M_2$  harmonic of the TPXO8-Atlas ocean-tide models has been retrieved by the user from Oregon State University (<http://volkov.oce.orst.edu/>



tides/tpxo8\_atlas.html). The script `input/LoadModels/TPX08-Atlas/get_TPX08.sh` will download the model automatically.

The TPX08-Atlas netCDF files should be converted to LoadDef format using `GRDGEN/load_files/gen_otl.py`, as described above. The grids are output to `output/GridFiles/`. Two sub-directories, GMT and LoadDef, were also generated to keep the files organized. If any of the directories do not exist, then LoadDef will create them automatically. The files that will be used as input to `working/run_cn.py` are placed in the `output/GridFiles/nc/OTL/` directory (or the `output/GridFiles/text/OTL/` directory if opting to work with plain-text files). Note that, for each different harmonic and/or model type, variables in the “user inputs” section of the `gen_otl.py` utility must be modified appropriately.

#### 4.5.2 Time-Series Loads

Examples of non-harmonic, time-dependent loads include non-tidal oceanic loads and atmospheric loads. Models are typically available at 6-hourly or daily epochs. Each model will need to be converted to LoadDef format [latitude, longitude, amplitude, phase]. For non-harmonic, time-dependent loads, the phase should be set to zero. We have included utilities in the `GRDGEN/load_files/` folder that will convert a variety of common load models into LoadDef format.

Time series of non-tidal oceanic models (based on the NASA ECCO2 model) may be prepared for input into LoadDef by running the `gen_ecco2.py` utility. Time series of atmospheric-pressure models (based on ECMWF) may be prepared for input into LoadDef by running the `gen_ecmwf.py` utility. Even harmonic ocean-tide models may be converted a time-series of load models using `gen_otl_tseries.py`. A utility function is also available to convert NASA GRACE mass-change grids into LoadDef format: `gen_grace.py`.

### 4.6 Predicting Load-Induced Surface Displacements

Once a set of load Green’s functions has been computed (using `run_gf.py`) and a load model has been generated in the appropriate format (using one of the scripts in the `GRDGEN/load_files/` folder), then the `run_cn.py` script in the `working` directory may be used to predict surface displacements caused by

the load. We currently have two examples set up in the `run_cn.py` script. Both require that LGFs were computed using `run_gf.py`, as described above (Sec. 4.3). The first example, for harmonic ocean tidal loading response, requires that the TPXO8-Atlas model be downloaded and converted into the `LoadDef` format (Sec. 4.5.1). The second example, for a time series of non-tidal oceanic loading response, requires that a time series of ECCO2 models be downloaded and converted into `LoadDef` format.

The program is MPI compatible to improve computational efficiency. From within the `working` directory, the script may be run by typing:

```
mpirun -np X python run_cn.py
```

where `X` specifies the number of processors to use. For serial computations, specify `X = 1`. For a small number of load models and/or for tight computational-memory constraints, it may be preferable to run the script in serial-mode. The specified number of processors should not exceed the number of jobs to be run.

The first example (Example 1) may be run straightaway (assuming the appropriate LGF and load files are available). To run the second example (Example 2), simply uncomment the `loadfile_directory`, `loadfile_prefix`, and `time_series` variables associated with “Example 2” (commented lines in the “user inputs” section at the top of the script).

The run-time of the convolution program depends on the resolution of the integration mesh, resolution of the land-sea mask, and resolution of the load model. For TPXO8-Atlas, the convolution may take a few minutes per station, primarily due to the interpolation of the high-resolution load model onto the integration mesh. The resolution of the integration mesh may be modified using optional input parameters (Sec. 3.4). Furthermore, the formats for the input land-sea mask and the input load model are designed to be straightforward. Output files are placed in the `output/Convolution/` directory.

## 4.7 Utility Functions

### 4.7.1 Station Grid

A utility script called `land_grid.py`, located within the `GRDGEN/station_grid/` directory, may be used to generate a grid of geographic point locations to be used with the convolution algorithm, `run_cn.py`. The user simply provides a desired grid spacing, bounds for the grid, and a land-sea mask (nominally used to return only those grid points that reside over designated land areas).

### 4.7.2 Plotting Results

Several simple plotting scripts are provided with LoadDef under `utility/plots/`. Following successful runs of `run_ln.py`, `run_pl.py`, and `run_gf.py`, most of the scripts should run straightaway. Figures will be plotted to screen and also saved as image files under the `utility/plots/output/` folder. If the folder does not exist, LoadDef will create one automatically.

The plotting scripts include the following:

1. **plot\_em.py** : Plot parameters associated with Earth models
  - :: Note: Multiple Earth models (and associated labels, colors, and weights) may be specified at the top of the script (in list format)
  - :: Note: Panels F, G, and H, which show maximum differences *between* models, are only meaningful when at least two Earth models have been supplied as input (in the example, only PREM is shown)
2. **plot\_gf.py** : Plot load Green's functions, which are generated by `run_gf.py`
3. **plot\_ld.py** : Plot load models
  - :: Note: The script is set up to plot the  $M_2$  harmonic from the TPX08-Atlas ocean-tide model (format: [lat, lon, amp, pha]), which may be generated using the `generate_otl_grid.py` utility in the `GRDGEN/load_files/` folder
  - :: Note: Options within the script may be modified to plot values in the format [lat, lon, value] (e.g., the land-sea mask). To plot the land-sea mask that was provided in the `input/LoadModels/` directory, simply uncomment the fields marked with "Example 2" and comment *out* the fields marked with "Example 1". The land-sea mask is sparse, and only show values within a few grid-points of the coastlines. Land points are shown as magenta and ocean points are shown as cyan.
4. **plot\_ln.py** : Plot load Love numbers, which are generated by `run_ln.py`
5. **plot\_pl.py** : Plot Love-number partial derivatives, which are generated by `run_pl.py`
6. **plot\_ts.py** : Plot time series of 3-component displacements, which are generated by `run_cn.py`

### 4.7.3 Custom Earth Models

A few simple scripts to generate and manipulate Earth models are provided in the `utility/emods/` folder. The subdirectory `PREM` includes scripts to generate an isotropic PREM model based on the polynomial functions provided in Dziewonski & Anderson (1981). The `run_generate_PREM.py` script allows for user inputs, and calls the function `generate_PREM.py`.

The `utility/emods/` folder also contains the following scripts:

1. **`emod_dispersion.py`** : Adjusts the elastic parameters of a reference Earth model to non-seismic frequencies by accounting for physical dispersion
2. **`emod_homogeneous.py`** : Generates a homogeneous Earth model
3. **`emod_perturb.py`** : Perturbs the parameters (elastic moduli and density) of an Earth model

### 4.7.4 Conversion of Harmonic Displacements to Horizontal Particle Motion Ellipses

For the response to harmonic loads, such as surface displacements caused by ocean tidal loading, the horizontal components of the deformation may be converted to particle motion ellipses (PMEs) using utility scripts available in the `utility/pmes/` folder.

To facilitate the comparison of different models, stations should be grouped together into a single file for each tidal harmonic. The convolution program, however, generates a single file for each station, which contains all available harmonics. Thus, it may be necessary to sort through the station files, pick out the response to individual harmonics, and organize new response files by harmonic. The **`run_combine_harmonics.py`** script will do this for you, provided that the filenames for each station are in a certain format.

The “user inputs” section at the top of the script allows the user to specify the directory, prefix, and suffix corresponding to station files of interest. Only the name of the station should appear between the prefix and the suffix. The station name will be extracted within the code, as the string that exists between the prefix and the suffix. The model and harmonic should appear after the final underscore. The harmonic should be separated from the model name with a dash. The model name may optionally include dashes as well. For example, a filename might be `cn_OceanOnly_P402_cm_convvgf-TPX08-Atlas-M2.txt`, where `P402` is the station name, `TPX08-Atlas` is the model name, and `M2` is the harmonic.

Whether the files are organized by station or harmonic, the **run\_env2pme.py** script may be used to convert east and north displacements into particle motion ellipses. The input file for `run_env2pme.py` must be the same format as the files output by `run_cn.py`. The output file from `run_env2pme.py` will be in expanded “PME” format, which includes horizontal ellipse parameters.

Once files have been generated in “PME” format, the **run\_compute\_residuals.py** script may be used to compute residuals between the results contained within two PME-formatted files. Comparisons should only be made between ellipse parameters of the same frequency. In other words, each file should contain response estimates for a single harmonic. Optionally, the file may contain multiple stations, but the stations should be consistent in order and number between the two files being compared. In addition to computing the residuals directly between the two models, `run_compute_residuals.py` also generates a second set of residuals, whereby an amplitude and phase response common to the entire network is computed and removed. For more information on the “common-mode” response, see Martens et al. (2016b).

## 5 Deformation Modeling

### 5.1 Introduction

For a more comprehensive discussion of the theory associated with computing Love numbers, load Green's functions, and predicted load-induced surface displacements, the reader is referred to Martens (2016). Here, we review some of the key concepts.

Predicting the displacement-response of a radially symmetric Earth to surface mass loading (SML) involves a convolution of displacement load Green's functions (LGFs) with a load model (e.g., Farrell, 1973; Jentzsch, 1997):

$$\bar{U}(\bar{r}, S, Z, \rho) = \int_{\Omega'} \rho(\bar{r}') G(|\bar{r}' - \bar{r}|, S) Z(\bar{r}') d\Omega', \quad (5.1)$$

where  $\bar{U}$  is the response of the solid Earth at position vector  $\bar{r}$  (the measurement location),  $\rho$  is the mass density of the load at position vector  $\bar{r}'$ ,  $G$  is the Green's function per kg load, and  $Z$  is the height of the load at position vector  $\bar{r}'$ . The integral is taken over the surface area of the Earth,  $\Omega'$ . The LGFs depend on the distance between the load vector and the observation vector,  $|\bar{r}' - \bar{r}|$ , where  $\bar{r}$  represents the position vector of the measurement location and  $\bar{r}'$  represents the position vector of the load (e.g., Jentzsch, 1997, Sec. 2.3). The LGFs additionally depend on Earth structure,  $S$ , where  $S$  represents radially symmetric structure (e.g., PREM). The LGFs are derived from combinations of load Love numbers (LLNs) (e.g., Farrell, 1972).

In `LoadDef`, self-gravitating, spherically symmetric, non-rotating, elastic, and isotropic (SNREI) Earth models are assumed (e.g., Longman, 1962). In future releases, we plan to include the facility to adopt more sophisticated models, such as allowing for mantle anelasticity (e.g., Pagiatakis, 1990; Bos et al., 2015).

### 5.2 Love Number Computation

#### 5.2.1 Introduction

Love numbers are dimensionless parameters that characterize the yielding of the elastic Earth to body forces and surface tractions (Love, 1911; Munk & MacDonald, 1960). For the response of an elastic Earth to an external gravitational potential,  $V$ , three Love numbers are defined:  $h_n(r)$ ,  $k_n(r)$ , and  $l_n(r)$ . The subscript  $n$  denotes a dependence on spherical harmonic degree and  $(r)$  indicates a radial dependence. Augustus

Edward Hough (A.E.H.) Love introduced  $h_n(r)$  and  $k_n(r)$  in 1909 (Love, 1909); Toshi Shida subsequently introduced  $l_n(r)$  in 1912. All three parameters are commonly referred to as *Love numbers*, or alternatively referred to as the *Love and Shida numbers*. Although the parameters exhibit a radial dependence, here we consider deformation observed only at Earth's surface, and thus drop the  $(r)$  notation.

The parameter  $h_n$  characterizes Earth's vertical displacement in response to an external potential. The radial displacement,  $u_n$ , of Earth's surface in response to an external gravitational potential of spherical harmonic degree,  $n$ , is given by (e.g., Munk & MacDonald, 1960; Farrell, 1972; Melchior, 1983; Baker, 1984; Agnew, 2015):

$$u_n = h_n \frac{V_n}{g}, \quad (5.2)$$

where  $g$  is the gravitational acceleration at Earth's surface,  $\frac{V_n}{g}$  represents the equilibrium tidal height, and  $h_n$  scales the equilibrium height to a realistic vertical displacement based on the density and elastic properties of Earth's interior. Gravitational self-attraction, generated by the redistributed mass, is accounted for in the response parameter  $h_n$  (Munk & MacDonald, 1960).

The parameter  $k_n$  characterizes the change in the gravitational potential resulting from the redistribution of mass that occurs in response to the external potential field. Due to the self-attraction effect, the magnitude of the gravitational potential increases by a factor  $k_n V_n$  from the location of the displaced surface. Thus, the total potential, accounting for self-attraction, becomes (e.g., Munk & MacDonald, 1960; Agnew, 2015):

$$V_n^{\text{total}} = (1 + k_n) V_n. \quad (5.3)$$

The Shida number  $l_n$  is defined as the horizontal displacement of Earth relative to the gradient of the equilibrium tide. The two components of the horizontal displacement are:

$$\begin{aligned} v_n^{\text{north}} &= -\frac{l_n}{g} \frac{\partial V_n}{\partial \delta} \\ v_n^{\text{east}} &= \frac{l_n}{g} \frac{1}{\sin \delta} \frac{\partial V_n}{\partial \lambda}, \end{aligned} \quad (5.4)$$

where  $\delta$  is colatitude and  $\lambda$  is east longitude (e.g., Munk & MacDonald, 1960; Harrison, 1985).

The Love and Shida numbers described so far characterize Earth's response to an external gravitational potential; thus, we refer to them as **potential Love numbers**. A second class of Love numbers, referred to

as **load Love numbers**, may also be introduced to describe the deformation of Earth under normal tractions, typically applied at Earth's surface (Munk & MacDonald, 1960; Lambeck, 2005). Surface mass loads come from a variety of sources, including glaciers, lakes, the atmosphere, and oceans. The load Love numbers are distinguished from the potential Love numbers by a superscript prime:  $h'_n$ ,  $k'_n$ , and  $l'_n$ . A third class of Love numbers exists to characterize Earth's response to surface-tangential tractions (Lambeck, 2005), distinguished from the other classes by superscript double primes ( $h''_n$ ,  $k''_n$ ,  $l''_n$ ) and known as **shear Love numbers**. Only six of the nine Love numbers from the three sets (potential, load, and shear) are independent, and expressions exist to relate the Love numbers to one another (Molodenskiy, 1977; Merriam, 1985; Lambeck, 1988).

### 5.2.2 Equilibrium Equations for Material Deformation

The equilibrium equations describing spheroidal deformations of an elastic, self-gravitating, and hydrostatically pre-stressed body are derived from the principle of conservation of linear momentum (e.g., Takeuchi, 1950; Alterman et al., 1959; Longman, 1962; Takeuchi, 1966; Farrell, 1972; Takeuchi & Saito, 1972; Cathles, 1975; Lanzano, 1982; Dahlen & Tromp, 1998; Bos & Scherneck, 2013; Smylie, 2013).

In continuum mechanics, conservation of linear momentum states:

$$\rho \bar{a} = \bar{\nabla} \cdot \bar{\sigma} + \rho \bar{F}, \quad (5.5)$$

where  $\bar{\sigma}$  is the stress tensor,  $\rho$  is the density,  $\bar{a}$  is the acceleration vector ( $\bar{a}_i = \left( \frac{\partial^2 \bar{u}}{\partial t^2} \right)_i = (\bar{u}_{,tt})_i = u_{i,tt}$ , where  $\bar{u}$  is a three-component displacement vector) and  $\bar{F}$  is the body-force vector per unit mass. In indicial notation,  $(\bar{\nabla} \cdot \bar{\sigma})_i = \sigma_{ij,j}$ , where Einstein's summation convention for repeated indices applies. The system of Eqs. 5.5 are also known as the *equations of motion* or the *momentum equations*. Note that we retain the acceleration term.

For a self-gravitating and hydrostatically pre-stressed body subjected to a small elastic displacement  $\bar{u}$ , the momentum equations are given by:

$$\begin{aligned} \rho \bar{a} = \rho_0 \bar{u}_{,tt} &= \bar{\nabla} \cdot \bar{\sigma}_1 + \rho_0 \bar{\nabla}(\bar{u} \cdot \bar{g}_0) + (\bar{u} \cdot \bar{g}_0) \bar{\nabla} \rho_0 + \rho_0 \bar{g}_1 - \\ &(\rho_0 \Delta + \bar{u} \cdot \bar{\nabla} \rho_0) \bar{g}_0, \end{aligned} \quad (5.6)$$



where  $\bar{\bar{\sigma}}_1$  represents the perturbation to the stress field due to the deformation,  $\rho_0$  represents the equilibrium density of the unperturbed medium,  $\bar{g}_0$  represents the equilibrium gravity of the unperturbed medium, and  $\bar{g}_1$  represents the perturbation in gravity due to the perturbation in the gravitational potential (e.g., Alterman et al., 1959; Longman, 1962; Lapwood & Usami, 1981; Lanzano, 1982; Sabadini & Vermeersen, 2004; Smylie, 2013).

We define the displacement vector  $\bar{u}$  as (e.g., Alterman et al., 1959):

$$\begin{aligned} u_r &= u \\ u_\theta &= v \\ u_\phi &= w. \end{aligned} \tag{5.7}$$

Assuming that the vertical load is at the pole, it follows that the deformation is symmetric about  $\theta = 0$  and the  $\phi$  component of the equations of motion will be zero (e.g., Longman, 1962). Thus, we expand the momentum equations for displacements only in the directions of  $\hat{r}$  ( $u_r = u$ ) and  $\hat{\theta}$  ( $u_\theta = v$ ).

In spherical coordinates, the momentum equations become:

$$\begin{aligned} \rho_0 \frac{\partial^2 u}{\partial t^2} &= \frac{\partial}{\partial r} \sigma_{rr} + \frac{1}{r} \frac{\partial}{\partial \theta} \sigma_{r\theta} + \frac{1}{r} [2\sigma_{rr} - \sigma_{\theta\theta} - \sigma_{\phi\phi} + \cot \theta \sigma_{r\theta}] - \\ &\quad \rho_0 \frac{\partial(g_0 u)}{\partial r} + \rho_0 \frac{\partial \psi}{\partial r} + \rho_0 g_0 \Delta \\ \rho_0 \frac{\partial^2 v}{\partial t^2} &= \frac{\partial}{\partial r} \sigma_{r\theta} + \frac{1}{r} \frac{\partial}{\partial \theta} \sigma_{\theta\theta} + \frac{1}{r} [(\sigma_{\theta\theta} - \sigma_{\phi\phi}) \cot \theta + 3\sigma_{r\theta}] + \\ &\quad \frac{\rho_0}{r} \frac{\partial \psi}{\partial \theta} - \rho_0 g_0 \frac{1}{r} \frac{\partial u}{\partial \theta}, \end{aligned} \tag{5.8}$$

where positive  $\hat{r}$  is directed outward normal to the surface, positive  $\hat{\theta}$  is directed outward from the load point, and  $\psi$  represents the perturbation to the gravitational potential. We have assumed radial forcing, which implies only spheroidal deformation, though we have not yet made any assumptions about a constitutive law. The Eqs. 5.8 are general to spheroidal deformation and may be used for multiple applications, including Earth's free oscillations, Earth's response to external gravitational potentials, and Earth's response to surface mass loading. The distinction between the different applications enters only through the boundary conditions applied at the surface, as we will discuss later on.

### 5.2.3 Linear Elastic Constitutive Relation

In the small-strain approximation, the strain tensor may be related to displacements by:

$$\bar{\epsilon} = \frac{1}{2} ((\nabla \bar{u})^T + (\nabla \bar{u})), \quad (5.9)$$

or in indicial notation by:

$$\epsilon_{ij} = \frac{1}{2} (u_{i,j} + u_{j,i}). \quad (5.10)$$

For linear elasticity, the constitutive relation is given by:

$$\sigma_{ij} = \mathbb{C}_{ijkl} \epsilon_{kl}, \quad (5.11)$$

where  $\mathbb{C}_{ijkl}$  represents the elasticity modulus (or *stiffness tensor*), which is a tensor of fourth-order. Eq. 5.11 is also known as Hooke's Law. For isotropic materials, the elasticity modulus reduces to:

$$\mathbb{C}_{ijkl} = \lambda \delta_{ij} \delta_{kl} + \mu (\delta_{ik} \delta_{jl} + \delta_{il} \delta_{jk}), \quad (5.12)$$

where  $\lambda$  and  $\mu$  are Lamé's constants, which are related to compressional ( $P$ ) and shear ( $S$ ) sound-wave velocities by:

$$V_P^2 = \frac{\lambda + 2\mu}{\rho} \quad (5.13)$$

$$V_S^2 = \frac{\mu}{\rho}. \quad (5.14)$$

Thus, for linear elastic and isotropic materials, the constitutive relation is given by (Eqs. 5.11 and 5.12):

$$\sigma_{ij} = \lambda \epsilon_{kk} \delta_{ij} + 2\mu \epsilon_{ij}. \quad (5.15)$$

In spherical coordinates, the components of the stress tensor,  $\bar{\bar{\sigma}}_1$ , arising from the material deformation (without the hydrostatic pre-stress terms) are given by (e.g., Takeuchi, 1966; Lapwood & Usami, 1981):

$$\sigma_{rr} = \lambda \Delta + 2\mu \epsilon_{rr} \quad (5.16)$$

$$\sigma_{\theta\theta} = \lambda \Delta + 2\mu \epsilon_{\theta\theta} \quad (5.17)$$

$$\sigma_{\phi\phi} = \lambda \Delta + 2\mu \epsilon_{\phi\phi} \quad (5.18)$$

$$\sigma_{r\theta} = 2\mu \epsilon_{r\theta} \quad (5.19)$$

$$\sigma_{r\phi} = 2\mu \epsilon_{r\phi} \quad (5.20)$$

$$\sigma_{\theta\phi} = 2\mu \epsilon_{\theta\phi}, \quad (5.21)$$

where

$$\epsilon_{rr} = \frac{\partial u}{\partial r} \quad (5.22)$$

$$\epsilon_{\theta\theta} = \left( \frac{1}{r} \frac{\partial v}{\partial \theta} + \frac{u}{r} \right) \quad (5.23)$$

$$\epsilon_{\phi\phi} = \left( \frac{1}{r \sin \theta} \frac{\partial w}{\partial \phi} + \frac{v}{r} \cot \theta + \frac{u}{r} \right) \quad (5.24)$$

$$\epsilon_{r\theta} = \left( \frac{1}{2} \frac{\partial v}{\partial r} - \frac{v}{2r} + \frac{1}{2r} \frac{\partial u}{\partial \theta} \right) \quad (5.25)$$

$$\epsilon_{r\phi} = \left( \frac{1}{2} \frac{1}{r \sin \theta} \frac{\partial u}{\partial \phi} + \frac{1}{2} \frac{\partial w}{\partial r} - \frac{w}{2r} \right) \quad (5.26)$$

$$\epsilon_{\theta\phi} = \left[ \frac{1}{2r} \left( \frac{\partial w}{\partial \theta} - w \cot \theta \right) + \frac{1}{2r \sin \theta} \frac{\partial v}{\partial \phi} \right]. \quad (5.27)$$

Thus, both elastic and gravitational restoring forces contribute to the deformation response. Note that definitions of the shear strain can differ by a factor of two in the literature, which must then be reflected consistently in the equations of motion (e.g., Alterman et al., 1959; Longman, 1962).

Inserting the constitutive relations into the equations of motion yields:

$$\begin{aligned} \rho_0 \frac{\partial^2 u}{\partial t^2} &= \frac{\partial}{\partial r} \left( \lambda \Delta + 2\mu \frac{\partial u}{\partial r} \right) + \frac{2\mu}{r} \frac{\partial \left( \frac{1}{2} \frac{\partial v}{\partial r} - \frac{v}{2r} + \frac{1}{2r} \frac{\partial u}{\partial \theta} \right)}{\partial \theta} + \\ &\quad \frac{2\mu}{r} \left[ 2 \frac{\partial u}{\partial r} - \frac{1}{r} \frac{\partial v}{\partial \theta} - \frac{2u}{r} + \cot \theta \left( \frac{1}{2} \frac{\partial v}{\partial r} - \frac{3v}{2r} + \frac{1}{2r} \frac{\partial u}{\partial \theta} \right) \right] - \\ &\quad \rho_0 \frac{\partial(g_0 u)}{\partial r} + \rho_0 \frac{\partial \psi}{\partial r} + \rho_0 g_0 \Delta \\ \rho_0 \frac{\partial^2 v}{\partial t^2} &= 2 \frac{\partial}{\partial r} \left( \mu \left( \frac{1}{2} \frac{\partial v}{\partial r} - \frac{v}{2r} + \frac{1}{2r} \frac{\partial u}{\partial \theta} \right) \right) + \frac{1}{r} \frac{\partial}{\partial \theta} \left( \lambda \Delta + 2\mu \left( \frac{1}{r} \frac{\partial v}{\partial \theta} + \frac{u}{r} \right) \right) + \\ &\quad \frac{2\mu}{r} \left[ \left( \frac{1}{r} \frac{\partial v}{\partial \theta} - \frac{v}{r} \cot \theta \right) \cot \theta + 3 \left( \frac{1}{2} \frac{\partial v}{\partial r} - \frac{v}{2r} + \frac{1}{2r} \frac{\partial u}{\partial \theta} \right) \right] + \\ &\quad \frac{\rho_0}{r} \frac{\partial \psi}{\partial \theta} - \rho_0 g_0 \frac{1}{r} \frac{\partial u}{\partial \theta}, \end{aligned} \quad (5.28)$$

where we have allowed for radial heterogeneity in the density and elastic moduli.

#### 5.2.4 Solutions to the Equations of Motion

The spheroidal-deformation Eqs. 5.28 for a self-gravitating, radially heterogeneous Earth may be satisfied by solutions of the form (e.g., Alterman et al., 1959; Longman, 1962):

$$\begin{aligned} u_n &= U_n(r) P_n(\cos \theta) e^{i\omega t} \\ v_n &= V_n(r) \frac{\partial P_n(\cos \theta)}{\partial \theta} e^{i\omega t} \\ \psi_n &= \Psi_n(r) P_n(\cos \theta) e^{i\omega t}, \end{aligned} \quad (5.29)$$

where  $U(r)$ ,  $V(r)$ , and  $\Psi(r)$  are radial coefficients of the spherical harmonic expansions,  $P_n(\cos \theta)$  is a Legendre polynomial of order  $n$ ,  $u$  represents the radial displacement (Eq. 5.7),  $v$  represents the horizontal displacement (Eq. 5.7), and  $\psi$  represents the perturbation to the gravitational potential field caused by the deformation (e.g. Alterman et al., 1959; Longman, 1962; Sabadini & Vermeersen, 2004; Smylie, 2013). For periodic forcing, such as loading by the ocean tides,  $\omega$  represents the frequency of the forcing.

Since tides exhibit periods much longer than the free oscillations of the Earth ( $\sim 1$  hour), a quasi-static formulation of the equations of motion is sometimes adopted (e.g., Longman, 1962; Takeuchi, 1966; Farrell, 1972; Guo et al., 2004). For static or quasi-static formulations,  $\omega = 0$ , and temporal variations in the loading are removed from the problem. For the static case, additional considerations must be made for fluid regions (e.g. Longman, 1963; Chinnery, 1975). Since the divergence of the stress tensor must balance the sum of all forces, the static equations are referred to as the equilibrium equations (e.g., Longman, 1962). To maintain generality and consistency through fluid regions, we retain the time-varying factors in the development of the deformation solution (e.g., Alterman et al., 1959; Lapwood & Usami, 1981; Na & Baek, 2011).

The dilatation,  $\Delta$ , may be written as:

$$\begin{aligned} \Delta &= \epsilon_{rr} + \epsilon_{\theta\theta} + \epsilon_{\phi\phi} \\ &= X(r) P_n(\cos \theta) e^{i\omega t}, \end{aligned} \quad (5.30)$$

where

$$X(r) = \dot{U} + \frac{2U}{r} - \frac{n(n+1)}{r}V, \quad (5.31)$$

and we have made use of the Legendre differential equation (e.g., Boas, 1983). A dot implies differentiation with respect to  $r$ .

From the set of Eqs. 5.29:

$$\begin{aligned} \frac{\partial u}{\partial \theta} &= -U \sin \theta P'_n e^{i\omega t} \\ \frac{\partial v}{\partial \theta} &= V \sin^2 \theta P''_n e^{i\omega t} - V \cos \theta P'_n e^{i\omega t} \\ \frac{\partial u}{\partial r} &= \dot{U} P_n e^{i\omega t} \\ \frac{\partial v}{\partial r} &= -\dot{V} \sin \theta P'_n e^{i\omega t} \\ \frac{\partial^2 u}{\partial \theta^2} &= U \sin^2 \theta P''_n e^{i\omega t} - U \cos \theta P'_n e^{i\omega t} \\ \frac{\partial^2 v}{\partial \theta^2} &= \frac{\partial}{\partial \theta} [V \sin^2 \theta P''_n - V \cos \theta P'_n] e^{i\omega t} \\ &= V [-\sin^3 \theta P'''_n + 3P''_n \sin \theta \cos \theta + \sin \theta P'_n] e^{i\omega t}, \end{aligned} \quad (5.32)$$

where

$$P'_n = \frac{\partial P_n(\cos \theta)}{\partial \cos \theta}, P''_n = \frac{\partial^2 P_n(\cos \theta)}{\partial \cos^2 \theta}, P'''_n = \frac{\partial^3 P_n(\cos \theta)}{\partial \cos^3 \theta}, \quad (5.33)$$

and, according to the Legendre differential equation (Boas, 1983),

$$\sin^2 \theta P''_n - 2 \cos \theta P'_n = -n(n+1)P_n. \quad (5.34)$$

Only  $P_n$  and  $P'_n$  are required to derive additional derivatives of the Legendre polynomials recursively. For example, the third derivative of the Legendre polynomial,  $P'''_n$ , is given by:

$$\begin{aligned} 0 &= \frac{\partial}{\partial \cos \theta} [(1 - \cos^2 \theta) P''_n - 2 \cos \theta P'_n + n(n+1)P_n] \\ &= P'''_n - 2 \cos \theta P''_n - \cos^2 \theta P'''_n - 2P'_n - 2 \cos \theta P''_n + n(n+1)P'_n \\ &= (1 - \cos^2 \theta) P'''_n - 4 \cos \theta P''_n + (-2 + n(n+1))P'_n \\ &= \sin^2 \theta P'''_n - 4 \cos \theta P''_n - (2 - n(n+1))P'_n \end{aligned}$$

$$\sin^2 \theta P_n''' = 4 \cos \theta P_n'' + 2P_n' - n(n+1)P_n'. \quad (5.35)$$

Rewriting the radial component of Eq. 5.28, we have:

$$\begin{aligned} \rho_0 \frac{\partial^2 u}{\partial t^2} &= \left\{ \frac{\partial}{\partial r} \left( \lambda X + 2\mu \dot{U} \right) + \dot{V} \frac{\mu}{r} (-n(n+1)) + U \frac{\mu}{r^2} (-n(n+1)) + \right. \\ &\quad \left. \frac{\mu}{r^2} [4r\dot{U} - 3V(-n(n+1)) - 4U] - \rho_0 \frac{\partial(g_0 U)}{\partial r} + \rho_0 \dot{\Psi} + \rho_0 g_0 X \right\} P_n(\cos \theta) e^{i\omega t} \\ -\omega^2 \rho_0 U &= \frac{\partial}{\partial r} \left( \lambda X + 2\mu \dot{U} \right) + \frac{\mu}{r^2} [4r\dot{U} - 4U + n(n+1)(3V - U - r\dot{V})] - \\ &\quad \rho_0 \frac{\partial(g_0 U)}{\partial r} + \rho_0 \dot{\Psi} + \rho_0 g_0 X, \end{aligned} \quad (5.36)$$

where common terms in  $e^{i\omega t}$  and  $P_n$  have been canceled in the second line (Alterman et al., 1959).

Similarly, the surface-tangential component of Eq. 5.28 may be written as:

$$\begin{aligned} \rho_0 \frac{\partial^2 v}{\partial t^2} &= \left\{ -\sin \theta P_n' \left( \frac{\partial}{\partial r} \left( \mu \dot{V} - \mu \frac{V}{r} + \mu \frac{U}{r} \right) + \frac{\lambda}{r} X \right) + \right. \\ &\quad \frac{\rho_0}{r} \Psi P_n' (-\sin \theta) - \frac{\rho_0 g_0}{r} U P_n' (-\sin \theta) + \\ &\quad \frac{\mu}{r^2} [2V(-\sin \theta P_n' + n(n+1) \sin \theta P_n') + \\ &\quad \left. 5U P_n' (-\sin \theta) - 3V P_n' (-\sin \theta) - 3r\dot{V} \sin \theta P_n'] \right\} e^{i\omega t} \\ -\omega^2 \rho_0 V &= \frac{\partial}{\partial r} \left( \mu \dot{V} - \mu \frac{V}{r} + \mu \frac{U}{r} \right) + \frac{\lambda}{r} X + \frac{\rho_0}{r} \Psi - \frac{\rho_0 g_0}{r} U + \\ &\quad \frac{\mu}{r^2} [5U - V - 2n(n+1)V + 3r\dot{V}], \end{aligned} \quad (5.37)$$

where common terms in  $e^{i\omega t}$  and  $[-\sin \theta P_n']$  have been canceled in the second line (Alterman et al., 1959).

Finally, Poisson's equation may be written as (Alterman et al., 1959):

$$\begin{aligned} \nabla^2 \psi &= 4\pi G \left( \rho_0 \Delta + u \frac{\partial \rho_0}{\partial r} \right) \\ &= \{4\pi G (\rho_0 X + U \dot{\rho}_0)\} P_n(\cos \theta) e^{i\omega t}. \end{aligned} \quad (5.38)$$

We can also write the Laplacian in spherical coordinates as (Alterman et al., 1959):

$$\nabla^2 \psi = \left\{ \frac{2}{r} \dot{\Psi} + \ddot{\Psi} - \frac{n(n+1)}{r^2} \Psi \right\} P_n(\cos \theta) e^{i\omega t}, \quad (5.39)$$

where

$$\begin{aligned}\frac{\partial \psi}{\partial \theta} &= -\sin \theta \Psi P'_n e^{i\omega t} \\ \frac{\partial^2 \psi}{\partial \theta^2} &= \Psi [\sin^2 \theta P''_n - \cos \theta P'_n] e^{i\omega t}.\end{aligned}$$

Combining Eq. 5.38 with Eq. 5.39 yields (Alterman et al., 1959):

$$\ddot{\Psi} + \frac{2}{r} \dot{\Psi} - \frac{n(n+1)}{r^2} \Psi = 4\pi G (\rho_0 X + U \dot{\rho}_0), \quad (5.40)$$

where we have canceled common factors of  $e^{i\omega t}$  and  $P_n$ .

The equations of motion for spheroidal deformation are now given by three second-order differential equations (Eqs. 5.36, 5.37, and 5.40) that may be solved for the coefficients  $U$ ,  $V$ , and  $\Psi$ .

### 5.2.5 Reduction of the Equations of Motion to First Order

For convenience, a set of handy substitutions may be made to simplify Eqs. 5.36, 5.37, and 5.40 prior to numerical integration (e.g., Alterman et al., 1959; Longman, 1962; Melchior, 1983, Ch. 5):

$$\begin{aligned}y_1 &= U \\ y_2 &= \lambda X + 2\mu \dot{U} \\ y_3 &= V \\ y_4 &= \mu \left( \dot{V} - \frac{V}{r} + \frac{U}{r} \right) \\ y_5 &= \Psi \\ y_6 &= \dot{\Psi} - 4\pi G \rho_0 U.\end{aligned} \quad (5.41)$$

With the substitutions, Eqs. 5.36, 5.37, and 5.40 become a system of six first-order differential equations (e.g. Alterman et al., 1959):

$$\begin{aligned}\dot{y}_1 &= \frac{-2\lambda}{\lambda + 2\mu} \frac{y_1}{r} + \frac{y_2}{\lambda + 2\mu} + \frac{\lambda n(n+1)}{\lambda + 2\mu} \frac{y_3}{r}, \\ \dot{y}_2 &= \left[ -\omega^2 \rho_0 r^2 - 4\rho_0 g_0 r + \frac{4\mu(3\lambda + 2\mu)}{\lambda + 2\mu} \right] \frac{y_1}{r^2} - \frac{4\mu}{\lambda + 2\mu} \frac{y_2}{r}\end{aligned}$$

$$\begin{aligned}
& + \left[ n(n+1)\rho_0 g_0 r - \frac{2\mu(3\lambda+2\mu)n(n+1)}{\lambda+2\mu} \right] \frac{y_3}{r^2} \\
& + n(n+1) \frac{y_4}{r} - \rho_0 y_6, \\
\dot{y}_3 &= -\frac{y_1}{r} + \frac{y_3}{r} + \frac{y_4}{\mu}, \\
\dot{y}_4 &= \left[ g_0 \rho_0 r - \frac{2\mu(3\lambda+2\mu)}{\lambda+2\mu} \right] \frac{y_1}{r^2} - \frac{\lambda}{\lambda+2\mu} \frac{y_2}{r} \\
& + \left[ -\omega^2 \rho_0 r^2 + \frac{2\mu}{\lambda+2\mu} [\lambda(2n^2+2n-1) + 2\mu(n^2+n-1)] \right] \frac{y_3}{r^2} \\
& - \frac{3y_4}{r} - \rho_0 \frac{y_5}{r}, \\
\dot{y}_5 &= 4\pi G \rho_0 y_1 + y_6, \\
\dot{y}_6 &= -4\pi G \rho_0 n(n+1) \frac{y_3}{r} + n(n+1) \frac{y_5}{r^2} - \frac{2y_6}{r}, \tag{5.42}
\end{aligned}$$

where dots represent differentiation with respect to  $r$ . Importantly, by reducing the equations of motion to first order, the derivatives of the elastic parameters no longer appear. The variables  $y_1$  and  $y_3$  characterize the radial and tangential displacements, respectively;  $y_2$  and  $y_4$  characterize the radial and tangential stress, respectively;  $y_5$  characterizes the gravitational potential; and the equation for  $\dot{y}_5$  defines  $y_6$ . Additional information about the equations of motion for spheroidal oscillations may be found in the literature (e.g., Takeuchi & Saito, 1972; Lapwood & Usami, 1981; Guo et al., 2004; Smylie, 2013).

Note that the six linear equations may now be written in the form  $\dot{y} = A y$ :

$$\begin{bmatrix} \frac{dy_1}{dr} \\ \frac{dy_2}{dr} \\ \frac{dy_3}{dr} \\ \frac{dy_4}{dr} \\ \frac{dy_5}{dr} \\ \frac{dy_6}{dr} \end{bmatrix} = \begin{bmatrix} -\frac{2\lambda\xi}{r} & \xi & \frac{k^2\lambda\xi}{r} & 0 & 0 & 0 \\ \left(-\omega^2\rho_0 - \frac{4g_0\rho_0}{r} + \frac{2\delta}{r^2}\right) & -\frac{4\mu\xi}{r} & \left(\frac{k^2g_0\rho_0}{r} - \frac{k^2\delta}{r^2}\right) & \frac{k^2}{r} & 0 & -\rho_0 \\ -\frac{1}{r} & 0 & \frac{1}{r} & \frac{1}{\mu} & 0 & 0 \\ \left(\frac{g_0\rho_0}{r} - \frac{\delta}{r^2}\right) & -\frac{\lambda\xi}{r} & \left(-\omega^2\rho_0 + \frac{\epsilon}{r^2}\right) & -\frac{3}{r} & -\frac{\rho_0}{r} & 0 \\ 4\pi G\rho_0 & 0 & 0 & 0 & 0 & 1 \\ 0 & 0 & -4\pi G\rho_0 \frac{k^2}{r} & 0 & \frac{k^2}{r^2} & -\frac{2}{r} \end{bmatrix} \begin{bmatrix} y_1 \\ y_2 \\ y_3 \\ y_4 \\ y_5 \\ y_6 \end{bmatrix}, \tag{5.43}$$

where

$$k^2 = n(n+1) \tag{5.44}$$

$$\xi = \frac{1}{\lambda+2\mu} \tag{5.45}$$



$$\delta = 2\mu(3\lambda + 2\mu)\xi \quad (5.46)$$

$$\epsilon = 4k^2\mu(\lambda + \mu)\xi - 2\mu. \quad (5.47)$$

The matrix equation,  $\dot{y} = A y$ , may be solved using numerical methods, such as the commonly adopted Runge-Kutta algorithm and the propagator matrix technique (Sec. 5.2.9) (Gilbert & Backus, 1966) .

For the special case of  $n = 0$ , the equations for  $y_3$  and  $y_4$  are undefined and the system reduces to (e.g., Smylie, 2013):

$$\begin{bmatrix} \frac{dy_1}{dr} \\ \frac{dy_2}{dr} \\ \frac{dy_5}{dr} \\ \frac{dy_6}{dr} \end{bmatrix} = \begin{bmatrix} -\frac{2\lambda\xi}{r} & \xi & 0 & 0 \\ \left(-\omega^2\rho_0 - \frac{4g_0\rho_0}{r} + \frac{2\delta}{r^2}\right) & -\frac{4\mu\xi}{r} & 0 & -\rho_0 \\ 4\pi G\rho_0 & 0 & 0 & 1 \\ 0 & 0 & 0 & -\frac{2}{r} \end{bmatrix} \begin{bmatrix} y_1 \\ y_2 \\ y_5 \\ y_6 \end{bmatrix}. \quad (5.48)$$

### 5.2.6 Non-dimensionalization

Suitable scaling parameters must be introduced to maintain numerical stability during the integration of the equations of motion (e.g., Longman, 1962; Crossley, 1975). We adopt a characteristic length scale,  $a$ , equal to Earth's mean radius (6371 km) and a characteristic mass scale close to Earth's mass,  $4\pi a^3 \bar{\rho}/3$ , where  $\bar{\rho}$  is an approximate value for Earth's average density (5500 kg/m<sup>3</sup>). A handy way of scaling the time is to define the characteristic time scale as  $1/\sqrt{\pi G \bar{\rho}}$ , where  $G$  is the universal gravitational constant. Since  $G$  has units of  $[M^{-1}L^3T^{-2}]$ , it becomes

$$G' = G/(\bar{\rho}^{-1}a^{-3}\pi G\bar{\rho}) = 1/\pi \quad (5.49)$$

in the scaled system.  $M$ ,  $L$ , and  $T$  represent units of mass, length, and time, respectively.

In summary, we have

Length :

$$l' = l/a \quad (5.50)$$

Mass :

$$m' = m/(4\pi\bar{\rho}a^3/3) \quad (5.51)$$

Time :

$$t' = t\sqrt{\pi G \bar{\rho}} \quad (5.52)$$

Another way of stating the above mass scaling is simply to say that we adopt a characteristic density scale equal to  $\bar{\rho}$ , where

$$\rho' = \rho/\bar{\rho}. \quad (5.53)$$

### 5.2.7 Starting Solutions: Power Series Expansion

The six first-order ordinary differential equations (Eq. 5.42) require six sets of starting solutions to initialize the Runge-Kutta integration. Three of the functions,  $y_1$ ,  $y_3$ , and  $y_5$ , diverge at  $r = 0$ ; thus, the starting solutions for  $U$  ( $= y_1$ ),  $V$  ( $= y_3$ ), and  $\Psi$  ( $= y_5$ ) are necessarily set to zero to ensure regularity at Earth's center (e.g., Crossley, 1975; Wu & Peltier, 1982). The remaining three linearly independent solutions at Earth's center may be computed by a power series expansion near the geocenter (Crossley, 1975; Smylie, 2013). Following the development of Crossley (1975) and Smylie (2013), the power series expansion of the  $y$  variables takes the form:

$$y_i(r) = r^\alpha \sum_{\nu=0}^{\infty} A_{i,\nu} r^\nu, \quad i = 1, 2, \dots, 6, \quad (5.54)$$

where  $\alpha$  and  $\nu$  are integers and the coefficients  $A_{i,\nu}$  are to be determined. The variable  $\alpha$  must be non-negative and the coefficients  $A_{i,\nu} = 0$  for  $\nu < 0$ . The derivate of Eq. 5.54 is given by (Crossley, 1975):

$$\frac{dy_i(r)}{dr} = r^{\alpha-1} \sum_{\nu=0}^{\infty} (\alpha + \nu) A_{i,\nu} r^\nu. \quad (5.55)$$

Additionally, gravity can be expanded as:

$$g_0(r) = \gamma r, \quad (5.56)$$

where terms beyond first-order have been dropped since the expansion will be implemented close to the geocenter, and

$$\gamma = \frac{4}{3}\pi G \rho_0. \quad (5.57)$$

Within an arbitrarily small radius, such as  $r = 1$  km, the density and elastic moduli are assumed to be constant and equivalent to their values at the geocenter.

Eqs. 5.54, 5.55, and 5.56 are inserted back into the system of equations (Eq. 5.42). Matching powers of the radius are equated to obtain a set of characteristic, or *indicial*, equations. Eigenvalues of the characteristic equations yield the acceptable values for variable  $\alpha$ , and the corresponding eigenvectors may then be used to compute the values of the coefficients  $A_{i,\nu}$  in terms of three free constants:  $A_{1,1}$ ,  $A_{6,1}$ , and  $A_{4,0}$  (Smylie, 2013). Choice of the free constants is arbitrary, since multiplying each of the  $y$  variables in a fundamental-solution set by the same constant factor does not affect the result; only ratios between the  $y$  variables are important. A convenient option is to set each of the three constants equal to one.

To facilitate numerical integration, we transform the variables (e.g., Smylie, 2013; Crossley, 1975):

$$\begin{aligned}
 z_1(r) &= \frac{y_1(r)}{r^{\alpha+1}} \\
 z_2(r) &= \frac{y_2(r)}{r^{\alpha}} \\
 z_3(r) &= \frac{y_3(r)}{r^{\alpha+1}} \\
 z_4(r) &= \frac{y_4(r)}{r^{\alpha}} \\
 z_5(r) &= \frac{y_5(r)}{r^{\alpha+2}} \\
 z_6(r) &= \frac{y_6(r)}{r^{\alpha+1}},
 \end{aligned} \tag{5.58}$$

where  $\alpha = n - 2$  for the starting solutions associated with the free constants  $A_{1,1}$  and  $A_{6,1}$  and  $\alpha = n$  for the starting solution associated with the free constant  $A_{4,0}$ . Appropriate modifications must be made for the special cases of  $n = 1$  and  $n = 0$  (Smylie, 2013). For  $n = 0$ , only two starting solutions are regular at the geocenter. More information about the starting solutions and how to compute them may be found in Smylie (2013) and Martens (2016).

### 5.2.8 Starting Solutions: Homogeneous Sphere

An alternative approach to the power series expansions is to compute the analytical solution for a homogeneous sphere (e.g., Farrell, 1972; Takeuchi & Saito, 1972; Lambeck, 1988; Dahlen & Tromp, 1998). Here, we review the analytical solutions of the equations of motion for a homogeneous sphere. Takeuchi & Saito (1972) provide a more comprehensive discussion.

Two of the independent solutions (note the  $\mp$  in the equation for  $b^2$  below) for spherical harmonic degree,

$n$ , and forcing frequency,  $\omega$ , are given by (e.g., Takeuchi & Saito, 1972):

$$\begin{aligned}
y_1 &= -\frac{r^{n+1}}{2n+3} \left[ \frac{1}{2} n h \chi_n(x) + f \phi_{n+1}(x) \right] \\
y_2 &= -(\lambda + 2\mu) r^n f \phi_n(x) + \frac{\mu r^n}{2n+3} [-n(n+1) h \chi_n(x) + 2(2f + k^2) \phi_{n+1}(x)] \\
y_3 &= -\frac{r^{n+1}}{2n+3} \left[ \frac{1}{2} h \chi_n(x) - \phi_{n+1}(x) \right] \\
y_4 &= \mu r^n \left[ \phi_n(x) - \frac{1}{2n+3} [(n-1) h \chi_n(x) + 2(f+1) \phi_{n+1}(x)] \right] \\
y_5 &= r^{n+2} \left[ \frac{V_P^2 f - (n+1) V_S^2}{r^2} - \frac{3\gamma f}{2(2n+3)} \chi_n(x) \right] \\
y_6 &= \frac{1}{r} \left[ (2n+1) y_5 + \frac{3n\gamma h r^{n+2}}{2(2n+3)} \chi_n(x) \right], \tag{5.59}
\end{aligned}$$

where  $V_P$  is the compressional wave velocity,  $V_S$  is the shear wave velocity,  $r$  is the radius,  $\lambda$  and  $\mu$  are Lamé parameters, and

$$\begin{aligned}
\gamma &= \frac{4}{3} \pi \rho G \\
x &= b r \\
b^2 &= \frac{1}{2} \left[ \frac{\omega^2 + 4\gamma}{V_P^2} + \frac{\omega^2}{V_S^2} \mp \left( \left( \frac{\omega^2}{V_S^2} - \frac{\omega^2 + 4\gamma}{V_P^2} \right)^2 + \frac{4k^2 \gamma^2}{V_P^2 V_S^2} \right)^{\frac{1}{2}} \right] \\
f &= \frac{V_S^2}{\gamma} \left( b^2 - \frac{\omega^2}{V_S^2} \right) \\
h &= f - (n+1). \tag{5.60}
\end{aligned}$$

Furthermore,

$$\begin{aligned}
\phi_n(x) &= \frac{(2n+1)!!}{x^n} j_n(x) \\
&= 1 - \frac{x^2}{2(2n+3)} + \frac{x^4}{2^2(2n+3)(2n+5)2} - \dots \tag{5.61}
\end{aligned}$$

$$\begin{aligned}
\chi_n(x) &= \frac{2(2n+3)}{x^2} [1 - \phi_n(x)] \\
&= 1 - \frac{x^2}{2(2n+5)2} + \frac{x^4}{2^2(2n+5)(2n+7)3} - \dots \tag{5.62}
\end{aligned}$$

where  $j_n(x)$  represents the spherical Bessel function of the first kind (e.g., Abramowitz & Stegun, 1964; Takeuchi & Saito, 1972). Since the Bessel functions tend toward zero at high  $n$ , we approximate them using

the power series expansions given by Eqs. 5.61 and 5.62, carried out to several terms.

The third independent solution is given by (e.g., Takeuchi & Saito, 1972):

$$\begin{aligned}
y_1 &= nr^{n-1} \\
y_2 &= 2\mu n(n-1)r^{n-2} \\
y_3 &= r^{n-1} \\
y_4 &= 2\mu(n-1)r^{n-2} \\
y_5 &= (n\gamma - \omega^2)r^n \\
y_6 &= \frac{1}{r}(2n+1)y_5(r) - 3n\gamma r^{n-1}.
\end{aligned} \tag{5.63}$$

### 5.2.9 Runge-Kutta Integration

We integrate the equations of motion from depth to Earth's surface using Runge-Kutta algorithms that are part of the `scipy` library. The starting radius for the integration can affect the numerical stability of the solution. `LoadDef` determines the starting radius for the integration based on the decaying influence of an external potential field with depth for any given harmonic (see Sec. 5.2.18). In practice, we have found that commencing the integration from Earth's center is appropriate for  $n < \text{about } 20$ , after which numerical stability may be improved by starting the integration within the mantle. For integrations that start at Earth's center and move through the core, `LoadDef` uses starting solutions computed from power series expansions with transformed  $z$  variables (Smylie, 2013). For integrations that start in the mantle, `LoadDef` uses starting solutions computed for a homogeneous sphere (Takeuchi & Saito, 1972).

From a set of starting solutions  $y_j(r_i)$  (or  $z_j(r_i)$  within the inner core) at an initial radius  $r_i$ , the solution vector  $y_j(r_{i+1})$  at the new radius  $r_i + h$  is given by:

$$y_j(r_{i+1}) = y_j(r_i) + \frac{h}{6}(k_{1j} + 2k_{2j} + 2k_{3j} + k_{4j}), \tag{5.64}$$

where  $h$  represents a suitably small step in radius,  $j = 1 \cdots 6$  for each of the six solutions to the system of six linear equations for spheroidal deformation (Eqs. 5.41), and

$$k_{1j} = A_{jl}(r_i) y_l(r_i) \tag{5.65}$$

$$k_{2j} = A_{jl} \left( r_i + \frac{h}{2} \right) \left[ y_l(r_i) + \frac{k_{1l}}{2} \right] \quad (5.66)$$

$$k_{3j} = A_{jl} \left( r_i + \frac{h}{2} \right) \left[ y_l(r_i) + \frac{k_{2l}}{2} \right] \quad (5.67)$$

$$k_{4j} = A_{jl}(r_i + h) [y_l(r_i) + k_{3l}]. \quad (5.68)$$

$A_{jl}$  is given by Eq. 5.43. The fourth-order Runge-Kutta formulation in Eq. 5.64 is derived from a Taylor series expansion of  $\dot{y}$ . The system of equations,  $\dot{y}$ , may be computed at each radial step using the propagator matrix technique (i.e.,  $\dot{y} = A y$ , as in Eqs. 5.65–5.68) (Gilbert & Backus, 1966).

### 5.2.10 Fluid Layers

In fluid regions, the shear modulus vanishes ( $\mu = 0$ ). Hence  $y_4 = 0$ ,  $y_2 = \lambda X$ , and  $\dot{y}_3$  is undefined (Alterman et al., 1959). Therefore, the system of equations for spheroidal deformation reduces to (e.g., Smylie, 2013):

$$\begin{bmatrix} \frac{dy_1}{dr} \\ \frac{dy_2}{dr} \\ 0 \\ \frac{dy_5}{dr} \\ \frac{dy_6}{dr} \end{bmatrix} = \begin{bmatrix} -\frac{2}{r} & \frac{1}{\lambda} & \frac{k^2}{r} & 0 & 0 \\ \left( -\omega^2 \rho_0 - \frac{4g_0 \rho_0}{r} \right) & 0 & \frac{k^2 g_0 \rho_0}{r} & 0 & -\rho_0 \\ \frac{g_0 \rho_0}{r} & -\frac{1}{r} & -\omega^2 \rho_0 & -\frac{\rho_0}{r} & 0 \\ 4\pi G \rho_0 & 0 & 0 & 0 & 1 \\ 0 & 0 & -4\pi G \rho_0 \frac{k^2}{r} & \frac{k^2}{r^2} & -\frac{2}{r} \end{bmatrix} \begin{bmatrix} y_1 \\ y_2 \\ y_3 \\ y_5 \\ y_6 \end{bmatrix}.$$

The third equation in the system can be solved for  $y_3$  as follows (Alterman et al., 1959):

$$\begin{aligned} 0 &= \frac{\rho_0 g_0}{r} y_1 - \frac{1}{r} y_2 - \omega^2 \rho_0 y_3 - \frac{\rho_0}{r} y_5 \\ \omega^2 \rho_0 y_3 &= \frac{\rho_0 g_0}{r} y_1 - \frac{1}{r} y_2 - \frac{\rho_0}{r} y_5 \\ y_3 &= \frac{1}{\omega^2 \rho_0} \left( \frac{\rho_0 g_0}{r} y_1 - \frac{1}{r} y_2 - \frac{\rho_0}{r} y_5 \right) \\ y_3 &= \frac{1}{\omega^2 r} \left( g_0 y_1 - \frac{1}{\rho_0} y_2 - y_5 \right). \end{aligned} \quad (5.69)$$

Note that, with  $\omega$  in the denominator, the zero-frequency case is problematic for fluid layers (e.g. Longman, 1963).

The equation for  $y_3$  is now written in terms of  $y_1$ ,  $y_2$ , and  $y_5$ , so it may be substituted back into the matrix

system, which reduces to:

$$\begin{bmatrix} \frac{dy_1}{dr} \\ \frac{dy_2}{dr} \\ \frac{dy_5}{dr} \\ \frac{dy_6}{dr} \end{bmatrix} = \begin{bmatrix} -\frac{2}{r} + \frac{k^2}{r} y_3^1 & \frac{1}{\lambda} + \frac{k^2}{r} y_3^2 & \frac{k^2}{r} y_3^5 & 0 \\ \left( -\omega^2 \rho_0 - \frac{4g_0 \rho_0}{r} + \frac{k^2 g_0 \rho_0}{r} y_3^1 \right) & \frac{k^2 g_0 \rho_0}{r} y_3^2 & \frac{k^2 g_0 \rho_0}{r} y_3^5 & -\rho_0 \\ 4\pi G \rho_0 & 0 & 0 & 1 \\ -4\pi G \rho_0 \frac{k^2}{r} y_3^1 & -4\pi G \rho_0 \frac{k^2}{r} y_3^2 & \left( \frac{k^2}{r^2} - 4\pi G \rho_0 \frac{k^2}{r} y_3^5 \right) & -\frac{2}{r} \end{bmatrix} \begin{bmatrix} y_1 \\ y_2 \\ y_5 \\ y_6 \end{bmatrix},$$

where

$$\begin{aligned} y_3^1 &= \frac{g_0}{\omega^2 r} \\ y_3^2 &= -\frac{1}{\rho_0 \omega^2 r} \\ y_3^5 &= -\frac{1}{\omega^2 r}. \end{aligned} \tag{5.70}$$

### 5.2.11 Boundary Conditions at Solid-Fluid Interfaces

All independent variables  $y_1, y_2, \dots, y_6$  are continuous at solid-solid internal boundaries (e.g., Alterman et al., 1959; Takeuchi & Saito, 1972; Guo et al., 2004). At solid-fluid boundaries, however, the shear stress vanishes; thus, all  $y$  variables are continuous with the exception of  $y_3$ , which is undefined across the interface. The system of six first-order ODEs within the solid layer reduces to a system of four first-order ODEs within the fluid layer. Thus, whereas three independent solutions are required for solid layers, only two independent solutions are required for fluid layers. See Takeuchi & Saito (1972) and Martens (2016) for more information on the boundary conditions at solid-fluid interfaces.

### 5.2.12 Surface Boundary Conditions

The surface boundary conditions differ depending on the type of response being investigated, such as Earth's free oscillations, Earth's response to an external gravitational potential, or Earth's response to surface mass loading. For a comprehensive discussion and derivation of the surface boundary conditions for several different response cases, the reader is referred to Martens (2016). Here, we provide an abbreviated summary.

For free oscillations of the Earth, the absence of an applied load requires that the radial and tangential stresses vanish at the surface (e.g., Alterman et al., 1959; Wiggins, 1968; Takeuchi & Saito, 1972). For an

<b>Surface Boundary Conditions (<math>n \neq 1</math>)</b>				
	(a) Free Oscillations	(b) External Potential	(c) Surface Mass Loading	(d) Surface Shear Forcing
$y_2$	0	0	$-g_S^2 \frac{2n+1}{4\pi G}$	0
$y_4$	0	0	0	$\frac{(2n+1)g_S^2}{4\pi G n(n+1)}$
$y_6 + \frac{n+1}{a} y_5$	0	$(2n+1)g_S$	$(2n+1)g_S$	0

Table 5.1: Summary of surface boundary conditions for the cases of (a) free oscillations, (b) the presence of an external gravitational potential field, (c) surface mass loading, and (d) surface shear forcing (e.g., Alterman et al., 1959; Longman, 1963; Wiggins, 1968; Lanzano, 1982; Melchior, 1983; Okubo & Saito, 1983; Okubo & Endo, 1986; Guo et al., 2004). Note that the boundary conditions stated in Longman (1963) are presented in terms of normalized y-variables, whereas here we state the boundary conditions directly in terms of the y-variables. Also note that the Love number definitions of Okubo & Saito (1983) differ from the definitions stated here by a factor of  $(a g_S)$ , where  $a$  is Earth's radius and  $g_S$  is the acceleration due to gravity. Different scalings for the Love numbers must be reflected in the boundary conditions.

<b>Surface Boundary Conditions (<math>n = 1</math>, CE frame)</b>					
	(a) Free Oscillations	(b) External Potential	(c) Surface Mass Loading	(d) Surface Shear Forcing	(e) Surface Stress
$y_2$	0	0	$-\frac{3g_S^2}{4\pi G}$	0	$-\frac{3g_S^2}{4\pi G}$
$y_4$	0	0	0	$\frac{3g_S^2}{8\pi G}$	$\frac{3g_S^2}{8\pi G}$
$y_5$	0	$a g_S$	$a g_S$	0	0

Table 5.2: Summary of surface boundary conditions for the cases of (a) free oscillations, (b) the presence of an external gravitational potential field, (c) surface mass loading, (d) surface shear forcing, and (e) surface stress (e.g., Alterman et al., 1959; Farrell, 1972; Saito, 1974; Merriam, 1985; Okubo & Endo, 1986; Blewitt, 2003; Guo et al., 2004). The surface stress solution satisfies the consistency relation and provides a linearly independent secondary solution for static degree-1 modes (Okubo & Endo, 1986).



external gravitational potential, caused by a mass  $m$  external to the Earth, the additional potential,  $\psi_E$ , must be added to the perturbed potential field,  $\psi$ , in the equations of motion (e.g., Farrell, 1972).

Since mass  $m$  exists entirely outside Earth, however, the external potential field satisfies Laplace's equation everywhere inside the Earth and thus is only implicit in the equations of motion. The surface boundary conditions, however, contain  $\psi_E$  explicitly. At the surface, both  $\psi$  and  $\psi_E$  must be continuous. Furthermore,  $\dot{\psi}_1 - 4\pi G \rho_0 u$  must be continuous, as stated previously, and additionally  $\dot{\psi}_E + 4\pi G \gamma$  must also be continuous, where  $\gamma$  represents a unit of external mass distributed uniformly over a disk of radius  $\alpha$  (e.g., Longman, 1962; Farrell, 1972). Following the method of Longman (1962), a unit of external mass  $\gamma$  distributed uniformly over a disk of radius  $\alpha$  may be expanded as a harmonic Legendre series of the form:

$$\gamma = \sum_{n=0}^{\infty} K_n P_n(\cos \theta) e^{i\omega t}. \quad (5.71)$$

The coefficients  $K_n$  are then given by (e.g., Longman, 1962; Farrell, 1972; Lanzano, 1982):

$$\begin{aligned} K_0 &= \frac{1}{4\pi a^2} \\ K_n &= \frac{P_{n-1}(\cos \alpha) - P_{n+1}(\cos \alpha)}{4\pi a^2(1 - \cos \alpha)}, \quad n > 0 \end{aligned} \quad (5.72)$$

where  $a$  is Earth's radius. In the limit  $\alpha \rightarrow 0$ ,

$$K_n = \frac{2n+1}{4\pi a^2}. \quad (5.73)$$

From a Legendre recursion relation,

$$P_{n-1}(x) - P_{n+1}(x) = \frac{2n+1}{n(n+1)}(1-x^2)P'_n(x); \quad (5.74)$$

therefore (Farrell, 1972),

$$K_n = \frac{2n+1}{4\pi a^2} \left[ -\frac{(1+\cos \alpha)}{n(n+1)\sin \alpha} \frac{\partial P_n(\cos \alpha)}{\partial \alpha} \right]. \quad (5.75)$$

The quantity in brackets is known as the **disk factor** and represents a mass distribution of finite size. The quantity in front of the bracketed terms represents the Legendre expansion of the delta function in spherical

coordinates (e.g., Farrell, 1972; Sun & Okubo, 1993).

For Earth's response to a gravitational potential field generated by an external mass *not* loading the Earth, the radial and tangential tractions vanish at the free surface (e.g., Melchior, 1983). Thus,  $y_2 = y_4 = 0$ , as for the free oscillations (e.g., Alterman et al., 1959; Takeuchi & Saito, 1972). For the case of surface mass loading, however, the radial traction will be non-zero (e.g., Longman, 1962; Farrell, 1972; Lanzano, 1982; Guo et al., 2004). The radial traction is given by the acceleration of gravity multiplied by the surface mass distribution (e.g., Lanzano, 1982, Sec. 3.06). Thus,

$$\begin{aligned} y_2 &= -g_S K_n \\ &= -g_S^2 \frac{2n+1}{4\pi G}. \end{aligned} \quad (5.76)$$

The surface boundary conditions for free oscillations, external potential fields, and surface mass loading (SML) are summarized in Table 5.1. Solving the spheroidal-deformation equations using external-potential boundary conditions yields potential Love numbers. Solving the equations using SML boundary conditions yields load Love numbers. Another set of boundary conditions may be developed to represent surface shear forcing (also listed in Table 5.1). Solutions generated from applying shear-forcing boundary conditions to the equations of motion yield shear Love numbers. Only six of the nine Love numbers (potential, load, and shear) are independent and there exist three independent linear relationships among them (e.g., Molodenskiy, 1977; Saito, 1978).

For the special case of  $n = 0$ , the equations for  $y_3$  and  $y_4$  (the tangential components) are undefined and the system reduces to four equations (Eq. 5.48) (e.g., Longman, 1963; Smylie, 2013). Furthermore, only two solutions and two boundary conditions exist for  $n = 0$ . The boundary conditions are identical to those listed in Table 5.1, with the exception that the conditions for  $y_4$  must be excluded.

For the special case of  $n = 1$ , the gravitational-potential load Love number,  $k'_1$ , must be zero in a reference frame centered at the center of mass of the solid Earth (CE) because deformation of the solid Earth caused by external surface loads, once the loads are in place, cannot affect the position of the center of mass of the solid Earth (Blewitt, 2003, Sec. 4.1). Ensuring that  $k'_1 = 0$  may be accomplished by adjusting the boundary conditions such that  $Y_5(a) = a g_S$ , since  $k'_1 = \frac{Y_5(a)}{a g_S} - 1$  (e.g. Guo et al., 2004).

Alternatively, the load Love numbers for  $n = 1$  may be computed using the same boundary conditions as

for all other spherical harmonic degrees (Table 5.1), and then subsequently adjusted to ensure that load-induced changes in the degree-one gravitational potential vanish outside the Earth (e.g. Merriam, 1985). The required adjustments satisfy the constraint of a vanishing gravitational potential outside the Earth by accounting for a rigid-body translation of the center of mass. Suppose that the load Love numbers derived from the solutions to the equations of motion (using boundary conditions from Table 5.1) are  $h_1^e$ ,  $l_1^e$ , and  $k_1^e$ . To satisfy the constraint of the vanishing gravitational potential,  $k_1^e$  should be subtracted from each of the Love numbers (e.g. Merriam, 1985):

$$\begin{aligned} h_1' &= h_1^e - k_1^e \\ l_1' &= l_1^e - k_1^e \\ k_1' &= k_1^e - k_1^e. \end{aligned} \tag{5.77}$$

Note that  $k_1' = 0$  after applying the correction. The other two load Love numbers,  $h_1'$  and  $l_1'$ , are also adjusted slightly to account for the translation of the center of mass.

As a third option, applying a rigid-body translation to the solution vectors at the surface *prior* to computation of the Love numbers, such that  $Y_5(a) + (\alpha g_S) = 0$  where  $\alpha = -\frac{Y_5(a)}{g_S}$  (e.g. Merriam, 1985), yields  $Y_5(a) = 0$ . With  $Y_5(a) = 0$ ,  $k_1' = \frac{Y_5(a)}{a g_S} - 1 = -1$ , which represents  $k_1'$  in the CM reference frame. The load Love numbers in the CM frame may then be converted to the CE frame using transformation equations (Blewitt, 2003). Sec. 5.3.8 provides a description of reference frames applicable to the loading problem, and more information on the special degree-1 case may be found in the literature (e.g. Farrell, 1972; Saito, 1974; Merriam, 1985; Okubo & Endo, 1986; Blewitt, 2003; Guo et al., 2004).

### 5.2.13 Load Love Numbers

Load Love numbers are computed by equating linear combinations of the three independent solutions to the equations of motion with boundary conditions at the surface. In matrix form,

$$\begin{bmatrix} -g_S^2 \frac{2n+1}{4\pi G} \\ 0 \\ (2n+1) g_S \end{bmatrix} = \begin{bmatrix} y_2^I & y_2^{II} & y_2^{III} \\ y_4^I & y_4^{II} & y_4^{III} \\ (y_6^I + \frac{n+1}{a} y_5^I) & (y_6^{II} + \frac{n+1}{a} y_5^{II}) & (y_6^{III} + \frac{n+1}{a} y_5^{III}) \end{bmatrix} \begin{bmatrix} m_1 \\ m_2 \\ m_3 \end{bmatrix}, \tag{5.78}$$

where the superscript Roman numerals represent each of the three independent solutions that were propagated to the surface. Note that if the y-variables are non-dimensional, then the other variables must be scaled appropriately (Sec. 5.2.6). The system of equations may now be solved for the model parameters  $m_1$ ,  $m_2$ , and  $m_3$ . When the system is solved using a direct matrix inversion or the normal equations, large instabilities in the Love numbers can arise, particularly at high spherical harmonic degrees (see Sec. 5.2.17). To promote stability, we solve the system of equations directly for all  $n$  using `numpy`, without inverting the matrix explicitly.

With the model parameters in hand,  $Y_1$ ,  $Y_3$ , and  $Y_5$  at the surface may now be derived:

$$Y_1(a) = m_1 y_1^{\text{I}} + m_2 y_1^{\text{II}} + m_3 y_1^{\text{III}} \quad (5.79)$$

$$Y_3(a) = m_1 y_3^{\text{I}} + m_2 y_3^{\text{II}} + m_3 y_3^{\text{III}} \quad (5.80)$$

$$Y_5(a) = m_1 y_5^{\text{I}} + m_2 y_5^{\text{II}} + m_3 y_5^{\text{III}}. \quad (5.81)$$

The load Love numbers are given by (e.g., Longman, 1962; Farrell, 1972; Guo et al., 2004):

$$h'_n = \frac{Y_1(a)}{a} \quad (5.82)$$

$$l'_n = \frac{Y_3(a)}{a} \quad (5.83)$$

$$k'_n = \frac{Y_5(a)}{a g_S} - 1. \quad (5.84)$$

Since we have assumed a spherically symmetric, non-rotating, elastic and isotropic (SNREI) Earth, the load Love numbers are real-valued and latitude independent. In future versions, we aim to relax the Earth-model assumptions. Rotation and ellipticity would introduce a latitudinal dependency (e.g., Lambeck, 1988) and anelastic effects would produce complex-valued load Love numbers (e.g., Pagiatakis, 1990).

#### 5.2.14 Potential Love Numbers

The potential, or “tidal” (e.g., Saito, 1978), Love numbers are computed analogously to the load Love numbers, with the exception of different boundary conditions. For potential Love numbers, boundary conditions for an external gravitational potential are applied to the equations of motion at the surface (e.g., Farrell,

1972; Melchior, 1983):

$$\begin{bmatrix} 0 \\ 0 \\ (2n+1)g_S \end{bmatrix} = \begin{bmatrix} y_2^{\text{I}} & y_2^{\text{II}} & y_2^{\text{III}} \\ y_4^{\text{I}} & y_4^{\text{II}} & y_4^{\text{III}} \\ (y_6^{\text{I}} + \frac{n+1}{a}y_5^{\text{I}}) & (y_6^{\text{II}} + \frac{n+1}{a}y_5^{\text{II}}) & (y_6^{\text{III}} + \frac{n+1}{a}y_5^{\text{III}}) \end{bmatrix} \begin{bmatrix} m_1 \\ m_2 \\ m_3 \end{bmatrix}. \quad (5.85)$$

The potential Love numbers are derived from

$$Y_1(a) = m_1 y_1^{\text{I}} + m_2 y_1^{\text{II}} + m_3 y_1^{\text{III}} \quad (5.86)$$

$$Y_3(a) = m_1 y_3^{\text{I}} + m_2 y_3^{\text{II}} + m_3 y_3^{\text{III}} \quad (5.87)$$

$$Y_5(a) = m_1 y_5^{\text{I}} + m_2 y_5^{\text{II}} + m_3 y_5^{\text{III}} \quad (5.88)$$

using the following formulae:

$$h_n = \frac{Y_1(a)}{a} \quad (5.89)$$

$$l_n = \frac{Y_3(a)}{a} \quad (5.90)$$

$$k_n = \frac{Y_5(a)}{a g_S} - 1. \quad (5.91)$$

### 5.2.15 Shear Love Numbers

The shear Love numbers are computed analogously to the load and potential Love numbers, except for different boundary conditions. Shear-traction boundary conditions are applied to derive the shear Love numbers (Table 5.1). Furthermore,

$$k_n = \frac{Y_5(a)}{a g_S}, \quad (5.92)$$

since the external force is free of a gravitational potential (e.g., Saito, 1978; Okubo & Saito, 1983).

### 5.2.16 Stress Love Numbers and Degree-1 Modes

Since potential and shear Love numbers are undefined for the degree-1 static case, stress Love numbers may be introduced to satisfy the consistency relation (e.g., Farrell, 1972; Okubo & Endo, 1986). The consistency

relation, given by

$$y_2(r) + 2 y_4(r) + \frac{g(r)}{4\pi G} y_6(r) = 0, \quad (5.93)$$

ensures that, in the static case for  $n = 1$ , the solid Earth experiences no net force (e.g., Saito, 1974; Okubo & Endo, 1986). As with the shear Love numbers, the stress Love numbers characterize Earth's response to potential-free external forcing (Table 5.1).

One additional special consideration must be made for the degree-1 mode: accounting for a rigid-body translation (e.g., Merriam, 1985; Okubo & Endo, 1986; Okubo, 1993; Blewitt, 2003). For a reference frame centered at the center of mass of the solid Earth (CE), the degree-1 potential field must vanish outside the Earth. To satisfy the restriction, a rigid-body translation may be added to the solution vector derived from the equations of motion for spheroidal deformation (e.g., Merriam, 1985; Okubo & Endo, 1986):

$$\begin{aligned} y_1(r) &= \alpha \\ y_2(r) &= 0 \\ y_3(r) &= \alpha \\ y_4(r) &= 0 \\ y_5(r) &= g(r) \alpha \\ y_6(r) &= \frac{-2 g(r)}{r} \alpha, \end{aligned} \quad (5.94)$$

where

$$y_5(a)^{Load} = 1 \quad (5.95)$$

$$y_5(a)^{Stress} = 0 \quad (5.96)$$

and  $a$  corresponds to an evaluation at Earth's surface. Thus,

$$\alpha^{Load} = -\frac{y_5(a)}{g(a)} \quad (5.97)$$

$$\alpha^{Stress} = -\frac{y_5(a)}{g(a)} + \frac{1}{g(a)}. \quad (5.98)$$

A careful reader might recognize that the set of Eqs. 5.94 correspond precisely to Eqs. 5.63 for the case of

$n = 1$ ,  $\omega = 0$ , and  $y_5(a) = 1$  for the load solution or  $y_5(a) = 0$  for the stress solution (Takeuchi & Saito, 1972). Note that definitions of the “y” equations (Eqs. 5.42) may differ in the literature. For example, to convert between the convention used here (Table 5.1) (e.g., Alterman et al., 1959) and the convention of Okubo & Saito (1983) and Okubo & Endo (1986), one must divide the y-variables by a factor  $[a g(a)]$ . Furthermore,  $y_6$  is also defined differently; thus, the convention adopted here requires an extra factor of  $[\frac{-(n+1)}{r} g(r) \alpha = \frac{-2g(r)}{r} \alpha]$  for the rigid-body translation.

### 5.2.17 Numerical Considerations

Numerical instabilities can easily arise in load Love number computations up to spherical harmonic degree  $n = 10000$  and greater, particularly since the three linearly independent starting solutions become less linearly independent with integration to the surface. In addition to non-dimensionalization, we compute the surface model parameters (Eq. 5.85) using a linear-algebra solver in NumPy, rather than invert the matrix explicitly. Furthermore, the integration solver can also influence stability. LoadDef uses a Runge-Kutta scheme with adaptive step-sizing within Python. We have found good stability with the scipy differential-equation solvers *dopri5* and *dopri853*, which perform explicit fourth- and eighth-order Runge-Kutta integration, respectively. Reducing the absolute and relative tolerance values for the integration can improve precision, albeit at the expense of computation time (e.g., Press et al., 2007). LoadDef allows the user to specify integration tolerances and solvers. Another method for improving stability involves variable transformations (e.g., Wang et al., 2012; Smylie, 2013). In addition, the starting solutions and choice of starting radius also have significant effects on precision and stability, as discussed in the following section.

### 5.2.18 Starting Radius within the Mantle

Vertical and horizontal displacements induced by either an external gravitational potential or by surface mass loading at spherical harmonic degree,  $n$ , are proportional to the external potential field, which is proportional to  $(\frac{r}{a})^n$  (e.g., Farrell, 1972; Baker, 1984; Jentzsch, 1997). Therefore, since the influence of the potential drops off rapidly inside Earth with increasing  $n$ , integration through the inner and outer cores becomes less important (and may cause numerical instabilities in the solution vectors) for spherical harmonic degrees higher than about  $n = 20$  (e.g., Na & Baek, 2011). In practice, we have found that commencing the integrations from a radius at which  $(\frac{r}{a})^n$  just exceeds a tolerance level of  $10^{-5}$  works well. With a tolerance

level of  $10^{-5}$ , the integration for spherical harmonic degrees  $n \geq 20$  will commence within the mantle. LoadDef allows the user to specify the tolerance level for integration starting-radius.

### 5.2.19 Asymptotic Solutions

As a function of spherical harmonic degree, the load Love numbers approach asymptotic values after about  $n = 1000$  (e.g., Farrell, 1972; Guo et al., 2004). The asymptotic expressions may be obtained by solving the flat-Earth Boussinesq problem (e.g., Farrell, 1972) or by deriving asymptotic solutions to the system of governing ordinary differential equations (e.g., Guo et al., 2004). Using the latter method, the asymptotic expressions are given by:

$$\begin{aligned} h'_n &= h_\infty^* + \frac{1}{n} h_\infty^{**} \\ nl'_n &= l_\infty^* + \frac{1}{n} l_\infty^{**} \\ nk'_n &= k_\infty^* + \frac{1}{n} k_\infty^{**}, \end{aligned} \quad (5.99)$$

where

$$\begin{aligned} h_\infty^* &= -\frac{g_S^2 \sigma_S}{4\pi G \mu_S \eta_S} \\ l_\infty^* &= \frac{g_S^2}{4\pi G \eta_S} \\ k_\infty^* &= -\frac{a \rho_S g_S}{2 \mu_S} \\ h_\infty^{**} &= \frac{g_S^2}{4\pi G \eta_S} \left[ -\frac{\mu_S}{\eta_S} + \frac{a \rho_S g_S (\lambda_S^2 + \lambda_S \mu_S - \mu_S^2)}{2 \mu_S^2 \eta_S} + \frac{2\pi G a \rho_S \eta_S}{g_S \mu_S} \right] \\ l_\infty^{**} &= \frac{g_S^2}{4\pi G \eta_S} \left[ -\frac{3\lambda_S^2 + 8\lambda_S \mu_S + 3\mu_S^2}{2\mu_S \eta_S} + \frac{a \rho_S g_S \sigma_S}{2\mu_S \eta_S} \right] \\ k_\infty^{**} &= \frac{a g_S \rho_S}{\mu_S} \left[ \frac{\lambda_S}{4\eta_S} + \frac{a \rho_S g_S (2\lambda_S + \mu_S)}{8\mu_S \eta_S} + \frac{\pi G a \rho_S}{g_S} \right] \end{aligned} \quad (5.100)$$

and

$$\begin{aligned} \sigma_S &= \lambda_S + 2\mu_S \\ \eta_S &= \lambda_S + \mu_S. \end{aligned} \quad (5.101)$$



A subscript  $S$  refers to the value of the parameter at Earth's surface.

### 5.3 Load Green's Functions

#### 5.3.1 Introduction

Infinite sums of Love numbers may be formed to determine the impulse-response function, or **Green's Function**, of a body to a certain stimulus. `LoadDef` computes Green's functions for surface mass loading boundary conditions, though a similar procedure may be applied to other types of boundary conditions, such as an external gravitational potential. The variables  $Y_1$ ,  $Y_3$ , and  $Y_5$  obtained in Sec. 5.2.13 represent the radial coefficients of the spherical harmonic expansions (Eqs. 5.29). Namely, for mass loading at Earth's surface,

$$\begin{aligned} U_n(r) &= Y_1 = a h'_n \\ V_n(r) &= Y_3 = a l'_n \\ \Psi_n(r) &= Y_5 = a g (k'_n + 1), \end{aligned} \tag{5.102}$$

where  $a$  is Earth's radius. Referring back to Eqs. 5.29, the radial displacement for spherical harmonic degree  $n$  is given by:

$$\begin{aligned} u_n &= U_n(r) P_n(\cos \theta) e^{i\omega t} \\ &= a h'_n P_n(\cos \theta) e^{i\omega t}, \end{aligned} \tag{5.103}$$

where  $e^{i\omega t}$  represents the temporal evolution of the applied load, such as a periodic ocean tide.

Since the boundary conditions in Sec. 5.2.12 were formulated based on the mass of the Earth, Eq. 5.103 may be rewritten to represent an arbitrary mass load  $m'$  (e.g., Longman, 1963):

$$\begin{aligned} u_n &= a \frac{m'}{m_E} h'_n P_n(\cos \theta) e^{i\omega t} \\ &= \frac{a}{m_E} h'_n P_n(\cos \theta) e^{i\omega t}, \end{aligned} \tag{5.104}$$

where, in the second line, we have taken  $m'$  to be a load of unit mass.

The vertical-displacement load Green's function (LGF) for a 1-kg load applied at Earth's surface is given by a summation of Eq. 5.104 over all  $n$ :

$$u = \frac{a}{m_E} \sum_{n=0}^{\infty} h'_n P_n(\cos \theta) e^{i\omega t}. \quad (5.105)$$

Similarly, the horizontal-displacement LGF for a 1-kg load at Earth's surface is given by:

$$v = \frac{a}{m_E} \sum_{n=1}^{\infty} l'_n \frac{\partial P_n(\cos \theta)}{\partial \theta} e^{i\omega t}. \quad (5.106)$$

Note that the sum for  $v$  begins at  $n = 1$ , since horizontal displacements do not apply to the degree-0 mode.

The radial coefficients of the spherical harmonic expansions may also be expressed in terms of the transformed surface potential for a point load of unit mass,  $\Phi_{2,n}$  (e.g., Munk & MacDonald, 1960; Farrell, 1972; Melchior, 1983; Jentzsch, 1997):

$$\begin{aligned} U_n(r) &= h'_n(r) \frac{\Phi_{2,n}}{g} \\ V_n(r) &= l'_n(r) \frac{\Phi_{2,n}}{g}, \end{aligned} \quad (5.107)$$

where

$$\Phi_{2,n} = \frac{4\pi G a}{2n+1} K_n = \frac{a g}{m_E}. \quad (5.108)$$

The displacement LGFs in Eqs. 5.105 and 5.106 may also be derived from Eqs. 5.107 and 5.108. In other words, the load Love numbers scale the equipotential height,  $\frac{\Phi_{2,n}}{g}$ , to the true displacements expected for Earth's material structure. To derive the predicted SML-induced displacements within Earth's interior, an extra factor of  $\left(\frac{r}{a}\right)^n$  must be included in Eq. 5.108 (e.g., Munk & MacDonald, 1960; Melchior, 1983).

In summary, the amplitudes of the displacement LGFs (i.e., written without the dynamic component of the forcing term) are:

$$u = \frac{a}{m_E} \sum_{n=0}^{\infty} h'_n P_n(\cos \theta) \quad (5.109)$$

and

$$v = \frac{a}{m_E} \sum_{n=1}^{\infty} l'_n \frac{\partial P_n(\cos \theta)}{\partial \theta}. \quad (5.110)$$

Displacement LGFs are appropriate for comparing predicted load-induced surface displacements with GNSS-inferred observations of surface displacements.

For surface displacements induced by an external gravitational potential, the potential Love numbers scale the equipotential height generated by the external gravitational potential,  $V_n$  (Eq. 5.2). For a mass a distance  $R$  away from Earth's center, the gravitational potential at Earth's surface,  $a$ , is given by:

$$V_n^{\text{potential}} = \frac{GM}{R} \left( \frac{a}{R} \right)^n P_n(\cos \theta) e^{i\omega t}, \quad (5.111)$$

where the time-dependent harmonic term ( $e^{i\omega t}$ ) has been included to account for periodic dynamic forcing. Thus, the vertical and horizontal displacements due to an external gravitational potential may be derived by inserting the expression for  $V_n$  (Eq. 5.111) into Eqs. 5.2 and 5.4, respectively, and summing over all  $n$ .

LoadDef also computes Green's functions for gravity, tilt and strain (e.g., Farrell, 1972; Francis & Dehant, 1987; Jentzsch, 1997; Guo et al., 2004; Na & Baek, 2011).

The equation for the indirect (elastic) effect of gravity is (e.g., Farrell, 1972; Guo et al., 2004):

$$g^E = \frac{g_a}{M_E} \sum_{n=0}^{\infty} 2h'_n P_n(\cos \theta) - (n+1) k'_n P_n(\cos \theta), \quad (5.112)$$

where  $g_a$  is the acceleration due to gravity at the surface and  $M_E$  is the mass of the Earth. The direct, or Newtonian, effect of gravity is given by (e.g., Farrell, 1972):

$$g^N = -\frac{g_a}{4 M_E \sin(\theta/2)}. \quad (5.113)$$

The equation for the indirect (elastic) effect of tilt is (e.g., Farrell, 1972; Guo et al., 2004):

$$t^E = -\frac{1}{M_E} \sum_{n=1}^{\infty} (-h'_n + k'_n) \frac{d}{d\theta} P_n(\cos \theta). \quad (5.114)$$

The direct, or Newtonian, effect of tilt is given by (e.g., Farrell, 1972):

$$t^N = \frac{\cos(\theta/2)}{4 M_E \sin^2(\theta/2)}. \quad (5.115)$$

The diagonal components of the strain tensor are given by (e.g., Farrell, 1972; Guo et al., 2004; Bos & Scherneck, 2013; Agnew, 2015, Sec. 3.06.4.2)

$$\epsilon_{\lambda\lambda} = \frac{1}{a} u + \frac{\cot \theta}{a} v \quad (5.116)$$

$$\epsilon_{\theta\theta} = \frac{1}{a} u + \frac{1}{a} \frac{\partial v}{\partial \theta} = \frac{1}{a} u + \frac{1}{M_E} \sum_{n=1}^{\infty} l'_n \frac{d^2}{d\theta^2} P_n(\cos \theta) \quad (5.117)$$

$$\epsilon_{rr} = \frac{\partial u}{\partial r} = -\frac{\lambda_a}{\lambda_a + 2\mu_a} (\epsilon_{\theta\theta} + \epsilon_{\lambda\lambda}), \quad (5.118)$$

where  $u$  represents radial displacement at the surface,  $v$  represents tangential displacement at the surface, and  $\lambda_a$  and  $\mu_a$  are the Lamé parameters at the surface. In the spherical coordinate system,  $\theta$  is the surface-tangential component in the longitudinal direction,  $\lambda$  is the surface-tangential component in the azimuthal direction, and  $r$  is the radial component. Eq. 5.135 may be solved directly using the displacement load Green's functions. Plugging in expressions for  $u$  and  $v$ , Eq. 5.117 becomes

$$\epsilon_{\theta\theta} = \frac{1}{M_E} \sum_{n=0}^{\infty} h'_n P_n(\cos \theta) + \frac{1}{M_E} \sum_{n=0}^{\infty} l'_n \frac{\partial^2 P_n(\cos \theta)}{\partial \theta^2}. \quad (5.119)$$

Bos & Scherneck (2013) discuss how to rotate the components of the strain tensor into a geographical configuration (Eqs. 1.114–1.117). Agnew (2015) provides an expression for computing strain along a desired azimuth (Eq. 52).

### 5.3.2 Kummer's Transformation and Series Convergence

The series in Eqs. 5.109, 5.110, and 5.112–5.118 can be slow to converge. Kummer's series transformation may be implemented to speed convergence (e.g., Farrell, 1972; Francis & Dehant, 1987; Guo et al., 2004; Na & Baek, 2011). The general form of Kummer's transformation is given by (e.g., Abramowitz & Stegun, 1964; Na & Baek, 2011):

$$\sum_n f(n) Q_n = f_{\infty} \sum_n Q_n + \sum_n (f(n) - f_{\infty}) Q_n, \quad (5.120)$$

where  $f_{\infty} = \lim_{n \rightarrow \infty} f(n)$ .

Thus, Eqs. 5.109 and 5.110 may be expressed in terms of the asymptotic expressions of the load Love

numbers as:

$$u = \frac{a}{m_E} h_\infty^* \sum_{n=0}^{\infty} P_n(\cos \theta) + \frac{a}{m_E} \sum_{n=0}^{\infty} (h'_n - h_\infty^*) P_n(\cos \theta) \quad (5.121)$$

and

$$v = \frac{a}{m_E} l_\infty^* \sum_{n=1}^{\infty} \frac{1}{n} \frac{\partial P_n(\cos \theta)}{\partial \theta} + \frac{a}{m_E} \sum_{n=1}^{\infty} (nl'_n - l_\infty^*) \frac{1}{n} \frac{\partial P_n(\cos \theta)}{\partial \theta}. \quad (5.122)$$

The factor  $\frac{1}{n}$  in Eq. 5.122 enters because  $l_\infty^*$  represents the asymptotic value of  $nl'_n$  (Eq. 5.99) (cf., Farrell, 1972; Guo et al., 2004).

Eqs. 5.121 and 5.122 include only the first term in the asymptotic expressions of the load Love numbers (Eq. 5.99). Guo et al. (2004) introduced an additional term to the asymptotic expressions, improving accuracy by a factor  $\frac{1}{n}$ . With the extra term included, Eqs. 5.109 and 5.110 become:

$$\begin{aligned} u = & \frac{a}{m_E} h_\infty^* \sum_{n=1}^{\infty} P_n(\cos \theta) + \frac{a}{m_E} h_\infty^{**} \sum_{n=1}^{\infty} \frac{1}{n} P_n(\cos \theta) + \\ & \frac{a}{m_E} h'_0 + \frac{a}{m_E} \sum_{n=1}^{N_{\max}} (h'_n - (h_\infty^* + \frac{1}{n} h_\infty^{**})) P_n(\cos \theta) \end{aligned} \quad (5.123)$$

and

$$\begin{aligned} v = & \frac{a}{m_E} l_\infty^* \sum_{n=1}^{\infty} \frac{1}{n} \frac{\partial P_n(\cos \theta)}{\partial \theta} + \frac{a}{m_E} l_\infty^{**} \sum_{n=1}^{\infty} \frac{1}{n^2} \frac{\partial P_n(\cos \theta)}{\partial \theta} + \\ & \frac{a}{m_E} \sum_{n=1}^{N_{\max}} (nl'_n - (l_\infty^* + \frac{1}{n} l_\infty^{**})) \frac{1}{n} \frac{\partial P_n(\cos \theta)}{\partial \theta}, \end{aligned} \quad (5.124)$$

where  $N_{\max}$  represents the maximum degree  $n$  after which the asymptotic values are assumed. Note that the second-order terms for the asymptotes are undefined for  $n = 0$ . In practice, the load Love number computations are often carried out to spherical harmonic degree  $n = 10000$ , beyond which the load Love numbers are assumed to be equivalent to the asymptotic values (Eq. 5.99) (e.g., Farrell, 1972; Guo et al., 2004). Thus, the arguments in Eqs. 5.123 and 5.124 that contain load Love numbers become zero beyond spherical harmonic degree,  $N$ . Furthermore, some Legendre sums are known analytically, which will be discussed in Sec. 5.3.3, and other Legendre polynomials and their derivatives may be computed recursively using the so-called *recursion relations*, which will be discussed in Sec. 5.3.5.

In summary, the displacement load Green's functions are computed using the formulae:

$$\begin{aligned}
 u(\theta) = & \frac{a}{m_E} h_\infty^* \sum_{n=1}^{\infty} P_n(\cos \theta) + \frac{a}{m_E} h_\infty^{**} \sum_{n=1}^{\infty} \frac{1}{n} P_n(\cos \theta) + \\
 & \frac{a}{m_E} h'_0 + \frac{a}{m_E} \sum_{n=1}^{N_{\max}} (h'_n - (h_\infty^* + \frac{1}{n} h_\infty^{**})) P_n(\cos \theta)
 \end{aligned} \tag{5.125}$$

for the vertical-displacement response, and

$$\begin{aligned}
 v(\theta) = & \frac{a}{m_E} l_\infty^* \sum_{n=1}^{\infty} \frac{1}{n} \frac{\partial P_n(\cos \theta)}{\partial \theta} + \frac{a}{m_E} l_\infty^{**} \sum_{n=1}^{\infty} \frac{1}{n^2} \frac{\partial P_n(\cos \theta)}{\partial \theta} + \\
 & \frac{a}{m_E} \sum_{n=1}^{N_{\max}} (nl'_n - (l_\infty^* + \frac{1}{n} l_\infty^{**})) \frac{1}{n} \frac{\partial P_n(\cos \theta)}{\partial \theta}
 \end{aligned} \tag{5.126}$$

for the horizontal-displacement response. The Legendre sums without Love-number coefficients may be determined analytically, as discussed in Sec. 5.3.3. The Legendre contributions to the final terms in Eqs. 5.125 and 5.126 are computed recursively (Sec. 5.3.5). For  $\theta = 180^\circ$ , we compute the limits of the Legendre functions and their derivatives, as well as the limits of the Legendre sums, as  $\theta$  approaches  $180^\circ$ .

The Kummer transformations for gravity, tilt, and strain are performed in a similar way.

For the indirect effect of gravity,

$$\begin{aligned}
 g^E &= \left( \frac{2g_a}{M_E} \sum_{n=0}^{\infty} h'_n P_n(\cos \theta) \right) - \left( \frac{g_a}{M_E} \sum_{n=0}^{\infty} (n+1) \frac{n k'_n}{n} P_n(\cos \theta) \right) \\
 &= \left( \frac{2g_a}{M_E} \sum_{n=0}^{\infty} h'_n P_n(\cos \theta) \right) - \left( \frac{g_a}{M_E} \sum_{n=0}^{\infty} \left[ n \frac{n k'_n}{n} P_n(\cos \theta) + \frac{n k'_n}{n} P_n(\cos \theta) \right] \right) \\
 &= \left( \frac{2g_a}{M_E} \sum_{n=0}^{\infty} h'_n P_n(\cos \theta) \right) - \left( \frac{g_a}{M_E} \sum_{n=0}^{\infty} \left[ n k'_n P_n(\cos \theta) + n k'_n \frac{1}{n} P_n(\cos \theta) \right] \right) \\
 &= 2g_a \left( \frac{u}{a} \right) - \left( \frac{g_a}{M_E} \sum_{n=0}^{\infty} \left[ n k'_n P_n(\cos \theta) + n k'_n \frac{1}{n} P_n(\cos \theta) \right] \right).
 \end{aligned} \tag{5.127}$$

Isolating components, we have:

$$\begin{aligned}
 \sum_{n=0}^{\infty} (n k'_n) P_n(\cos \theta) &= k_\infty^* \sum_{n=0}^{\infty} P_n(\cos \theta) + k_\infty^{**} \sum_{n=0}^{\infty} \frac{1}{n} P_n(\cos \theta) \\
 &+ \sum_{n=0}^{N_{\max}} [(n(n k'_n - k_\infty^*) - k_\infty^{**}) / n] P_n(\cos \theta)
 \end{aligned} \tag{5.128}$$

and

$$\sum_{n=0}^{\infty} (n k'_n) \frac{1}{n} P_n(\cos \theta) = k_{\infty}^* \sum_{n=0}^{\infty} \frac{1}{n} P_n(\cos \theta) + \sum_{n=0}^{N_{\max}} (n k'_n - k_{\infty}^*) \frac{1}{n} P_n(\cos \theta). \quad (5.129)$$

For the second sum (Eq. 5.129), we opted to perform only a first-order Kummer transformation, which still facilitates a sufficient convergence of the series.

For the indirect effect of tilt,

$$\begin{aligned} t^E &= -\frac{1}{M_E} \sum_{n=1}^{\infty} (-h'_n + k'_n) \frac{d}{d\theta} P_n(\cos \theta) \\ &= \left[ -\frac{1}{M_E} \sum_{n=1}^{\infty} (-h'_n) \frac{d}{d\theta} P_n(\cos \theta) \right] + \left[ -\frac{1}{M_E} \sum_{n=1}^{\infty} (k'_n) \frac{d}{d\theta} P_n(\cos \theta) \right] \\ &= \left[ \frac{1}{M_E} \sum_{n=1}^{\infty} h'_n \frac{d}{d\theta} P_n(\cos \theta) \right] + \left[ -\frac{1}{M_E} \sum_{n=1}^{\infty} \frac{n k'_n}{n} \frac{d}{d\theta} P_n(\cos \theta) \right] \\ &= \left[ \frac{1}{M_E} \sum_{n=1}^{\infty} h'_n \frac{d}{d\theta} P_n(\cos \theta) \right] - \left[ \frac{1}{M_E} \sum_{n=1}^{\infty} (n k'_n) \frac{1}{n} \frac{d}{d\theta} P_n(\cos \theta) \right]. \end{aligned} \quad (5.130)$$

Isolating components, we have:

$$\begin{aligned} \sum_{n=1}^{\infty} h'_n \frac{d}{d\theta} P_n(\cos \theta) &= h_{\infty}^* \sum_{n=1}^{\infty} \frac{d}{d\theta} P_n(\cos \theta) + h_{\infty}^{**} \sum_{n=1}^{\infty} \frac{1}{n} \frac{d}{d\theta} P_n(\cos \theta) \\ &\quad + \sum_{n=1}^{N_{\max}} [(n(h'_n - h_{\infty}^*) - h_{\infty}^{**}) / n] \frac{d}{d\theta} P_n(\cos \theta) \end{aligned} \quad (5.131)$$

and

$$\begin{aligned} \sum_{n=1}^{\infty} (n k'_n) \frac{1}{n} \frac{d}{d\theta} P_n(\cos \theta) &= k_{\infty}^* \sum_{n=1}^{\infty} \frac{1}{n} \frac{d}{d\theta} P_n(\cos \theta) + k_{\infty}^{**} \sum_{n=1}^{\infty} \frac{1}{n^2} \frac{d}{d\theta} P_n(\cos \theta) \\ &\quad + \sum_{n=1}^{N_{\max}} [(n(n k'_n - k_{\infty}^*) - k_{\infty}^{**}) / n] \frac{1}{n} \frac{d}{d\theta} P_n(\cos \theta). \end{aligned} \quad (5.132)$$

For the strain component  $\epsilon_{\theta\theta}$ ,

$$\begin{aligned} \epsilon_{\theta\theta} &= \frac{u}{a} + \frac{1}{M_E} \sum_{n=1}^{\infty} l'_n \frac{d^2}{d\theta^2} P_n(\cos \theta) \\ &= \frac{u}{a} + \frac{1}{M_E} \sum_{n=1}^{\infty} (n l'_n) \frac{1}{n} \frac{d^2}{d\theta^2} P_n(\cos \theta), \end{aligned} \quad (5.133)$$

where

$$\begin{aligned} \sum_{n=1}^{\infty} (nl'_n) \frac{1}{n} \frac{d^2}{d\theta^2} P_n(\cos \theta) &= l_{\infty}^* \sum_{n=1}^{\infty} \frac{1}{n} \frac{d^2}{d\theta^2} P_n(\cos \theta) + l_{\infty}^{**} \sum_{n=1}^{\infty} \frac{1}{n^2} \frac{d^2}{d\theta^2} P_n(\cos \theta) \\ &+ \sum_{n=1}^{N_{\max}} \left[ (n(nl'_n - l_{\infty}^*) - l_{\infty}^{**}) / n \right] \frac{1}{n} \frac{d^2}{d\theta^2} P_n(\cos \theta). \end{aligned} \quad (5.134)$$

The strain component  $\epsilon_{\lambda\lambda}$  may be computed directly from the vertical and horizontal displacements:

$$\epsilon_{\lambda\lambda} = \frac{1}{a} u + \frac{\cot \theta}{a} v. \quad (5.135)$$

Finally, the strain component  $\epsilon_{rr}$  may be computed directly from  $\epsilon_{\theta\theta}$  and  $\epsilon_{\lambda\lambda}$ :

$$\epsilon_{rr} = -\frac{\lambda_a}{\lambda_a + 2\mu_a} (\epsilon_{\theta\theta} + \epsilon_{\lambda\lambda}). \quad (5.136)$$

To further improve the convergence of the series, we adopt the method of recursive averages suggested by Guo et al. (2004). The recursive averaging can be performed by developing a set of coefficients for each harmonic degree  $n$  that effectively “taper” the summands as the series approaches  $n = n_{\max}$ , where  $n_{\max}$  is often taken to be 10 000. Most of the coefficients will be one, except for as  $n = n_{\max}$  is approached and the coefficients are reduced towards zero. The point at which the taper starts depends on the number of recursive averages performed. `LoadDef` nominally selects 200 iterations for the taper.

### 5.3.3 Legendre Sums

Hobson (1955), Farrell (1972), Guo et al. (2004), Na & Baek (2011) and Bos & Scherneck (2013) provide closed-form expressions for several Legendre sums. Guo et al. (2004) include the most comprehensive collection of formulas. Equation B9 from Guo et al. (2004), however, contains a typo and should instead read (J.-Y. Guo, personal communication, 20 June 2016):

$$\begin{aligned} \sum_{n=1}^{\infty} \frac{1}{n^2} x^n \frac{d^2}{d\theta^2} P_n(\cos \theta) &= -\frac{\cos \theta}{\sin^2 \theta} \ln \frac{(x - l + 1)^2 (1 - \cos \theta)}{2(l - 1 + x \cos \theta)(1 + \cos \theta)} \\ &+ \frac{1}{\sin^2 \theta} \ln \frac{x^2 \sin^2 \theta}{2(l - 1 + x \cos \theta)} \end{aligned}$$



$$+ \frac{x(\cos \theta - 1)(1 - l)}{(l - 1 + x \cos \theta)l} - \frac{2x}{(x - l + 1)l} + 2. \quad (5.137)$$

The only difference is that  $(\cos \theta - l)$  should instead be  $(\cos \theta - 1)$  in the final line. The equation may then be further reduced using half-angle formulas from trigonometry.

Many of the Legendre sums that appear in Eqs. 5.123–5.134 are known analytically (e.g., J.-Y. Guo, personal communication, 20 June 2016; Farrell, 1972; Guo et al., 2004; Na & Baek, 2011):

$$\begin{aligned} \sum_{n=0}^{\infty} P_n(\cos \theta) &= \frac{1}{2 \sin(\theta/2)} \\ \sum_{n=0}^{\infty} n P_n(\cos \theta) &= -\frac{1}{4 \sin(\theta/2)} \\ \sum_{n=1}^{\infty} \frac{1}{n} P_n(\cos \theta) &= \ln \frac{1}{\sin(\theta/2) [1 + \sin(\theta/2)]} \\ \sum_{n=1}^{\infty} \frac{\partial P_n(\cos \theta)}{\partial \theta} &= -\frac{\cos(\theta/2)}{4 \sin^2(\theta/2)} \\ \sum_{n=1}^{\infty} \frac{1}{n} \frac{\partial P_n(\cos \theta)}{\partial \theta} &= -\frac{\cos(\theta/2) [1 + 2 \sin(\theta/2)]}{2 \sin(\theta/2) [1 + \sin(\theta/2)]} \\ \sum_{n=1}^{\infty} \frac{1}{n^2} \frac{\partial P_n(\cos \theta)}{\partial \theta} &= \frac{1}{\sin \theta} \ln \frac{\sin(\theta/2) [1 - \sin(\theta/2)]}{\cos^2(\theta/2)} - \frac{\cos \theta}{\sin \theta} \ln \frac{\sin(\theta/2) \cos^2(\theta/2)}{1 - \sin(\theta/2)} \\ \sum_{n=1}^{\infty} \frac{1}{n} \frac{\partial^2 P_n(\cos \theta)}{\partial \theta^2} &= \frac{1 + \sin(\theta/2) + \sin^2(\theta/2)}{4 \sin^2(\theta/2) [1 + \sin(\theta/2)]} \\ \sum_{n=1}^{\infty} \frac{1}{n^2} \frac{\partial^2 P_n(\cos \theta)}{\partial \theta^2} &= -\frac{\cos \theta}{\sin^2 \theta} \ln \frac{\sin(\theta/2) [1 - \sin(\theta/2)]}{\cos^2(\theta/2)} \\ &\quad + \frac{1}{\sin^2 \theta} \ln \frac{\sin(\theta/2) \cos^2(\theta/2)}{1 - \sin(\theta/2)} - \frac{1 - 2 \sin(\theta/2)}{2 \sin(\theta/2)}. \end{aligned} \quad (5.138)$$

$$(5.139)$$

### 5.3.4 Legendre Sums: Limit as $\theta \rightarrow 180^\circ$

In the limit  $\theta \rightarrow 180^\circ$ , the Legendre sums reduce to:

$$\begin{aligned} \sum_{n=0}^{\infty} P_n(\cos \theta) &= \frac{1}{2} \\ \sum_{n=0}^{\infty} n P_n(\cos \theta) &= -\frac{1}{4} \end{aligned}$$

$$\begin{aligned}
\sum_{n=1}^{\infty} \frac{1}{n} P_n(\cos \theta) &= \ln\left(\frac{1}{2}\right) = -\ln(2) \\
\sum_{n=1}^{\infty} \frac{\partial P_n(\cos \theta)}{\partial \theta} &= 0 \\
\sum_{n=1}^{\infty} \frac{1}{n} \frac{\partial P_n(\cos \theta)}{\partial \theta} &= 0 \\
\sum_{n=1}^{\infty} \frac{1}{n^2} \frac{\partial P_n(\cos \theta)}{\partial \theta} &= 0 \\
\sum_{n=1}^{\infty} \frac{1}{n} \frac{\partial^2 P_n(\cos \theta)}{\partial \theta^2} &= \frac{3}{8} \\
\sum_{n=1}^{\infty} \frac{1}{n^2} \frac{\partial^2 P_n(\cos \theta)}{\partial \theta^2} &= \frac{\ln(2)}{2} + \frac{1}{4}.
\end{aligned}
\tag{5.140}$$

$$\tag{5.141}$$

We computed the sums directly where possible, and otherwise used the Python package `SymPy`.

### 5.3.5 Legendre Polynomial Recursion Relations

To evaluate the final terms in Eqs. 5.125 and 5.126, the Legendre functions and their derivatives must be determined for every  $n$ . Recursion relations, derived from the Legendre generating function, are commonly used (e.g., Farrell, 1972; Guo et al., 2004; Na & Baek, 2011).

Two useful recursion, or recurrence, relations are (e.g., Boas, 1983):

$$nP_n(x) = (2n-1)xP_{n-1}(x) - (n-1)P_{n-2}(x) \tag{5.142}$$

$$(1-x^2)\frac{\partial P_n(x)}{\partial x} = nP_{n-1}(x) - nxP_n(x). \tag{5.143}$$

For  $x = \cos \theta$ , the recursion relations become:

$$\begin{aligned}
nP_n(\cos \theta) &= (2n-1)\cos \theta P_{n-1}(\cos \theta) - \\
&\quad (n-1)P_{n-2}(\cos \theta)
\end{aligned}
\tag{5.144}$$

$$(1-\cos^2 \theta)\frac{\partial P_n(\cos \theta)}{\partial \cos \theta} = nP_{n-1}(\cos \theta) - n\cos \theta P_n(\cos \theta). \tag{5.145}$$

Since Eq. 5.126 requires the derivative of the Legendre function with respect to  $\theta$  (as opposed to  $\cos \theta$ ),

each side of Eq. 5.145 can be multiplied by  $\frac{\partial \cos \theta}{\partial \theta}$ , leading to:

$$\begin{aligned}
 (1 - \cos^2 \theta) \frac{\partial P_n(\cos \theta)}{\partial \cos \theta} \frac{\partial \cos \theta}{\partial \theta} &= [nP_{n-1}(\cos \theta) - n \cos \theta P_n(\cos \theta)] \frac{\partial \cos \theta}{\partial \theta} \\
 (\sin^2 \theta) \frac{\partial P_n(\cos \theta)}{\partial \theta} &= [nP_{n-1}(\cos \theta) - n \cos \theta P_n(\cos \theta)] (-\sin \theta) \\
 \frac{\partial P_n(\cos \theta)}{\partial \theta} &= -\frac{n}{\sin \theta} [P_{n-1}(\cos \theta) - \cos \theta P_n(\cos \theta)].
 \end{aligned} \tag{5.146}$$

Legendre's differential equation is given by (e.g., Boas, 1983; Arfken & Weber, 2005, Eq. 12.40)

$$(1 - x^2) \frac{\partial^2 P(x)}{\partial x^2} - 2x \frac{\partial P(x)}{\partial x} + l(l+1)P(x) = 0. \tag{5.147}$$

For  $x = \cos \theta$ , Eq. 5.147 becomes

$$(1 - \cos^2 \theta) \frac{d^2 P(\cos \theta)}{d \cos^2 \theta} - 2 \cos \theta \frac{dP(\cos \theta)}{d \cos \theta} + l(l+1)P(\cos \theta) = 0. \tag{5.148}$$

To evaluate the strain load Green's functions (SLGFs), however, we need to derive a recurrence relation for  $\frac{d^2 P(\cos \theta)}{d \theta^2}$  rather than for  $\frac{d^2 P(\cos \theta)}{d \cos^2 \theta}$ . From the chain rule in calculus, we can write

$$\frac{d}{d \cos \theta} = \frac{d \theta}{d \cos \theta} \frac{d}{d \theta}, \tag{5.149}$$

which, when operating on  $P(\cos \theta)$ , becomes

$$\begin{aligned}
 \frac{dP(\cos \theta)}{d \cos \theta} &= \frac{d \theta}{d \cos \theta} \frac{dP(\cos \theta)}{d \theta} \\
 &= -\frac{1}{\sin \theta} \frac{dP(\cos \theta)}{d \theta}.
 \end{aligned} \tag{5.150}$$

The second derivative term in Eq. 5.148,  $\frac{d^2 P(\cos \theta)}{d \cos^2 \theta}$ , becomes

$$\begin{aligned}
 \frac{d}{d \cos \theta} \left[ \frac{dP(\cos \theta)}{d \cos \theta} \right] &= \frac{d \theta}{d \cos \theta} \frac{d}{d \theta} \left[ \frac{dP(\cos \theta)}{d \cos \theta} \right] \\
 &= -\frac{1}{\sin \theta} \frac{d}{d \theta} \left[ \frac{d \theta}{d \cos \theta} \frac{d}{d \theta} P(\cos \theta) \right] \\
 &= -\frac{1}{\sin \theta} \frac{d}{d \theta} \left[ -\frac{1}{\sin \theta} \frac{dP(\cos \theta)}{d \theta} \right]
 \end{aligned}$$

$$\begin{aligned}
&= \frac{1}{\sin \theta} \frac{d}{d\theta} \left[ \frac{1}{\sin \theta} \frac{dP(\cos \theta)}{d\theta} \right] \\
&= \frac{1}{\sin \theta} \left[ \frac{dP(\cos \theta)}{d\theta} \left( \frac{-\cos \theta}{\sin^2 \theta} \right) + \frac{1}{\sin \theta} \frac{d^2 P(\cos \theta)}{d\theta^2} \right] \\
&= \frac{1}{\sin^2 \theta} \left[ \frac{d^2 P(\cos \theta)}{d\theta^2} - \frac{\cos \theta}{\sin \theta} \frac{dP(\cos \theta)}{d\theta} \right]. \tag{5.151}
\end{aligned}$$

Thus, plugging Eq. 5.151 into Eq. 5.148, we have (e.g., Kamigaichi, 1998; Arfken & Weber, 2005, Eq. 12.29)

$$\begin{aligned}
0 &= \sin^2 \theta \left[ \frac{1}{\sin^2 \theta} \left\{ \frac{d^2 P(\cos \theta)}{d\theta^2} - \frac{\cos \theta}{\sin \theta} \frac{dP(\cos \theta)}{d\theta} \right\} \right] \\
&\quad - 2 \cos \theta \left[ -\frac{1}{\sin \theta} \frac{dP(\cos \theta)}{d\theta} \right] + l(l+1)P(\cos \theta) \\
&= \frac{d^2 P(\cos \theta)}{d\theta^2} - \frac{\cos \theta}{\sin \theta} \frac{dP(\cos \theta)}{d\theta} + 2 \frac{\cos \theta}{\sin \theta} \frac{dP(\cos \theta)}{d\theta} + l(l+1)P(\cos \theta) \\
&= \frac{d^2 P(\cos \theta)}{d\theta^2} + \frac{\cos \theta}{\sin \theta} \frac{dP(\cos \theta)}{d\theta} + l(l+1)P(\cos \theta). \tag{5.152}
\end{aligned}$$

Thus,

$$\frac{d^2 P(\cos \theta)}{d\theta^2} = -\frac{\cos \theta}{\sin \theta} \frac{dP(\cos \theta)}{d\theta} - l(l+1)P(\cos \theta). \tag{5.153}$$

### 5.3.6 Legendre Polynomial Recursion Relations: Limit as $\theta \rightarrow 180^\circ$

In the limit  $\theta \rightarrow 180^\circ$ , the Legendre function are given by:

$$\begin{aligned}
P_n(\cos \theta) &= (-1)^n \\
\frac{dP_n(\cos \theta)}{d\theta} &= 0 \\
\frac{d^2 P_n(\cos \theta)}{d\theta^2} &= (-1)^{n+1} \left( \frac{n(n+1)}{2} \right). \tag{5.154}
\end{aligned}$$

We evaluated the limits at  $\theta = 180^\circ$  using using the `Python` package `SymPy`.

For the tangential component of strain,  $\epsilon_{\lambda\lambda}$  (Eq. 5.135), a factor of  $\cos \theta$  appears in the second term that must also be evaluated in the limit that  $\theta \rightarrow 180^\circ$ . For this component, we evaluate the limit as  $\theta \rightarrow 180^\circ$  of:

$$\cot(\theta) \frac{dP_n(\cos \theta)}{d\theta}, \tag{5.155}$$

where the Legendre polynomial arises from the series expansion for horizontal displacement,  $v$  (Eq. 5.126).

From `SymPy`, the limit evaluates to:

$$(-1)^{n+1} \left( \frac{n(n+1)}{2} \right), \quad (5.156)$$

which is equivalent to the limit as  $\theta \rightarrow 180^\circ$  of  $\frac{d^2 P_n(\cos \theta)}{d\theta^2}$ . As a result,  $\epsilon_{\lambda\lambda} = \epsilon_{\theta\theta}$  at  $\theta = 180^\circ$ .

### 5.3.7 Disk Factor

To speed the convergence of the series in Eqs. 5.125 and 5.126, distant loads (e.g., several tens of degrees away from the observer) may be approximated by finite circular caps rather than delta functions (e.g., Farrell, 1972). In practice, the disk factor from Eq. 5.75 may be inserted back into Eqs. 5.125 and 5.126. For displacement LGFs, which converge relatively rapidly, disk factors are generally not necessary; however, disk factors can be very useful for other types of LGFs, such as tilt and strain (e.g., Na & Baek, 2011).

The disk factor,

$$\left[ -\frac{(1 + \cos \alpha)}{n(n+1) \sin \alpha} \frac{\partial P_n(\cos \alpha)}{\partial \alpha} \right], \quad (5.157)$$

is only valid in the limit  $\alpha \rightarrow 0$ , where  $\alpha$  specifies the finiteness of the circular cap (e.g., Farrell, 1972); thus, the disk factor should only be invoked with small  $\alpha$  (e.g.,  $\sim 0.004^\circ$ ) or only at large angular distances.

### 5.3.8 Reference Frames

The vector displacement field generated by surface mass loading depends both on the physical characteristics of the deformation as well as the chosen reference frame (e.g., Blewitt, 2003; Petit & Luzum, 2010). The load Love numbers and corresponding load Green's functions described thus far have been computed in a reference frame fixed to the center of mass of the solid Earth, abbreviated CE. The CE reference frame is convenient for computing Love numbers and Green's functions, but not directly observable in practice (e.g., Farrell, 1972; Blewitt, 2003; Agnew, 2013). More appropriate reference frames for GNSS-inferred surface displacements are defined by the center of mass of the entire Earth system, abbreviated CM, which includes the solid Earth as well as its fluid exterior (e.g., oceans and atmosphere), or the center of figure, abbreviated CF (e.g., Blewitt, 2003; Fu et al., 2012).

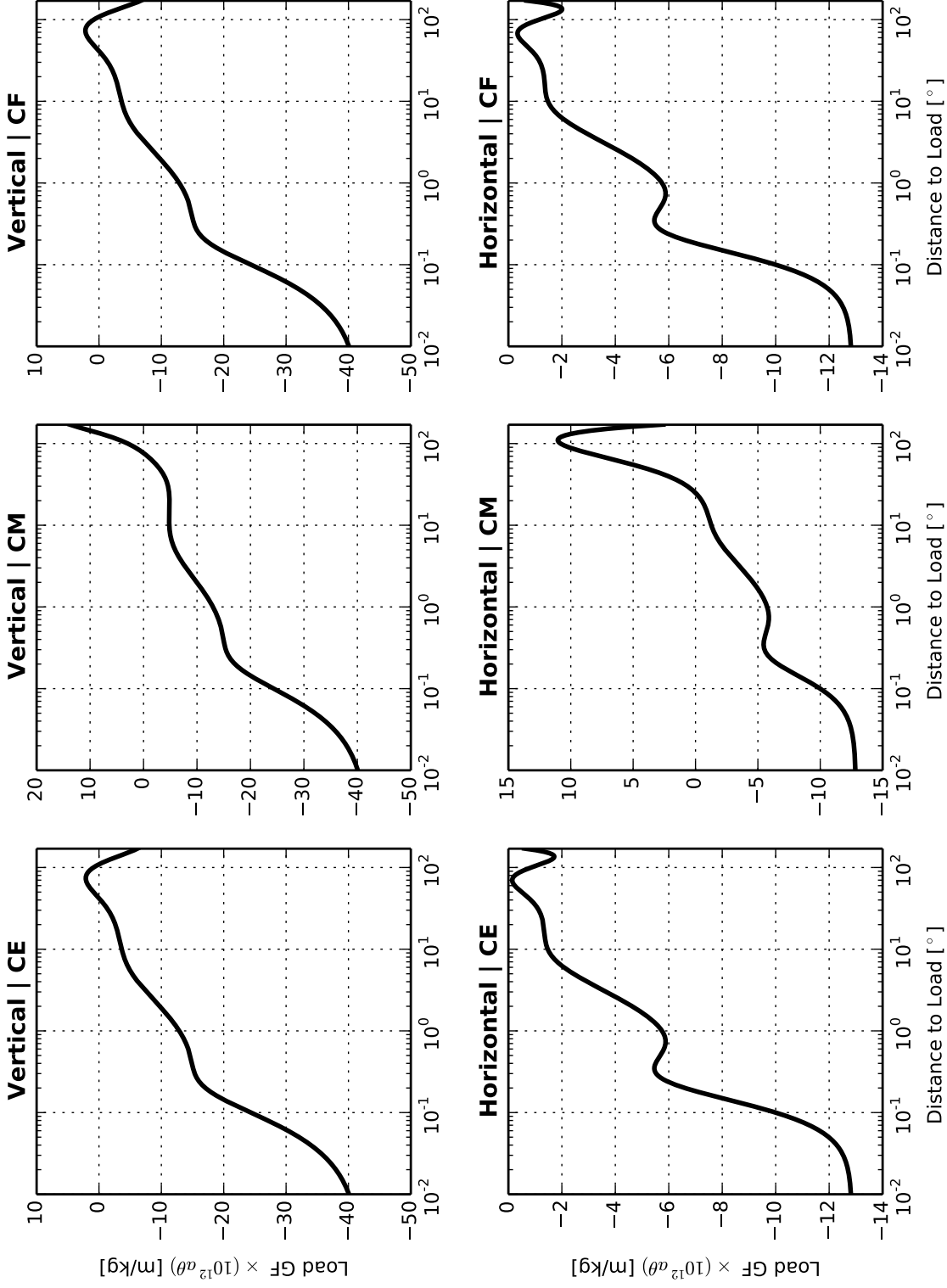


Figure 5.1: Vertical (top) and horizontal (bottom) displacement load Green's functions (LGFs) for a 1 kg surface mass load, computed using an isotropic and oceanless version of PREM. The left panels show the LGFs in the CE reference frame, the central panels show the LGFs in the CM reference frame, and the right panels show the LGFs in the CF reference frame (Blewitt, 2003). The load Green's functions have been normalized according to the Farrell convention (Farrell, 1972): displacement  $\times (a \theta) 10^{12}$ , where  $a$  is the radius of the Earth in meters and  $\theta$  is the angular distance from the load in radians.

Blewitt (2003) demonstrated that conversions between the various reference frames involve only simple transformations of the degree-one load Love numbers. The conversions for CE to CM, for example, are given by:

$$\begin{aligned} [h'_1]_{CM} &= [h'_1]_{CE} - 1 \\ [l'_1]_{CM} &= [l'_1]_{CE} - 1 \\ [1 + k'_1]_{CM} &= [1 + k'_1]_{CE} - 1. \end{aligned} \quad (5.158)$$

Similarly, the conversions for CE to CF (center of figure) are given by:

$$\begin{aligned} [h'_1]_{CF} &= \frac{2}{3} [h'_1 - l'_1]_{CE} \\ [l'_1]_{CF} &= -\frac{1}{3} [h'_1 - l'_1]_{CE} \\ [1 + k'_1]_{CF} &= \left[ 1 - \frac{1}{3} h'_1 - \frac{2}{3} l'_1 \right]_{CE}. \end{aligned} \quad (5.159)$$

From the equations for the displacement LGFs (Eqs. 5.109 and 5.110), the degree-1 components are:

$$u_1 = \frac{a}{m_E} h'_1 \cos \theta \quad (5.160)$$

and

$$v_1 = \frac{a}{m_E} l'_1 \frac{\partial}{\partial \theta} \cos \theta = -\frac{a}{m_E} l'_1 \sin \theta \quad (5.161)$$

for the vertical- and horizontal-displacement components, respectively.

The difference between LGFs computed in the CM and CE frames involves only a degree-one transformation. Thus, (e.g., Agnew, 2013):

$$u^{\text{CM}} - u^{\text{CE}} = u_1^{\text{CM}} - u_1^{\text{CE}} = \frac{a}{m_E} \cos \theta ([h'_1]_{\text{CM}} - [h'_1]_{\text{CE}}) = -\frac{a}{m_E} \cos \theta \quad (5.162)$$

for the vertical-displacement component, and

$$v^{\text{CM}} - v^{\text{CE}} = v_1^{\text{CM}} - v_1^{\text{CE}} = -\frac{a}{m_E} \sin \theta ([l'_1]_{\text{CM}} - [l'_1]_{\text{CE}}) = \frac{a}{m_E} \sin \theta \quad (5.163)$$

for the horizontal-displacement component.

The straightforward conversions between the CE and CM LGFs simplify to (Agnew, 2013):

$$u^{\text{CM}} = u^{\text{CE}} - \frac{a}{m_E} \cos \theta \quad (5.164)$$

for the vertical-displacement component, and

$$v^{\text{CM}} = v^{\text{CE}} + \frac{a}{m_E} \sin \theta \quad (5.165)$$

for the horizontal-displacement component.

The vertical- and horizontal-displacement LGFs computed in the CE, CM, and CF reference frames for the Preliminary Reference Earth Model (PREM) (Dziewonski & Anderson, 1981) are shown in Fig. 5.1.

## 5.4 Convolution Methods

SML-induced surface displacements may now be computed by convolving LGFs with a load model. Eqs. 5.109 and 5.110 represent the load-induced displacements per 1-kg load. For an applied load of arbitrary mass,  $dm$ , the induced displacements,  $du$  and  $dv$ , are given by (e.g., Scherneck & Bos, 2002):

$$du = \frac{a}{m_E} \sum_{n=0}^{\infty} h'_n P_n(\cos \theta) dm = G_u(\theta) dm \quad (5.166)$$

and

$$dv = \frac{a}{m_E} \sum_{n=1}^{\infty} l'_n \frac{\partial P_n(\cos \theta)}{\partial \theta} dm = G_v(\theta) dm, \quad (5.167)$$

where  $G_u(\theta)$  and  $G_v(\theta)$  represent the vertical- and horizontal-displacement LGFs, respectively.

For a spatially variable, non-point-source load, the LGFs are convolved with a load model:

$$\bar{U}_j(\bar{r}, S, \rho_{sea}, Z_j) = \int_{\Omega'} G(|\bar{r} - \bar{r}'|, S) \rho_{sea}(\bar{r}') Z_j(\bar{r}') d\Omega'. \quad (5.168)$$

In the context of ocean tidal loading (OTL),  $\bar{U}_j$  represents the surface displacement at observation point  $r$  due to loading by tidal harmonic  $j$ ,  $\rho_{sea}$  is the density of seawater at the load point  $r'$ ,  $G$  represents



the displacement LGF, and  $Z_j$  is the complex-valued tidal height at the load point  $r'$  (e.g., Farrell, 1973; Melchior, 1983; Baker, 1984; Harrison, 1985; Francis & Mazzega, 1990; Scherneck, 1991; Agnew, 1997; Jentzsch, 1997; Bos & Baker, 2005; Agnew, 2013; Bos & Scherneck, 2013). The LGF depends on distance to the load as well as Earth structure,  $S$ , which is assumed radially symmetric (e.g., PREM). The mass of the load,  $dm$ , at each load point,  $r'$ , is equivalent to the product of the amplitude, area element for a spherical surface, and density of the load (Eqs. 5.166 and 5.167).

Since OTL is confined to Earth's surface, Eq. 5.168 may be re-expressed as:

$$\bar{U}_j(\Theta, \lambda, \rho_{sea}, Z_j, S) = \int_0^{2\pi} \int_0^\pi \rho_{sea}(\Theta', \lambda') Z_j(\Theta', \lambda') G(\theta, S) T(\alpha) a^2 \sin \Theta' d\Theta' d\lambda', \quad (5.169)$$

where  $\Theta$  and  $\lambda$  are the co-latitude and longitude of the observation point, respectively;  $\Theta'$  and  $\lambda'$  are the co-latitude and longitude of the load point;  $G$  is the displacement LGF;  $T(\alpha)$  is a trigonometric factor that decomposes the horizontal-displacement response into two-component vectors (for the vertical response,  $T(\alpha) = 1$ );  $\alpha$  is the azimuth (measured clockwise from north);  $Z_j$  is the complex-valued tide height at the load point; and  $a$  is Earth's radius.

As an alternative to the spatial-convolution approach, the load model and the predicted response may be developed in the frequency domain in terms of spherical harmonics (e.g., Farrell, 1972; Agnew, 2015, Sec. 3.06.4.1). The spherical-harmonic approach can be highly efficient, particularly when seeking the deformation response globally (Farrell, 1972; Agnew, 2015, Sec. 3.06.4.1). The spatial-convolution method, on the other hand, allows for enhanced accuracy very near to the receiver without requiring a global refinement in the integration mesh (e.g., Farrell, 1972; Bos & Baker, 2005; Agnew, 2015, Sec. 3.06.4.2). Furthermore, the spatial convolution allows for easy combination of multiple loading models from different grids (e.g., Agnew, 1997, 2015, Sec. 3.06.4.2). We have adopted the spatial-convolution approach in the development presented here; however, with modern computing power and recent advancements in ocean-tide modeling, the spherical-harmonic method might now be a preferred option, and may be implemented in future releases.

#### 5.4.1 Integration Mesh

For practical implementation, the integral in Eq. 5.169 is replaced by a sum over discrete cells. The discrete cells are collectively known as the integration mesh. The integration mesh may be defined in two primary

ways (e.g., Hofmann-Wellenhof & Moritz, 2005): templates or gridlines. Templates are formed by subdividing concentric circles about the observation point. Gridlines are formed by subdividing a geographic coordinate system into discrete blocks. Since ocean-tide and other surface-fluid models are commonly distributed in gridline format, and the gridline method is not specific to an observation point, defining the integration mesh in terms of gridlines may seem the natural and obvious choice (e.g., Scherneck, 1991; Scherneck & Bos, 2002; Bos & Baker, 2005; Yeh et al., 2008). Defining the integration mesh in terms of templates, however, has distinct advantages for SML analysis (e.g., Goad, 1980; Harrison, 1985; Agnew, 1997, 2013). First, since the LGFs depend only on the angular distance between the load and receiver, the station-centric coordinate system requires relatively few LGFs to be computed. Second, the integration mesh does not change with the load model and, thus, easily facilitates the combination of multiple load models, even on irregular grids. Third, the singularity in the LGFs at small  $\theta$  is easily mitigated through appropriate scaling factors and integration over the area of the cells.

A drawback to the template method is that it requires interpolation of the load model onto the integration mesh and, therefore, takes time and does not represent the load model exactly. The ocean model itself, however, is also an approximation of the true load. Moreover, the gridline method also might require some interpolation of the load model (e.g., if a finer integration mesh is adopted near the station). In practice, Bos & Baker (2005) determined through rigorous testing that the choice of template or gridline method had little effect on predicted OTL-induced surface displacements.

As a result of the straightforward implementation and algorithmic flexibility, we have adopted the template method. Since the template grid is centered on the station, Eq. 5.169 becomes (e.g., Harrison, 1985; Agnew, 1997):

$$\bar{U}_j(\Theta, \lambda, \rho_{sea}, Z_j, S) = \int_0^{2\pi} \int_0^\pi \rho_{sea}(\theta, \alpha) Z_j(\theta, \alpha) G(\theta, S) T(\alpha) a^2 \sin \theta d\theta d\alpha, \quad (5.170)$$

where the load model,  $Z$ , and load density,  $\rho_{sea}$ , have been interpolated onto the integration mesh. Due to the rapid changes in the LGFs as  $\theta \rightarrow 0$ , the integration mesh should be refined near the station and neighboring coastlines in order to obtain accurate response predictions (e.g., Scherneck & Bos, 2002; Bos & Baker, 2005; Penna et al., 2008; Agnew, 2013).

### 5.4.2 Interpolation and Integration of Load Green's Function

One method to alleviate the singularity in the displacement LGFs at  $\theta = 0$  is to scale the LGFs by a factor proportional to  $\theta$ . Following (Agnew, 2013),

$$G'(\theta) = a^2 G(\theta) 2 \sin(\theta/2), \quad (5.171)$$

where  $G'(\theta)$  is the normalized LGF,  $G(\theta)$  is the original LGF, and  $a$  is Earth's radius. With the singularity reduced, the normalized LGFs are easily interpolated to intermediary values of  $\theta$  using, e.g., cubic-spline interpolation. Since tabulated LGFs necessarily contain a greater number of entries at small  $\theta$ , where the LGFs vary rapidly, interpolation on  $\log \theta$  provides a more even spacing (e.g., Bos & Baker, 2005). When working with a template grid, another option is to integrate the LGFs directly at the LLN-summation stage (e.g., Goad, 1980), which has the added benefit of improving the convergence of the series.

Using the normalized LGFs, Eq. 5.170 becomes:

$$\bar{U}_j(\Theta, \lambda, \rho_{sea}, Z_j, S) = \int_0^{2\pi} \int_0^\pi \rho_{sea} Z(\theta, \alpha) G'(\theta) T(\alpha) \frac{\sin \theta}{2 \sin(\theta/2)} d\theta d\alpha. \quad (5.172)$$

The tide height, seawater density, and normalized LGFs are given by the value at the mid-point of each cell.

Thus, we rewrite Eq. 5.172 as:

$$\bar{U}_j(\Theta, \lambda, \rho_{sea}, Z_j, S) = \rho_{sea} Z(\theta, \alpha) G'(\theta) \int_0^\pi \frac{\sin \theta}{2 \sin(\theta/2)} d\theta \int_0^{2\pi} T(\alpha) d\alpha. \quad (5.173)$$

In this form, the integration may be performed over individual cells and then summed together (Agnew, 2013):

$$\bar{U}_j(\Theta, \lambda, \rho_{sea}, Z_j, S) = \sum_{i=1}^N \rho_i Z_i G'(\theta_i) \int_{\theta_i - \frac{\delta}{2}}^{\theta_i + \frac{\delta}{2}} \frac{\sin \theta}{2 \sin(\theta/2)} d\theta \int_{\alpha_i - \frac{\beta}{2}}^{\alpha_i + \frac{\beta}{2}} T(\alpha) d\alpha, \quad (5.174)$$

where  $N$  is the total number of cells in the integration mesh,  $Z_i$  is the tide height at the center of cell  $i$ ,  $\rho_i$  is the seawater density at the center of cell  $i$ ,  $G'(\theta_i)$  is the normalized LGF computed for the center of cell  $i$ ,  $\theta_i$  is the angular separation between the station and the center of the load patch,  $\delta_i$  is the inclination width of the load patch,  $\alpha_i$  is the azimuth between the station and center of the load patch (as measured at the station

in degrees clockwise from north), and  $\beta_i$  is the azimuthal width of the load patch.

For vertical-displacement response,  $T(\alpha) = 1$ . For the north component of the horizontal response,  $T(\alpha) = -\cos(\alpha)$ . For the east component of the horizontal response,  $T(\alpha) = -\sin(\alpha)$ . The minus signs are required because the horizontal response is directed radially outwards from the load point; thus, the azimuth of the response at the receiver is  $\alpha + 180^\circ$ , where  $\alpha$  is the vector geodesic pointing from the receiver to the load point (e.g., Scherneck, 1991).

The integral over  $\theta$  reduces to (Agnew, 2013):

$$\int_{\theta_i - \frac{\delta_i}{2}}^{\theta_i + \frac{\delta_i}{2}} \frac{\sin \theta}{2 \sin(\theta/2)} d\theta = 4 \cos\left(\frac{\theta_i}{2}\right) \sin\left(\frac{\delta_i}{4}\right). \quad (5.175)$$

Since  $\theta_i$  and  $\delta_i$  are determined solely from the integration mesh, the integrated LGFs may be computed and stored prior to convolution with a load model. The integral over  $\alpha$  for the vertical-displacement response reduces to:

$$\int_{\alpha_i - \frac{\beta_i}{2}}^{\alpha_i + \frac{\beta_i}{2}} T(\alpha) d\alpha = \int_{\alpha_i - \frac{\beta_i}{2}}^{\alpha_i + \frac{\beta_i}{2}} d\alpha = \beta_i. \quad (5.176)$$

The integral over  $\alpha$  for the horizontal-displacement response (north component) reduces to:

$$\begin{aligned} \int_{\alpha_i - \frac{\beta_i}{2}}^{\alpha_i + \frac{\beta_i}{2}} T(\alpha) d\alpha &= - \int_{\alpha_i - \frac{\beta_i}{2}}^{\alpha_i + \frac{\beta_i}{2}} \cos(\alpha) d\alpha \\ &= - \left\{ \sin\left(\alpha_i + \frac{\beta_i}{2}\right) - \sin\left(\alpha_i - \frac{\beta_i}{2}\right) \right\} \\ &= - \left[ \sin(\alpha_i) \cos\left(\frac{\beta_i}{2}\right) + \cos(\alpha_i) \sin\left(\frac{\beta_i}{2}\right) \right] + \\ &\quad \left[ \sin(\alpha_i) \cos\left(\frac{\beta_i}{2}\right) - \cos(\alpha_i) \sin\left(\frac{\beta_i}{2}\right) \right] \\ &= -2 \sin\left(\frac{\beta_i}{2}\right) \cos(\alpha_i). \end{aligned} \quad (5.177)$$

The integral over  $\alpha$  for the horizontal-displacement response (east component) reduces to:

$$\begin{aligned} \int_{\alpha_i - \frac{\beta_i}{2}}^{\alpha_i + \frac{\beta_i}{2}} T(\alpha) d\alpha &= - \int_{\alpha_i - \frac{\beta_i}{2}}^{\alpha_i + \frac{\beta_i}{2}} \sin(\alpha) d\alpha \\ &= - \left\{ \cos\left(\alpha_i - \frac{\beta_i}{2}\right) - \cos\left(\alpha_i + \frac{\beta_i}{2}\right) \right\} \end{aligned}$$

$$\begin{aligned}
&= - \left[ \cos(\alpha_i) \cos\left(\frac{\beta_i}{2}\right) + \sin(\alpha_i) \sin\left(\frac{\beta_i}{2}\right) \right] + \\
&\quad \left[ \cos(\alpha_i) \cos\left(\frac{\beta_i}{2}\right) - \sin(\alpha_i) \sin\left(\frac{\beta_i}{2}\right) \right] \\
&= -2 \sin\left(\frac{\beta_i}{2}\right) \sin(\alpha_i).
\end{aligned} \tag{5.178}$$

### 5.4.3 Convolution Procedure

After the integration mesh has been defined and the LGFs have been normalized and integrated, the next step is to determine the geographic coordinates for the midpoint of each cell. From spherical trigonometry, we compute the latitude and longitude of the cell midpoints  $(\Phi_i, \lambda_i)$  using the so-called direct geodesic problem (e.g., Karney, 2013):

$$\Phi_i = \arcsin(\sin \Phi_R \cos \theta_i + \cos \Phi_R \sin \theta_i \cos \alpha_i) \tag{5.179}$$

$$\lambda_i = \lambda_R + \arctan\left(\frac{\sin \alpha_i \sin \theta_i \cos \Phi_R}{\cos \theta_i - \sin \Phi_R \sin \Phi_i}\right), \tag{5.180}$$

where  $\Phi_i = 90 - \Theta_i$  is the latitude at the midpoint of mesh cell  $i$ ,  $\lambda_i$  is the longitude at the midpoint of mesh cell  $i$ ,  $\Phi_R$  is the latitude of the station,  $\lambda_R$  is the longitude of the station,  $\theta_i$  is the inclination angle between the station and the midpoint of mesh cell  $i$ , and  $\alpha_i$  is the azimuth from the station to the midpoint of mesh cell  $i$  (measured at the station in degrees clockwise from north). Note that to account for Earth flattening effects, the geographic coordinates may be converted to geocentric coordinates when computing azimuth and inclination.

The load model, provided on a geographic coordinate grid, may now be interpolated to the specific geographic coordinates at the center of each integration-mesh cell. One option is to use bilinear interpolation of the four neighboring load points (e.g., Penna et al., 2008; Agnew, 2013). Another option, as long as the grid is rectangular, is to use two-dimensional bivariate spline interpolation, which is provided as a built-in function within `scipy`.

The discrete convolution now may be written as (e.g., Harrison, 1985; Agnew, 1997):

$$\bar{U}_{\text{vert}}(\Theta, \lambda) = 4 \sum_{i=1}^N Z_i \rho_i G'(\theta_i) \cos\left(\frac{\theta_i}{2}\right) \sin\left(\frac{\delta_i}{4}\right) \beta_i \tag{5.181}$$

$$\bar{U}_{\text{north}}(\Theta, \lambda) = 8 \sum_{i=1}^N Z_i \rho_i G'(\theta_i) \cos\left(\frac{\theta_i}{2}\right) \sin\left(\frac{\delta_i}{4}\right) \sin\left(\frac{\beta_i}{2}\right) \cos(\alpha_i + 180^\circ) \quad (5.182)$$

$$\bar{U}_{\text{east}}(\Theta, \lambda) = 8 \sum_{i=1}^N Z_i \rho_i G'(\theta_i) \cos\left(\frac{\theta_i}{2}\right) \sin\left(\frac{\delta_i}{4}\right) \sin\left(\frac{\beta_i}{2}\right) \sin(\alpha_i + 180^\circ). \quad (5.183)$$

For complex-valued loads, including the ocean tides, the amplitudes and phases are partitioned into real and imaginary components (e.g., Bos & Baker, 2005):

$$Z_i = A_i \cos \phi_i + i A_i \sin \phi_i = c + i s, \quad (5.184)$$

where  $A_i$  is the amplitude of the load at the center of mesh cell  $i$  and  $\phi_i$  is the phase at the center of mesh cell  $i$ . The real and imaginary components are convolved separately over all cells in the integration mesh using Eqs. 5.181–5.183. The convolution results for each harmonic coefficient,  $U_c$  and  $U_s$ , are then recombined into the amplitude and phase for each spatial component:

$$A = \sqrt{U_c^2 + U_s^2} \quad (5.185)$$

$$\phi = \text{atan2}(U_s, U_c). \quad (5.186)$$

In addition to a spatially variable load model, a spatially variable model for seawater densities may also be included (e.g., Bos & Baker, 2005; Agnew, 2013; Ray, 2013). As with the load model, the densities would be interpolated onto the integration mesh, designed such that the average density within each cell is approximately equal to the value at the midpoint of each cell. Alternatively, the seawater density may be approximated as constant everywhere and applied after the convolution. The approximation of constant seawater density is good to about 1% (e.g., Bos & Baker, 2005).

#### 5.4.4 Additional Considerations

To improve the convolution further, the load model may be refined around coastal boundaries using a land-sea mask and bilinear interpolation (e.g., Agnew, 2013). Recent ocean tide models, such as TPX08-Atlas and FES2014, do a much better job of fitting the coastline than former-generation models (e.g., Penna et al.,

2008); thus, refining the ocean tide models around the coastline has become less critical, but still influential.

It is also worth noting that the development presented here applies to an elastic Earth. For a viscoelastic Earth, the elastic moduli are frequency dependent and the load Love numbers become complex-valued (e.g., Lambeck, 1988; Pagiatakis, 1990; Bos et al., 2015). Francis & Mazzega (1990) reported differences between OTL-induced surface displacements of up to 1.5% in amplitude and  $0.3^\circ$  in phase when comparing elastic and anelastic models. More recently, Bos et al. (2015) found that discrepancies between observed and predicted OTL-induced surface displacements in western Europe could be reduced by about 0.2 mm on average by accounting for mantle anelasticity.

## References

- Abramowitz, M. & Stegun, I. A., 1964. *Handbook of mathematical functions: With formulas, graphs, and mathematical tables*, Courier Corporation, Dover Publications, New York.
- Agnew, D. C., 1997. NLOADF: A program for computing ocean-tide loading, *J. Geophys. Res.*, **102**(B3), 5109–5110.
- Agnew, D. C., 2013. SPOTL: Some programs for ocean-tide loading, *Scripps Institute of Oceanography Technical Report*.
- Agnew, D. C., 2015. Earth Tides, *Treatise on Geophysics, 2nd Ed.*, **3**(06), 151–178.
- Alterman, Z., Jarosch, H., & Pekeris, C., 1959. Oscillations of the Earth, *Proc. R. Soc. London, Ser. A*, **252**(1268), 80–95.
- Amante, C. & Eakins, B. W., 2009. ETOPO1 1 arc-minute global relief model: Procedures, data sources and analysis, *NOAA Technical Memorandum NESDIS NGDC-24*.
- Arfken, G. B. & Weber, H. J., 2005. *Mathematical methods for physicists, Sixth Ed.*, Academic press.
- Baker, T., 1984. Tidal deformations of the Earth, *Sci. Prog. Oxford*, **69**, 197–233.
- Blewitt, G., 2003. Self-consistency in reference frames, geocenter definition, and surface loading of the solid Earth, *J. Geophys. Res.*, **108**(B2), 2103.
- Boas, M. L., 1983. *Mathematical Methods in the Physical Sciences, 2nd Edition*, John Wiley & Sons., Inc.
- Bos, M. & Baker, T., 2005. An estimate of the errors in gravity ocean tide loading computations, *J. Geod.*, **79**(1), 50–63.
- Bos, M. & Scherneck, H.-G., 2013. Computation of Green's Functions for Ocean Tide Loading, in *Sciences of Geodesy II*, ed. Xu, G., Springer-Verlag, Berlin.
- Bos, M. S., Penna, N. T., Baker, T. F., & Clarke, P. J., 2015. Ocean tide loading displacements in western Europe. Part 2: GPS-observed anelastic dispersion in the asthenosphere, *J. Geophys. Res. Solid Earth*, **120**(9), 6540–6557.



- Carrère, L., Lyard, F., Cancet, M., Guillot, A., & Roblou, L., 2012. FES2012: A new global tidal model taking advantage of nearly 20 years of altimetry, in *Proceedings of meeting “20 Years of Altimetry”*, Venice.
- Cathles, L. M., 1975. *The viscosity of the Earth’s mantle*, vol. 386, Princeton University Press: Princeton, NJ.
- Chinnery, M. A., 1975. The static deformation of an earth with a fluid core: a physical approach, *Geophys. J. R. Astron. Soc.*, **42**(2), 461–475.
- Crossley, D., 1975. The free-oscillation equations at the centre of the Earth, *Geophys. J. Int.*, **41**(2), 153–163.
- Dahlen, F. & Tromp, J., 1998. *Theoretical global seismology*, Princeton University Press: Princeton, NJ.
- Desai, S. D. & Ray, R. D., 2014. Consideration of tidal variations in the geocenter on satellite altimeter observations of ocean tides, *Geophys. Res. Lett.*, **41**(7), 2454–2459.
- Dziewonski, A. M. & Anderson, D. L., 1981. Preliminary reference Earth model, *Phys. Earth Planet. Inter.*, **25**(4), 297–356.
- Egbert, G. D. & Erofeeva, S. Y., 2002. Efficient inverse modeling of barotropic ocean tides, *J. Atmos. Oceanic Technol.*, **19**(2), 183–204.
- Egbert, G. D., Bennett, A. F., & Foreman, M. G., 1994. TOPEX/POSEIDON tides estimated using a global inverse model, *J. Geophys. Res. Oceans*, **99**(C12), 24821–24852.
- Egbert, G. D., Erofeeva, S. Y., & Ray, R. D., 2010. Assimilation of altimetry data for nonlinear shallow-water tides: Quarter-diurnal tides of the Northwest European Shelf, *Cont. Shelf Res.*, **30**(6), 668–679.
- Farrell, W., 1972. Deformation of the Earth by surface loads, *Rev. Geophys.*, **10**(3), 761–797.
- Farrell, W., 1973. Earth tides, ocean tides and tidal loading, *Philos. Trans. R. Soc. London, Ser. A*, **274**(1239), 253–259.
- Francis, O. & Dehant, V., 1987. Recomputation of the Green’s functions for tidal loading estimations, *Bull. Inf. Mar. Terr.*, **no. 100**, 6962–6986.

- Francis, O. & Mazzega, P., 1990. Global charts of ocean tide loading effects, *J. Geophys. Res. Oceans*, **95**(C7), 11411–11424.
- Fu, Y., Freymueller, J. T., & van Dam, T., 2012. The effect of using inconsistent ocean tidal loading models on GPS coordinate solutions, *J. Geod.*, **86**(6), 409–421.
- Gilbert, F. & Backus, G. E., 1966. Propagator matrices in elastic wave and vibration problems, *Geophysics*, **31**(2), 326–332.
- Goad, C. C., 1980. Gravimetric tidal loading computed from integrated Green's functions, *J. Geophys. Res. Solid Earth*, **85**(B5), 2679–2683.
- Guo, J., Li, Y., Huang, Y., Deng, H., Xu, S., & Ning, J., 2004. Green's function of the deformation of the Earth as a result of atmospheric loading, *Geophys. J. Int.*, **159**(1), 53–68.
- Harrison, J., 1985. *Earth Tides (Benchmark Papers in Geology)*, Van Nostrand Reinhold Company Inc.
- Hobson, E., 1955. *The Theory of Spherical and Ellipsoidal Harmonics*, Chelsea, New York.
- Hofmann-Wellenhof, B. & Moritz, H., 2005. *Physical Geodesy, Second Edition*, Springer.
- Jentzsch, G., 1997. Earth tides and ocean tidal loading, in *Tidal Phenomena*, pp. 145–171, Springer.
- Kamigaichi, O., 1998. Green functions of the earth at borehole sensor installation depths for surface point load, *Papers in Meteorology and Geophysics*, **48**(4), 89–100.
- Karney, C. F., 2013. Algorithms for geodesics, *J. Geod.*, **87**(1), 43–55.
- Lambeck, K., 1988. *Geophysical Geodesy: The slow deformations of the Earth*, Clarendon Press, Oxford.
- Lambeck, K., 2005. *The Earth's variable rotation: Geophysical causes and consequences*, Cambridge University Press.
- Lambert, A., Pagiatakis, S., Billyard, A., & Dragert, H., 1998. Improved ocean tide loading corrections for gravity and displacement: Canada and northern United States, *J. Geophys. Res. Solid Earth*, **103**(B12), 30231–30244.
- Lanzano, P., 1982. *Deformations of an elastic earth (International Geophysics Series; v. 31)*, Academic Press, New York.

- Lapwood, E. R. & Usami, T., 1981. *Free Oscillations of the Earth*, Cambridge University Press.
- Le Provost, C., Genco, M., Lyard, F., Vincent, P., & Canceil, P., 1994. Spectroscopy of the world ocean tides from a finite element hydrodynamic model, *J. Geophys. Res. Oceans*, **99**(C12), 24777–24797.
- Longman, I., 1962. A Green's function for determining the deformation of the Earth under surface mass loads: 1. Theory, *J. Geophys. Res.*, **67**(2), 845–850.
- Longman, I., 1963. A Green's function for determining the deformation of the Earth under surface mass loads: 2. Computations and numerical results, *J. Geophys. Res.*, **68**(2), 485–496.
- Love, A., 1909. The yielding of the Earth to disturbing forces, *Proc. R. Soc. London, Ser. A*, **82**(551), 73–88.
- Love, A. E. H., 1911. *Some Problems of Geodynamics: Being an essay to which the Adams Prize in the University of Cambridge was Adjudged in 1911*, Cambridge University Press.
- Lyard, F., Lefevre, F., Letellier, T., & Francis, O., 2006. Modelling the global ocean tides: Modern insights from FES2004, *Ocean Dyn.*, **56**(5-6), 394–415.
- Martens, H. R., 2016. *Using Earth deformation caused by surface mass loading to constrain the elastic structure of the crust and mantle*, Ph.D. thesis, California Institute of Technology.
- Martens, H. R., Rivera, L., Simons, M., & Ito, T., 2016a. The sensitivity of surface mass loading displacement response to perturbations in the elastic structure of the crust and mantle, *J. Geophys. Res. Solid Earth*, **121**.
- Martens, H. R., Simons, M., Owen, S., & Rivera, L., 2016b. Observations of ocean tidal load response in South America from sub-daily GPS positions, *Geophys. J. Int.*, **205**, 1637–1664.
- Melchior, P., 1983. *The tides of the planet Earth, 2nd Ed.*, Pergamon Press: Oxford, UK.
- Merriam, J., 1985. Toroidal love numbers and transverse stress at the earth's surface, *J. Geophys. Res. Solid Earth*, **90**(B9), 7795–7802.
- Molodenskiy, S., 1977. Relation between Love numbers and load factors, *Izvestiya, Earth Physics*, **13**(3), 147–149.
- Munk, W. & MacDonald, G., 1960. *The Rotation of the Earth*, Cambridge University Press: New York.

- Na, S.-H. & Baek, J., 2011. Computation of the load Love number and the load Green's function for an elastic and spherically symmetric earth, *J. Korean Phys. Soc.*, **58**(5), 1195–1205.
- Okubo, S., 1993. Reciprocity theorem to compute the static deformation due to a point dislocation buried in a spherically symmetric earth, *Geophys. J. Int.*, **115**(3), 921–928.
- Okubo, S. & Endo, T., 1986. Static spheroidal deformation of degree 1 - Consistency relation, stress solution and partials, *Geophys. J. Int.*, **86**(1), 91–102.
- Okubo, S. & Saito, M., 1983. Partial derivative of Love numbers, *Bulletin Géodésique*, **57**(1), 167–179.
- Pagiatakis, S. D., 1990. The response of a realistic earth to ocean tide loading, *Geophys. J. Int.*, **103**(2), 541–560.
- Penna, N. T., Bos, M. S., Baker, T. F., & Scherneck, H.-G., 2008. Assessing the accuracy of predicted ocean tide loading displacement values, *J. Geod.*, **82**(12), 893–907.
- Petit, G. & Luzum, B., 2010. IERS Technical Note No. 36, IERS Conventions (2010), *International Earth Rotation and Reference Systems Service: Frankfurt, Germany*.
- Press, W. H., Teukolsky, S. A., Vetterling, W. T., & Flannery, B. P., 2007. *Numerical recipes, 3rd Edition: The art of scientific computing*, Cambridge University Press.
- Ray, R., 2013. Precise comparisons of bottom-pressure and altimetric ocean tides, *J. Geophys. Res. Oceans*, **118**(9), 4570–4584.
- Ray, R., Egbert, G., & Erofeeva, S., 2011. Tide predictions in shelf and coastal waters: Status and prospects, in *Coastal Altimetry*, pp. 191–216, Springer.
- Ray, R. D., 1999. A global ocean tide model from TOPEX/POSEIDON altimetry: GOT99. 2., *NASA Technical Memorandum 209478*.
- Ray, R. D. & Egbert, G. D., 2004. The global S1 tide, *J. Phys. Oceanogr.*, **34**(8), 1922–1935.
- Sabadini, R. & Vermeersen, B., 2004. *Global dynamics of the Earth: Applications of normal mode relaxation theory to solid-earth geophysics*, Kluwer Academic Publishers.
- Saito, M., 1974. Some problems of static deformation of the Earth., *J. Phys. Earth*, **22**(1), 123–140.

- Saito, M., 1978. Relationship between tidal and load Love numbers, *J. Phys. Earth*, **26**(1), 13–16.
- Savcenko, R. & Bosch, W., 2012. EOT11a—empirical ocean tide model from multi-mission satellite altimetry, *DGFI Report*, **89**.
- Scherneck, H.-G., 1991. A parametrized solid earth tide model and ocean tide loading effects for global geodetic baseline measurements, *Geophys. J. Int.*, **106**(3), 677–694.
- Scherneck, H.-G. & Bos, M. S., 2002. Ocean tide and atmospheric loading, in *IVS 2002 General Meeting Proceedings*, pp. 205–214.
- Smylie, D., 2013. *Earth Dynamics: Deformations and Oscillations of the Rotating Earth*, Cambridge University Press.
- Stammer, D., Wunsch, C., Fukumori, I., & Marshall, J., 2002. State estimation improves prospects for ocean research, *Eos Transactions*, **83**(27), 289–295.
- Sun, W. & Okubo, S., 1993. Surface potential and gravity changes due to internal dislocations in a spherical earth – i. theory for a point dislocation, *Geophys. J. Int.*, **114**(3), 569–592.
- Takeuchi, H., 1950. On the Earth tide of the compressible Earth of variable density and elasticity, *Eos Transactions*, **31**(5), 651–689.
- Takeuchi, H., 1966. *Theory of the Earth's Interior*, Blaisdell Publishing Company.
- Takeuchi, H. & Saito, M., 1972. Seismic surface waves, in *Methods in Computational Physics, Volume 11/Seismology: Surface Waves and Earth Oscillations*, pp. 217–295, Academic Press.
- van Dam, T., Wahr, J., Chao, Y., & Leuliette, E., 1997. Predictions of crustal deformation and of geoid and sea-level variability caused by oceanic and atmospheric loading, *Geophys. J. Int.*, **129**(3), 507–517.
- Wang, H., Xiang, L., Jia, L., Jiang, L., Wang, Z., Hu, B., & Gao, P., 2012. Load Love numbers and Green's functions for elastic Earth models PREM, iasp91, ak135, and modified models with refined crustal structure from Crust 2.0, *Computers & Geosciences*, **49**, 190–199.
- Wessel, P., Smith, W. H., Scharroo, R., Luis, J., & Wobbe, F., 2013. Generic mapping tools: Improved version released, *Eos Transactions*, **94**(45), 409–410.

- Wiggins, R. A., 1968. Terrestrial variational tables for the periods and attenuation of the free oscillations, *Phys. Earth Planet. Inter.*, **1**(4), 201–266.
- Wu, P. & Peltier, W., 1982. Viscous gravitational relaxation, *Geophys. J. Int.*, **70**(2), 435–485.
- Wunsch, C. & Stammer, D., 1997. Atmospheric loading and the oceanic “inverted barometer” effect, *Rev. Geophys.*, **35**(1), 79–107.
- Yeh, T.-K., Huang, C., & Xu, G., 2008. GPS height and gravity variations due to ocean tidal loading around Taiwan, *Surv. Geophy.*, **29**(1), 37–50.